

NUMERICAL STUDY OF COAXIAL
TURBULENT JETS WITH SUDDEN
AXISYMMETRIC EXPANSION



by

RABINDRA NATH DAS

A Thesis Submitted to the Department of Mechanical Engineering in
Partial Fulfilment of the Requirements for the Degree of

Master of Science

in

Mechanical Engineering

December, 1992.

Bangladesh University of Engineering and Technology
Dhaka, Bangladesh.

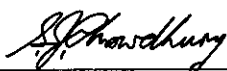


#85784#

532, 01
1992
DAS

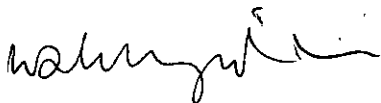
RECOMMENDATION OF THE BOARD OF EXAMINERS

The Board of Examiners hereby recommends to the Department of Mechanical Engineering, Bangladesh University of Engineering and Technology, Dhaka, the acceptance of the thesis, "NUMERICAL STUDY OF COAXIAL TURBULENT JETS WITH SUDDEN AXISYMMETRIC EXPANSION", submitted by Rabindra Nath Das, in partial fulfilment of the requirements for the degree of Master of Science in Mechanical Engineering.



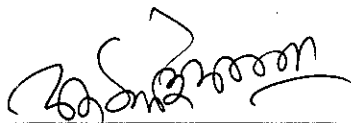
Dr. Showkat Jahan Chowdhury (Supervisor)
Assistant Professor
Department of Mechanical Engineering
BUET, Dhaka.

Chairman



Dr. Md. Wahhaj Uddin
Professor & Head
Department of Mechanical Engineering
BUET, Dhaka.

Member
(Ex-officio)



Dr. A. K. M. Sadrul Islam
Associate Professor
Department of Mechanical Engineering
BUET, Dhaka.

Member



Dr. Md. Abdul Matin
Assistant Professor
Department of Water Resources Engineering
BUET, Dhaka.

Member
(External)

ABSTRACT

This thesis deals with the numerical study of coaxial turbulent jets with sudden axisymmetric expansion, which has many practical applications. The computer program used for this analysis utilizes the $k-\epsilon$ model. The governing equations are discretized over the appropriate control volumes using the hybrid differencing scheme and nonuniform staggered grid.

The capability of the model in predicting such complex flows having recirculation, is tested by comparing with available experimental data. It is shown that the model can predict complicated flows like coaxial turbulent jet with sudden expansion with reasonable accuracy. The effect of changing the jet velocity ratio, computational grid size, Reynolds number and expansion ratio on the flow field is also examined. It is observed that, by proper nondimensionalization, we can plot profiles from which the required flow variables can be interpreted at different jet velocity ratio and Reynolds number. Grid size of 46 x 34 node points is adopted for the present computation. Computational time is observed to increase as square of the nodal points used in the analysis and thus the minimum number of nodal points required for attaining reasonably accurate results is necessary.

ACKNOWLEDGEMENT

The author would like to express his sincere gratitude and indebtedness to his Supervisor, Dr. Showkat Jahan Chowdhury, Assistant Professor, Department of Mechanical Engineering, Bangladesh University of Engineering and Technology (BUET), Dhaka, for his careful supervision, constant encouragement, invaluable suggestions and untiring assistance throughout this research work.

The author is also very grateful to Dr. Md. Wahhaj Uddin, Professor & Head, Department of Mechanical Engineering, Bangladesh University of Engineering and Technology for his cooperation and inspiration.

Special thanks to Mr. Maniruzzaman, Assistant Professor, Department of Mechanical Engineering, BUET, Dhaka, for his assistance and valuable suggestions while working on the computer.

The author also expresses his gratitude to Md. Fakhrul Islam Hazra, Accounts Assistant Cum-Typist, Department of Mechanical Engineering, BUET for typing this thesis.

Finally, the author would like to thank all others who, directly or indirectly, helped him while the research work was going on.

TABLE OF CONTENTS

	PAGE
Title Page	i
Certificate of Acceptance	ii
Abstract	iii
Acknowledgement	iv
Table of Contents	v
List of Figures	vii
List of Tables	ix
List of Symbols	x
CHAPTER - 1 INTRODUCTION	1
1.1 Background	1
1.2 Motivation of the Present Investigation	2
1.3 Literature Review	3
1.3.1 History of Turbulence	3
1.3.2 Previous Work	9
1.4 Objective of this Study	10
1.5 Outline of the Thesis	11
CHAPTER - 2 METHODOLOGY OF SOLUTION	12
2.1 Scope	12
2.2 Governing Equations	12
2.3 Solution Technique	15
2.4 Boundary Conditions	17
2.5 Solution Procedure	18
2.6 Closure	20

CHAPTER - 3	RESULTS & DISCUSSIONS	21
3.1	Scope	21
3.2	Problem Statement	21
3.3	Comparison with Available Experimental Data	22
3.4	Effect of Grid Size	25
3.5	Effect of Velocity Ratio U_1/U_2	25
3.6	Effect of Reynolds number	30
3.7	Effect of Expansion Ratio	31
3.8	Closure	33
CHAPTER - 4	CONCLUSION	34
4.1	Summary of Main Findings	34
4.2	Suggestions for Future Work	35
REFERENCES		37
FIGURES		42
APPENDIX - A	COMPUTER PROGRAMME FLOW CHART	88

LIST OF FIGURES

FIGURE		PAGE
1:	Geometry of confined coaxial jet expansion setup	42
2:	Staggered grid	43
3:	Three control volumes associated with points of the three grids	43
4:	Nonuniform rectangular grid system	44
5:	Comparison of mean axial velocity profiles	45
6:	Comparison of turbulent kinetic energy profiles	47
7:	Dissipation rate profiles at different axial locations	49
8:	Dimensionless mean axial velocity profiles for different axial locations	51
9:	Dimensionless turbulent kinetic energy profiles for different axial locations	52
10:	Comparison of mean axial velocity profiles	53
11:	Mean axial velocity profiles for $U_1/U_2 = 0.2$	55
12:	Turbulent kinetic energy profiles for $U_1/U_2 = 0.2$	57
13:	Dissipation rate profiles for $U_1/U_2 = 0.2$	59
14:	Dimensionless mean axial velocity profiles for different axial locations	61
15:	Dimensionless turbulent kinetic energy profiles for different axial locations	62
16:	Mean axial velocity profiles for $U_1/U_2 = 0.5$	63
17:	Turbulent kinetic energy profiles for $U_1/U_2 = 0.5$	65
18:	Dissipation rate profiles for $U_1/U_2 = 0.5$	67
19:	Dimensionless mean axial velocity profiles for different axial locations	69

20:	Dimensionless turbulent kinetic energy profiles for different axial locations	70
21:	Comparison of dimensionless mean axial velocity profiles	71
22:	Comparison of dimensionless turbulent kinetic energy profiles	73
23:	Comparison of nondimensional centerline velocities	75
24:	Comparison of dimensionless mean axial velocity profiles	76
25:	Comparison of mean axial velocity profiles	78
26:	Comparison of dimensionless turbulent kinetic energy profiles	80
27:	Comparison of turbulent kinetic energy profiles	82
28:	Comparison of dimensionless mean axial velocity profiles	84
29:	Comparison of dimensionless turbulent kinetic energy profiles	86

LIST OF TABLES

	PAGE
Table 2.1 Source Terms for the General Equation	14

LIST OF SYMBOLS

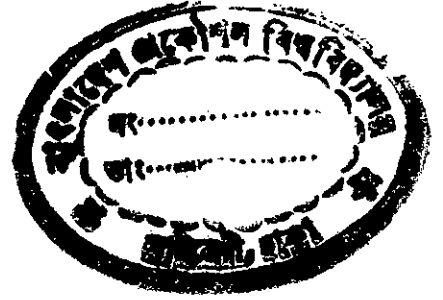
Symbol	Meaning
C_1	Turbulence model constant
C_2	Turbulence model constant
C_D	Turbulence model constant
C_μ	Turbulence model constant
k	Kinetic energy of turbulence
l	Length scale
p	Mean pressure
Q_1, Q_2	Jet flow rate
r	Radial distance
r_1, r_2	Radius of inner and outer jets
R_e	Reynolds number
S_φ	Source term for variable φ
u	Mean axial velocity
U_0	Reference velocity
U_1, U_2	Jet velocity
v_i	Instantaneous velocity
v_i'	Fluctuating velocity
x	Axial coordinate
x_R	Reattachment length

Greek Symbol Meaning

ϵ	Dissipation rate of turbulent kinetic energy
ν	Kinetic viscosity
ν_T	Turbulent (eddy) kinetic viscosity
μ	Dynamic viscosity
μ_l	Laminar dynamic viscosity
μ_T	Turbulent dynamic viscosity
ρ	Constant mass density
σ_φ	Prandtl number for variable φ
ω'_i	Turbulent fluctuating vorticity

CHAPTER - 1

INTRODUCTION



1.1 Background

When a fluid flows from a region of high pressure to a region of low pressure through some nozzle, it forms a jet. The jet may be, (i) a Free jet, if it is allowed to expand freely in the low pressure region; (ii) a Wall jet, if it impinges on a wall, (iii) a Confined jet, if it is allowed to expand in a closed conduit on the low pressure side. Although all these three types of jets have many practical engineering applications, confined jets are mainly used in the combustion chambers of gas turbines, ramjets, and in industrial furnaces, and hence are receiving special attention in the recent years.

When a confined jet is surrounded by another concentric circular jet, it is called confined coaxial jet. In combustors, usually the inlet flow comes as confined coaxial jets with fuel flowing as the inner jet and air flowing as the outer annular jet. The incoming coaxial jets which are normally turbulent in nature like other real flow, may again have sudden axisymmetric expansion in the combustion chamber. Due to this sudden expansion, the turbulence kinetic energy increases and the mixing rate is enhanced, which is desired. Such a flow is shown in Fig. 1. The resulting flow-field after expansion may include recirculation zones, due to which heat

and mass transfer increases several times than that for fully-developed turbulent pipe flow at the same Reynolds number.

In the development of combustion chambers for gas turbines, ramjets, and various industrial furnaces, designers usually depend on experiments. But as a supplement to them, economical design and operation can be greatly facilitated by the availability of prior predictions of the flowfield. These may be obtained by use of a mathematical model incorporating a numerical finite difference prediction procedure. A mathematical solution of the flowfield of interest should provide results more cheaply, quickly and correctly than possible by experiments on real-life systems or models.

1.2 Motivation of the Present Investigation:

The mixing of nonreacting and reacting fluids is encountered in many practical engineering applications. One example is that of two confined coaxial jets mixing in a chamber with sudden axisymmetric expansion. Mixing of confined coaxial jet with sudden axisymmetric expansion may have numerous practical engineering applications, e.g., in combustors of gas turbine engines, ramjet combustors, I.C. engines, jet engines, boilers, etc. As stated above, the sudden-expansion geometry produces mixing rates downstream of the expansion that are substantially higher than those that would be obtained at the same Reynolds number in the entrance region of a pipe. The elevated mixing rates are due to very high levels of

turbulence kinetic energy generated by shearing as the core flow issues into the larger pipe. Detail knowledge of the flow properties are required before manufacturing equipment having these types of flow. Experimental investigations are quite expensive. This thesis, therefore, suggests numerical studies to investigate the effects of the different flow parameters and to generate information which will be helpful for production, in a cost effective way.

1.3 Literature Review:

1.3.1 History of Turbulence:

With more than a century of intensive research, turbulence remains as the unsolved problem of classical physics. Although the Navier-Stokes equations govern the instantaneous turbulence fluid motion, effort in direct simulation of turbulence has been limited to low Reynolds number ($Re \leq 5000$) and to relatively simple parallel flows. As the Reynolds number of the flow increases, the range of length and time scales required for solving the instantaneous turbulent motions by direct simulation increases rapidly exceeding the storage capacity of the largest computers in the foreseeable future even for simple flows. On the other hand, most industrially important flows are quite complex and requires only knowledge of the averaged quantities. Thus, turbulence modeling remains as the economically feasible approach for simulating mean flow fields in industrial applications.

Extensive reviews of the historical and recent developments in turbulence modeling were provided by Launder and Spalding [1972], Lumley [1978, 1983], Donaldson [1972], Reynolds [1976], Bradshaw, Cebeci and Whitelaw [1981], Rodi [1982] and Zeman [1981]. In this section a brief review of the fundamental assumptions is given.

The existing turbulence models can be categorized in several ways. The most common way is to classify them according to the number of differential equations solved in addition to the mean flow equations [Reynolds 1976]. These classifications are: (i) zero-equation models, (ii) one-equation models, (iii) two-equation models and (iv) stress-transport models.

Historically, turbulence models were initiated by Boussinesq [1877], Prandtl [1925] and Taylor [1932]. Zero-equation models (classical phenomenological models) employ Boussinesq eddy viscosity concept. In the later part of the nineteenth century, Boussinesq suggested modeling turbulent mean motion as a laminar flow with a greatly increased viscosity (termed an eddy viscosity). The value of the eddy viscosity is to be determined from experiment. This approach allows the use of the same solution procedure for turbulent flows which is similar to that of laminar flows. The fundamental assumption in these early phenomenological models is that the state of motion of the mean field fluid is fully determined by the mean velocity vector \underline{v} , and the mean pressure p at a point.

Prandtl's mixing length hypothesis, which was developed in midtwenties, utilizes the eddy viscosity concept to relate the turbulent transport terms to the local gradients of mean flow quantities. Though the mixing length model has been successfully applied to a large number of thin shear layer flows [Spalding 1982], it has several serious shortcomings. One of the major drawbacks of this hypothesis is that it assumes local equilibrium conditions for turbulence. This implies that, at any point in the flow, turbulence production is balanced by the dissipation-rate, and there is no diffusion or convection. Hence the mixing length model ignores transport and history effects of turbulence altogether. The model also erroneously leads to zero values for eddy viscosity and turbulent heat and mass diffusivities whenever the mean velocity gradient is zero. Furthermore, the effects due to buoyancy, rotation or streamline curvature on turbulence can only be introduced in an entirely empirical way, and hence generally applicable expressions are hard to formulate. Moreover, for complex flows, such as separated flows, empirical specification of the mixing length becomes impossible.

Recent generations of turbulence modelings are essentially motivated by the so-called Kolmogorov-Prandtl [Kolmogorov 1968, Prandtl 1945] hypothesis,

$$\mu_T = \rho u^* l^*, \quad [1.1]$$

where μ_T is the turbulent (eddy) viscosity, u^* is a characteristic turbulent velocity scale and l^* is a characteristic turbulent

length scale. While most existing models make use of Equation [1.1], the methods for obtaining the relevant scales differ.

In one-equation models, a transport equation for a suitable turbulent velocity scale is used to account for the transport and history effects of turbulence. Usually, \sqrt{k} acts as an appropriate velocity scale, where k is the kinetic energy of turbulent motion. The transport equation for k is derived from the Navier-Stokes equations [Launder and Spalding 1972]. Based on the Kolmogorov-Prandtl hypothesis, the eddy viscosity $\nu_t = \mu_t/\rho$ is expressed as $\nu_t = C^*k^{1/2}l$. In these models, the length scale l is still specified algebraically and hence the approach can not account for convection and diffusion of l . Moreover, for complex flows with separation, streamline curvature or rotation, the empirical specification of the length scale faces a number of difficulties. Due to significant limitations of algebraic expressions for the length scale, one equation models provided only little improvement over the zero equation models.

Two equation models, employ transport equations for both turbulent velocity scale and turbulent length scale. The use of a transport equation for the length scale l , accounts for the evolution of the spatial scale of turbulent throughout the flow region. In this length scale transport equation, the dependent variable can be any combination of l and k . Various combinations of two equation models have been proposed, but the k - ϵ model as developed by Launder &

Spalding [1972, 1974] and Jones & Launder [1972, 1973] using an equation for the dissipation rate, $\epsilon = C_D k^{\frac{3}{2}} / l$, has been widely used in most industrial applications. Here C_D is a constant. One reason for popularity of the two-equation model is that it can be conveniently accommodated in the computer codes for solving the Navier-Stokes equation. It also offers considerable saving in computational time when compared to the more sophisticated stress transport models. However, it is also known that the standard $k-\epsilon$ model is unable to handle unequal turbulent normal stresses and has limitation in using isotropic eddy viscosity and diffusivity. Due to the use of isotropic eddy viscosity, the model becomes incapable of predicting the observed secondary flows in rectangular ducts. The effects of curvature, rotation and buoyancy forces have to be modeled separately. In addition the model can not account for the convection and diffusion of the shear stresses.

In the stress transport model, to account for the evolution of the individual stress components, transport equations for each component of $\overline{v_i v_j}$ have been introduced. Exact equations for the $\overline{v_i v_j}$ can be obtained directly from the Navier-Stokes equation. However, these transport equations contain unknown higher order correlations which have to be approximated by closure assumptions. In exact Reynolds stress equation, however, terms accounting for buoyancy, rotation and other effects are introduced automatically. In modeling, turbulence processes are assumed to be characterized by a single time-scale, k/ϵ , where k is the kinetic energy of

fluctuating motion. Furthermore, local isotropy for dissipation is assumed to prevail so that the dissipation is same for all three normal components. The modeled Reynolds stress transport equations along with that for energy dissipation rate ϵ , have to be solved simultaneously. Thus, considerable computational effort is needed for solving practical engineering problems. Elaborate stress transport models were also developed by Daley and Harlow [1970], Hanjalic and Launder [1972, 1976], Lumley and Khajeh-Nouri [1974], Launder, Reece and Rodi [1975] and Newman, Launder and Lumley [1981].

In the stress transport models, one has to solve a large number of differential equations for each component of turbulent stresses and fluxes, which requires extensive computational effort. To reduce the required computational work, algebraic stress models have been developed by Rodi [1976], Yoshizawa [1984, 1985], Speziale [1987], Ahmadi & Chowdhury [1991] and Chowdhury [1990].

In spite of the extensive research effort to develop more accurate turbulence models, the linear $k-\epsilon$ model of turbulence is still widely used in industries for solving practical flow problems. One main reason is that, the needed computational effort for application of stress transport models to industrial fluid engineering problems is quite extensive, since the transport equations for each component of the Reynolds stress tensor have to be solved. In addition, in order to close the exact transport equations for the Reynolds stresses, closure approximations for the

higher order turbulence correlations such as pressure-strain terms are required which are difficult to achieve. Many turbulence researchers [Speziale 1987] believe that these shortcomings outweigh the main advantage of second order closures in practical applications. The other reason for the popularity of the $k-\epsilon$ model is that it has been accommodated into many commercially available computer codes.

1.3.2 Previous Work

Turbulent flow downstream of an abrupt pipe expansion was studied numerically by Amano [1983]. In this paper, the sudden expansion flow for a single jet was simulated. Here, expansion of concentric jets were not considered. Computations employed a hybrid method of central and upwind finite differencing to solve the Navier-Stokes equations with the $k-\epsilon$ turbulence model.

Experimental and numerical study of confined coaxial turbulent jets were performed by Khodadadi and Vlachos [1989]. The turbulent mixing of a primary jet and its surrounding fluid in a pipe was studied. But, in this experiment, the sudden expansion geometry was not considered. A hybrid difference scheme that combines central and upwind differencing was used for computation.

Numerical study in the developing region of coaxial axisymmetric confined jets was also carried out by Paul [1992]. Here also, the sudden expansion of the jets was not considered.

This thesis, therefore, analyses the flow of coaxial turbulent jets with sudden axisymmetric expansion, and uses the hybrid differencing scheme and $k-\epsilon$ turbulence model in the computer code of Chowdhury [1990].

1.4 Objective of this study

The objective of this thesis is to investigate numerically some important flow characteristics, valuable for greater understanding of the behavior of the nonreacting confined coaxial jets with sudden axisymmetric expansion. A fast and reliable computer program was adopted from Chowdhury [1990], for solving the governing finite-difference equations for given boundary conditions. The velocity components, turbulence kinetic energy, dissipation rate, etc., should be calculated at different sections of the mixing chamber (combustion chamber) for different input parameters. These parameters are Reynolds number, velocity ratio of jets, expansion ratio, etc. The specific objectives of this research are:

- (i) to test the capability of the model in predicting complex recirculating flows,
- (ii) to study the effect of jet velocity ratio on the flow field,
- (iii) to observe the effect of Reynolds number on the flow properties,

- (iv) to study the effect of grid spacing, and
- (v) to analyze the effect of expansion ratio on the flow field.

1.5. Outline of the Thesis

The main purpose of this thesis is to analyze numerically, the flow of coaxial turbulent jets with sudden axisymmetric expansion. The governing equations required for this numerical analysis, along with the solution technique and boundary conditions are briefly given in Chapter 2 of this thesis.

Chapter 3 contains the results and discussion. In this chapter, the predicted results are first compared with the available experimental data to prove the capability of the program. Then the effect of changing the jet velocity ratio, grid spacing, Reynolds number and expansion ratio on the flow properties is studied.

The summary of main findings of this thesis and the suggestions for future work are presented in Chapter 4.

References and figures are given at the end of this thesis.

CHAPTER - 2

METHODOLOGY OF SOLUTION

2.1 Scope:

In this chapter, the method of the numerical simulation is briefly described. As already mentioned in the previous chapter, k- ϵ model is used to solve this axisymmetric, steady, turbulent flow. The governing equations are first summarized. The solution technique is then briefly outlined. Boundary conditions are described in short. Finally, the solution procedure along with under-relaxation principle is briefly discussed. Closing remarks are also given.

2.2 Governing Equations:

The equations which govern the flow of an incompressible fluid are:

Conservation of mass

$$\frac{\partial v_i}{\partial x_i} = 0 \quad [2.1]$$

Linear momentum

$$\rho \frac{dv_i}{dt} = - \frac{\partial p}{\partial x_i} + \mu \frac{\partial^2 v_i}{\partial x_j \partial x_j} \quad [2.2]$$

But in a state of turbulent motion the field quantities become random functions of space and time. The instantaneous motions will still satisfy Equations [2.1] and [2.2], but will become too

complex and mathematically untractable. The usual approach is to use an averaging technique and to deal with the rather smooth variation of the mean flow field. In turbulence modeling, the complex motion of a simple (Newtonian) fluid is replaced by a simple motion of a complex mean field fluid.

During turbulent motions, the flow parameters may be decomposed into mean and fluctuating parts, i.e.

$$\psi = \bar{\psi} + \psi' \quad [2.3]$$

where $\bar{\psi}$ is the mean (expected value) and ψ' is the fluctuating part of the variable Ψ .

The governing equations then have more unknowns than the number of equations and hence require closure assumptions. These are the functions of turbulence modeling. In this thesis, the k- ϵ turbulence model of Launder and Spalding [1974] is used. In this model, there are also two transport equations for kinetic energy of turbulence, k and dissipation rate, ϵ . The turbulent kinetic energy and its dissipation rate are defined as,

$$k = \frac{1}{2} \overline{v'_i v'_i}, \quad \epsilon = 2\nu \overline{\omega'_i \omega'_i} \quad [2.4]$$

where v'_i is the fluctuating velocity and ω'_i is the fluctuating vorticity of turbulence.

The resulting governing equations are all similar and hence can be put in the common form:

$$\frac{1}{r} \left[\frac{\partial}{\partial x} (\rho u r \phi) + \frac{\partial}{\partial r} (\rho v r \phi) - \frac{\partial}{\partial x} (r \Gamma_{\phi} \frac{\partial \phi}{\partial x}) - \frac{\partial}{\partial r} (r \Gamma_{\phi} \frac{\partial \phi}{\partial r}) \right] = S_{\phi} \quad [2.5]$$

Here, $\phi = 1$ gives the continuity equation, $\phi = u$ and v gives the momentum equations, and $\phi = k$ and ϵ gives the transport equation for k and ϵ . In Equation [2.5] the first two terms are the convection terms, third and fourth terms are the diffusion terms and S_{ϕ} is the source term which contains terms describing the generation (creation) and consumption (dissipation) of variable ϕ . The forms for the source term S_{ϕ} are given in Table 2.1.

Table 2.1: Source Terms for the General Equation [2.5].

Name of Equation	ϕ	Source Term, S_{ϕ}
Continuity	1	0
u-momentum	u	$-\frac{\partial p}{\partial x} + S^u$
v-momentum	v	$-\frac{\partial p}{\partial r} - \frac{2\mu v}{r^2} + S^v$
k-equation	k	$G - C_D \rho \epsilon$
ϵ -equation	ϵ	$C_1 \frac{\epsilon G}{k} - C_2 \frac{\rho \epsilon^2}{k}$

Here,

$$S^u = \frac{\partial}{\partial x} \left(\mu \frac{\partial u}{\partial x} \right) + \frac{1}{r} \frac{\partial}{\partial r} \left(r \mu \frac{\partial v}{\partial x} \right) \quad [2.6]$$

$$S^v = \frac{\partial}{\partial x} \left(\mu \frac{\partial u}{\partial r} \right) + \frac{1}{r} \frac{\partial}{\partial r} \left(r \mu \frac{\partial v}{\partial r} \right) \quad [2.7]$$

$$G = \mu \left[2 \left\{ \left(\frac{\partial u}{\partial x} \right)^2 + \left(\frac{\partial v}{\partial r} \right)^2 + \left(\frac{v}{r} \right)^2 \right\} + \left(\frac{\partial u}{\partial r} + \frac{\partial v}{\partial x} \right)^2 \right] \quad [2.8]$$

$$\mu = C_\mu \rho k^2 / \epsilon + \mu_1, \quad \Gamma_\phi = \mu / \sigma_\phi \quad [2.9]$$

According to Launder and Spalding [1974], the empirical constants are taken as,

$$C_D = 1.0, \quad C_\mu = 0.09, \quad C_1 = 1.44 \quad \text{and} \quad C_2 = 1.92 \quad [2.10]$$

These equations have to be solved for the time mean pressure and velocity components.

2.3 Solution Technique:

The differential equations presented in the previous section are in their exact form. In order to solve these equations, the exact differential equations are first to be converted into approximate finite difference equations. The finite difference equations are solved on a complex mesh illustrated in Figure 2. The intersections, the point P for example, of the solid lines mark the grid nodes where all variables except u and v velocity components are stored. The latter are stored at points which are denoted by arrows located midway between the grid intersections, and the boomerang-shaped envelope encloses a triad of points with reference

location P at (I,J). This is known as staggered grid system. Details of the special merits of this staggered grid system have been reported by Patankar [1980]. The different control volumes C, U and V which are appropriate for the P, w and s locations respectively are given in Figure 3.

The finite difference equations for each ϕ are obtained by integrating Equation [2.5] over the appropriate control volume and expressing the result in terms of neighboring grid point values. Here, a hybrid scheme which is a combination of the so-called central and upwind finite differencing have been employed to discretize the equations. The advantages of this hybrid differencing scheme over central-difference and upwind scheme have been described in detail by Patankar [1980]. The discretized equations can finally be written in the following general form:

$$a_p \phi_p = \sum_j a_j \phi_j + S_u \quad [2.11]$$

where $a_p = \sum_j a_j - S_p$

\sum_j = sum over N, S, E and W neighbors thus linking each ϕ -value at a point P with its four neighboring values.

2.4 Boundary Conditions:

The flowfield is covered with a nonuniform rectangular grid system as shown in Figure 4. Typically the boundary of the solution domain falls halfway between its immediate nearby parallel gridlines. Clearly, specification of the x and r co-ordinates of the gridlines, together with the specification of JMAX(I) for each I is sufficient to determine the flowfield of interest. The finite difference formulation requires amendment for the near boundary points through insertion of correct boundary conditions. The boundary conditions for the present flowfield are briefly described below.

Inlet Boundary:

At the inlet, the axial velocity (u-velocity) is specified. No data was available for the radial velocity, and hence the radial velocity at inlet was set to zero. The turbulence kinetic energy k and dissipation rate ϵ were also specified at the inlet through the following relations,

$$k_{in} = \lambda_1 U_{in}^2, \quad \epsilon_{in} = \frac{k_{in}^{3/2}}{\lambda_2 R} \quad [2.12]$$

where U_{in} is the mean inlet velocity, and λ_1 and λ_2 are some constants.

Outlet Boundary:

The axial velocities at the outlet are deduced from their immediate upstream values. Zero normal gradient is specified for all other variables at the outlet.

Top and Side Wall:

At the top and side solid wall, no slip boundary conditions were applied. Near wall tangential velocities are connected with their zero wall values by way of the tangential shear stress wall functions.

Symmetry Axis:

At the axis of symmetry, zero normal gradient were specified for all the variables except the radial velocity. The radial velocity was given zero value at this symmetry axis.

2.5 Solution Procedure:

The finite difference equations and boundary conditions constitute a system of strongly-coupled simultaneous algebraic equations. They form a set of nonlinear equations. The nonlinear algebraic equations are solved by an iterative technique. Values of all the variables are first guessed. Then using the tridiagonal matrix

algorithm (TDMA), the set of equations are solved. This solution is considered as improved guess and the iteration is repeated until convergence criteria is satisfied.

At each iteration it is necessary to employ some degree of under-relaxation. A weighted average of the newly calculated value and the previous value is taken at each point. Because, if the corrections are too large per iteration, the nonlinearity of the finite difference equations causes divergence. Velocity and pressure corrections per iteration become smaller as the solution proceeds towards convergence.

Final convergence is decided by way of a residual-source criterion, which measures the departure from exactness for the variable ϕ at the point. The residual sources are defined for each variable at each point by equation like,

$$R_p = a_p \phi_p - \sum_j a_j \phi_j - S_v \quad [2.13]$$

The solution is considered to be converged if the cumulative sum of the absolute residuals throughout the field for all variables is less than 0.4 percent of the inlet flow rate of the corresponding variable.

2.6 Closure:

The governing differential equations are presented in this chapter in a form which is used in the computer programme. The solution technique and boundary conditions are discussed briefly. Finally, the solution procedure is also outlined.

An available computer programme is used to simulate the present flowfield and the results are discussed in the next chapter.

CHAPTER-3

RESULTS AND DISCUSSIONS

3.1 Scope

This chapter presents the results of numerical simulation of the coaxial turbulent jet with sudden axisymmetric expansion, using a modified version of the TEACH computer code of Chowdhury [1990]. The governing equations using the $k-\epsilon$ model, presented in the previous chapter, are used for the present study. First, the problem is defined. Then, the problem is solved for a particular case for which experimental data are available, and comparison is made for verifying the validity of the programme. The effect of changing the grid size on the flow-field simulation is observed. The effect of changing the jet velocity ratio (flow ratio) is also presented. Computations were also done by changing the jet Reynolds number and the results are discussed. Finally, the effect of changing the expansion ratio is studied, and closing remarks are given.

3.2 Problem Statement

As already mentioned, the confined coaxial turbulent jet with sudden axisymmetric expansion is analyzed in this thesis. The flow geometry is shown in Figure 1. Two coaxial jets of velocity U_1 and U_2 are coming in through the inner pipe of radius $r_1 = 0.012\text{m}$ and outer annular pipe of radius $r_2 = 0.0295\text{m}$, respectively. The jets

then suddenly expand into a larger pipe of radius $R = 0.061\text{m}$, for better mixing. Uniform profiles for the mean velocity, turbulence kinetic energy and dissipation rate are assumed at the inlet. The inlet turbulence kinetic energy and dissipation rate are taken by,

$$k_{in} = 0.03 U_{in}^2 \quad , \quad e_{in} = \frac{k_{in}^{3/2}}{0.02R} \quad [3.1]$$

where U_{in} is the inlet mean velocity, i.e. U_1 or U_2 . The flowfield is solved for a nonuniform staggered grid of size 46×34 (i.e. there are 46 grids in the axial direction and 34 grids in the radial direction) with finer spacing in the regions of large spatial gradients. In order to study the effect of grid size variation, the flow-field is also solved for 46×24 grids. The results are described in the subsequent sections.

3.3 Comparison with Available Experimental Data

Flow of coaxial jets with sudden axisymmetric expansion was studied experimentally by Johnson and Bennett [1981] in a water test rig for the test configuration shown in Figure 1 and described in the previous section. Measurements for mean velocity and turbulence fluctuations were made using a laser Doppler velocimeter. The inner jet has a velocity of $U_1 = 0.52 \text{ m/s}$ and the outer annular jet velocity is $U_2 = 1.66 \text{ m/s}$. The ratio of the velocities of the inner and outer jets, $U_1/U_2 = 0.31$, and the ratio of the flow rates for the inner and outer jets, $Q_1/Q_2 = 1/16$. The average velocity of the outer annular jet is taken as the reference velocity, $U_0 = U_2 = 1.66 \text{ m/s}$.

Based on this reference velocity and $2r_2$, the flow Reynolds number is 97000. The above flow is simulated using the computer code of Chowdhury [1990], which is a modified version of the TEACH computer code. A nonuniform grid of 46 x 34 node points is used. The governing equations employing the k- ϵ model are given in Chapter 2 of this thesis. The inlet turbulence energy and dissipation rate are calculated by Equation [3.1]. The predictions of the numerical model are compared with the experimental results of Johnson and Bennett [1981] in Figures 5 and 6. In these figures, the solid lines correspond to the numerical predictions of the present model and the boxes correspond to the experimental data.

The mean axial velocity distribution across the flow as predicted by the present numerical model at different axial locations are shown in Figure 5. The experimental data of Johnson and Bennett [1981] are also shown in this figure for comparison. It is observed that the model predictions for the mean velocity are in good agreement with the data. The reattachment length was found to be $x_R = 27.2$ cm, or $x_R/H = 8.64$, where H is the expansion step height of 3.15 cm.

Figure 6 compares the predicted turbulence kinetic energy distribution across the flow with the experimental data of Johnson and Bennett (1981). It is observed that the present model predictions are in good agreement with the data.

The dissipation rate profiles as predicted by the present model at different axial locations are shown in Figure 7. The trends of variations of the dissipation rate profiles appear to be quite reasonable; however, no experimental data for dissipation rate for the particular flow were reported in the literature for comparison.

Figure 8 shows the distributions of the dimensionless mean axial velocity as predicted by the present model for different axial locations. The mean velocities are nondimensionalized with the aid of the reference velocity which is the average velocity of the annular jet. In these velocity profiles we find the presence of the recirculation zone caused by the sudden expansion, which ultimately helps in mixing.

Distributions of the dimensionless turbulence kinetic energy across the flow at different axial locations are shown in Figure 9. Here also, the turbulence kinetic energy is nondimensionalized with the aid of the reference velocity, $U_0 = U_2$. The high level of turbulence kinetic energy generated due to high rate of shearing of the flow helps in the mixing process.

Based on the above presented results and comparison with experimental data, it may be concluded that the present numerical model has the capability of predicting turbulent flows with reasonable accuracy. Hence, this model will be used for further simulations in the following sections.

3.4 Effect of Grid Size

In the previous section, for Figures 5-9, the particular flow was simulated based on a grid of 46 x 34 node points. However, the effect of grid size variation on the simulated results, needs to be checked. So, the above flow was also simulated using 46 x 24 node points and the results presented.

Figure 10 shows the distribution of the mean axial velocity across the flow, for the conditions of the previous section, and for both the grid sizes of 46 x 34 and 46 x 24. The plots for 46 x 34 node points shown by solid lines are almost similar to those for 46 x 24 node points shown by dotted lines, except for a few places where the larger grid size has better matching with the experimental data. The distribution of turbulence kinetic energy and dissipation rate across the flow were also plotted for both the grid size and found to almost superimpose, and so were not presented here.

Hence, the use of 46 x 34 grid size seems to be reasonable, and so will be used for the present computation.

3.5 Effect of Velocity Ratio U_1/U_2

In section 3.3 of this thesis, computations for the coaxial turbulent jets with sudden expansion were performed for jet velocity ratio $U_1/U_2 = 0.31$, which corresponds to flow rate ratio

$Q_1:Q_2 = 1:16$, where Q_1 and Q_2 are the flow rates of the inner and outer annular jets, respectively. In practice, flow rate ratio different from the above might be required for the design of combustion chambers. Hence, the effect of changing this flow rate ratio or consequently jet velocity ratio on the flowfield will be studied in this section.

First, the coaxial turbulent jet flow for the geometry of Figure 1 is again simulated for $U_2 = 1.66$ m/s but $U_1 = 0.33$ m/s, which corresponds to $U_1/U_2 = 0.2$ or $Q_1:Q_2 = 1:25$, and the results are presented in Figs. 11-15.

Figure 11 shows the distribution of the mean axial velocity across the flow at different axial locations. Here x means the axial distance from the sudden expansion geometry. Here also, we observe the presence of the recirculation zone due to the sudden expansion. The reattachment length was found to be, $x_R = 27.8$ cm or $x_R/H = 8.83$, where H is the step height. The recirculation length has slightly increased compared to that for $U_1/U_2 = 0.31$.

The predicted variation of the turbulent kinetic energy across the flow at different sections are shown in Figure 12. Here, we find that the turbulent kinetic energy level is high at points where shearing of the flow is maximum. This high level of turbulent energy helps in the mixing process. The turbulent energy is generated more in the initial region after expansion and the profile flattens as goes away from the expansion section.

The predicted dissipation rate profiles at different locations are also shown in Figure 13. The peak of the dissipation rate profile is quite high near the expansion section, and decreases rapidly as we move along the axial direction.

Figure 14 shows the distribution of the dimensionless mean axial velocity across the flow at different axial locations. The mean velocity is nondimensionalized by the reference velocity $U_0 = U_2 = 1.66$ m/s. Here we observe that the centerline velocity recovers faster than that for $U_1/U_2 = 0.31$.

The predicted variation of the nondimensional turbulence kinetic energy is shown in Figure 15. In this figure, the solid line stands for $x = 5.1$ cm, and the dotted lines with increasing dot lengths represent the subsequent sections of 10.2 cm, 15.2 cm, 20.3 cm, 25.4 cm and 30.5 cm. The corresponding values of x/R for these sections are 0.84, 1.67, 2.49, 3.33, 4.16 and 5.0 respectively.

Next, the coaxial turbulent jet flow for the geometry for Figure 1 is simulated for $U_2 = 1.66$ m/s but $U_1 = 0.83$ m/s, which corresponds to $U_1/U_2 = 0.5$ or $Q_1:Q_2 = 1:10$, and the results are presented in Figures 16-20.

The mean axial velocity distribution across the flow as predicted by the present model at different sections are shown in Figure 16. The reattachment length for the recirculation zone near the wall,

was found to be $x_R = 26.7$ cm or $x_R/H = 8.48$, where H is the step height. The reattachment length is slightly less than that for $U_1/U_2 = 0.31$.

Figure 17 shows the variation of the turbulent kinetic energy across the flow at different axial locations. The turbulent kinetic energy is generated more at the regions of the larger shearing of flow.

The dissipation rate profiles as predicted by the present model at different axial locations are shown in Figure 18. The peak of the dissipation rate profile in the first section is quite large, whereas in the last section it has decreased a lot.

The predicted variation of the dimensionless mean axial velocity across the flow at different locations have been plotted in Figure 19. From this figure we can see how the velocity profile changes from section to section and the changes in the recirculation zone.

Figure 20 shows the dimensionless turbulent kinetic energy profiles for different sections. The reference velocity $U_0 = U_2$ has been used for nondimensionalization.

Now, the distribution of the dimensionless mean axial velocity across the flow at different axial positions for $U_1/U_2 = 0.2, 0.31$ and 0.5 are shown in Figure 21, for comparison. Nondimensionalization has been done with the aid of the reference

velocity $U_0 = U_2 = 1.66$ m/s. From the figure we find that the nondimensional curves are very similar except near the centerline. It can be seen that, the mean velocity for $U_1/U_2 = 0.2$, near the centerline, recovers much faster unlike that for $U_1/U_2 = 0.5$. At sections away from the expansion, the curves almost superimpose. From this figure, the mean velocity for different flow ratios of the two jets, can be predicted by interpolation.

Figure 22 compares the distribution of the dimensionless turbulent kinetic energy across the flow for $U_1/U_2 = 0.2, 0.31$ and 0.5 . Here we observe that the nondimensional turbulent kinetic energy profiles are very similar except near the centerline for the initial sections.

The predicted nondimensional centerline mean velocities are plotted in Figure 23, for $U_1/U_2 = 0.2, 0.31$ and 0.5 . From the figure we find that, in the initial region, the centerline velocity for $U_1/U_2 = 0.2$ drops rapidly after sudden expansion and then recovers very fast. The centerline velocity for $U_1/U_2 = 0.31$ drops slowly and again recovers, unlike that for $U_1/U_2 = 0.5$. At a certain distance away from the expansion section, the centerline velocity for all the three cases decreases at the same rate.

From the above figures we may conclude that, though there are certain changes in the flow field due to the change of jet velocity or flow ratio, but the properties can be predicted from the dimensionless figures like Figures 21 and 22, by interpolation.

3.6 Effect of Reynolds Number

The flow of the coaxial turbulent jet with sudden axisymmetric expansion was studied in section 3.3 for $U_1 = 0.52$ m/s and $U_2 = 1.66$ m/s, corresponding to which the velocity ratio $U_1/U_2 = 0.31$ and the Reynolds number $Re = 97000$, based on the outer jet velocity U_2 and diameter $2r_2$. The effect of changing the Reynolds number will be observed in this section.

The coaxial turbulent jet flow of section 3.3 is again simulated for $U_1 = 1.04$ m/s and $U_2 = 3.32$ m/s, while keeping other parameters constant. The Reynolds number now becomes, $Re = 194000$ i.e. doubled as before, while U_1/U_2 and $Q_1:Q_2$ still remain the same as 0.31 and 1:16 respectively. The simulated results are shown in Figures 24-27. In these figures, the solid line corresponds to $Re = 97000$, and the dotted line corresponds to $Re = 194000$.

Figure 24 compares the distribution of the dimensionless mean axial velocity across the flow for the two Reynolds number, at different axial locations. In this figure, the mean velocities have been nondimensionalized with the aid of the reference velocity U_o . For $Re = 97000$, $U_o = U_2 = 1.66$ m/s, while for $Re = 194000$, $U_o = U_2 = 3.32$ m/s. The nondimensional profiles for the mean velocity for both the Reynolds number are almost the same. The mean axial velocity distributions for the above Reynolds number have also been plotted in Figure 25, but without nondimensionalizing. In Figure 25, we

find that the curves for different Reynolds numbers are quite different. Hence, if the mean velocity profiles are plotted in the above nondimensional form, they can be used for predicting the flow at different Reynolds number.

The distribution of the nondimensional turbulent kinetic energy across the flow at different sections for $Re = 97000$ and 194000 have been plotted in Figure 26. Here, both the nondimensional figures coincide. The reference velocity $U_0 = U_2$ has been used for nondimensionalization, where the value of U_2 is different for each Re . The predicted dimensional turbulent kinetic energy distributions for the above Reynolds number are also shown in Figure 27. From this figure we observe that the dimensional profiles are quite different.

From the above study, it may be concluded that, if the variables are nondimensionalized with the aid of the reference velocity, then the figures can be used to predict the properties for different Reynolds number.

3.7 Effect of Expansion Ratio

In this thesis, the flow of the coaxial turbulent jet with sudden axisymmetric expansion is being studied. The sudden-expansion geometry produces mixing rates downstream of the expansion that are substantially higher than that without it. Therefore, the effect of changing this expansion ratio on the flow field needs to be

observed. Expansion ratio may be defined in terms of the change of radius or flow-area. The jet flow of section 3.3 is again studied in this section by increasing the radius of the larger pipe, R by 10%, while keeping other parameters constant. The results are presented in Figures 28 and 29. In these figures, the solid line represents the flow of section 3.3, where $R/r_2 = 2.07$, and the dotted line represents the flow due to the increased R , corresponding to which $R/r_2 = 2.27$.

The distribution of the predicted dimensionless mean axial velocity across the flow has been shown in Figure 28, for both expansion ratios $R/r_2 = 2.07$ and 2.27 , for comparison. In this figure, the mean velocity has been nondimensionalized with the reference velocity $U_0 = U_2$, and the radial distance has been nondimensionalized with the radius of the larger pipe R , which is different for the two cases. The peak of the mean velocities are shifted towards the centerline for larger R . Also, the length of the recirculation zone has increased for larger R . In section 3.3, the recirculation length was, $x_R = 27.2$ cm and $x_R/H = 8.64$, where H is the expansion step height of 3.15 cm. Here, due to increase of R by 10%, the recirculation length has become, $x_R = 32.5$ cm, but the expansion step height has also increased to 3.76 cm. So, for this increased R , nondimensional recirculation length becomes $x_R/H = 8.64$, which is the same as that of section 3.3.

Figure 29 compares the nondimensional turbulent kinetic energy distributions for both the expansion ratios. Here also we observe that the peaks are shifted towards the centerline.

3.8 Closure

The present computer code is used to simulate the mean flow of the coaxial turbulent jets with sudden axisymmetric expansion. The predicted results are compared with the available experimental data and found to have reasonably good matching. The flow is studied by changing the jet velocity ratio or flow ratio, and useful nondimensional results are presented. The effect of changing the grid size and flow Reynolds number is also studied. It is shown that 46 x 34 grid size is stable, and properly nondimensionalized plots can be used for different Reynolds number. Finally, the expansion ratio is changed and simulated results compared.

CHAPTER 4

CONCLUSION

In this chapter, the main findings of the present computational study are presented, along with suggestions for developments in the future.

4.1 Summary of Main Findings

Based on the presented results the following conclusions may be drawn:

- i. The present computational model is capable of predicting complex flows like coaxial turbulent jet expansion, with reasonable accuracy.
- ii. Due to the change in jet velocity ratio, the mean velocity and turbulence kinetic energy profiles have some variation near the centerline. The mean velocity profiles for different jet velocity ratio can be interpreted from the presented results.
- iii. With the increase of jet velocity ratio U_1/U_2 from 0.2 to 0.5, the recirculation length x_r/H slightly decreases from 8.83 to 8.48.

- iv. The centerline velocity for $U_1/U_2 = 0.2$, decreases sharply after expansion and again increases rapidly in the initial region, unlike that for $U_1/U_2 = 0.5$.
- v. The grid size of 46 x 34 node points used in the present computation for simulating the coaxial turbulent jet expansion, is sufficient. Further increase of node points will only increase the computational time and cost, without appreciable improvement of flow predictions.
- vi. The change of Reynolds number, changes the mean velocity, turbulent energy, etc. But if the results are plotted in proper nondimensional form, the profiles coincide.
- vii. The increase of expansion ratio, increases the recirculation length, but remains as a constant multiple of the expansion step height.

4.2 Suggestions for Future Work

The following works can be done in future:

- i. Swirl velocity can be added to the jets to study the effect of swirl, as used in swirl combustors.

- ii. Higher order schemes can be used to have better accuracy of prediction.
- iii. More sophisticated turbulence model can be employed.
- iv. Transport equation for temperature can be added.

REFERENCES

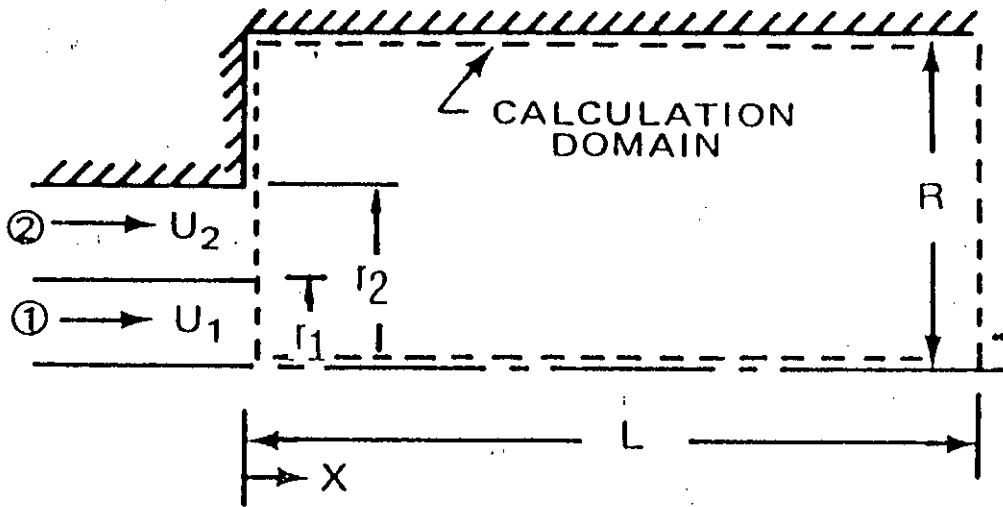
1. Ahmadi, G. and Chowdhury, S. J., "A Rate-Dependent Algebraic Stress Model for Turbulence," J. Appl. Math. Modelng, 15, 516-524 [1991].
2. Amano, R.S., "A Study of Turbulent Flow Downstream of an Abrupt Pipe Expansion," J. AIAA, 21, 1400-1405 [1983].
3. Boussinesq, J., "Theory del' eroulement tourbillant," Mem. Pre par. div. Sav. XXI, Paris [1877].
4. Bradshaw, P., Cebeci, T. and Whitelaw, J. H., "Engineering Calculation Methods for Turbulent Flow," Academic Press, New York [1981].
5. Chowdhury, S.J., "Thermodynamically Consistent Rate-Dependent Models for Turbulence," Ph.D. Thesis, Clarkson Universty, New York [1990].
6. Daley, R. J. and Harlow, F. H., "Transport Equation in Turbulence," Phys. Fluids 13, 2634 [1970]
7. Donaldson, C., "Calculation of Turbulent Shear Flows for Atmospheric and Vortex Motion," AIAA J. 10, pp. 4-12 [1972].

8. Hanjalic, K. and Launder, B. E., "A Reynolds Stress Model of Turbulence and its Application to Thin Shear Layer," J. Fluid Mech. 52, 609 [1972].
9. Hanjalic, K. and Launder, B. E., "Contribution Toward a Reynolds-Stress Closure for Low-Reynolds-Number Turbulence," J. Fluid Mech. 74, 593-610 [1976].
10. Jones, W. P. and Launder, B. E., "The Prediction of Laminarization with a Two-equation Model of Turbulence," Int. J. Heat Mass Transfer 15, 301-314 [1972].
11. Jones, W. P. and Launder, B. E., "The Calculation of Low-Reynolds Number Phenomena with a Two-equation Model of Turbulence," Int. J. Heat Mass Transfer 16, 1119-1130 [1973].
12. Khodadadi, J.M. and Vlachos, N.S., "Experimental and Numerical Study of Confined Coaxial Turbulent Jets," J. AIAA, 27, 532-541 [1989].
13. Kolmogorov, A. N., Izv. Akad. Nauk. SSR Seria Fizicheskaya V., No. 1-2, 56 [1942]. English Translation Mech. Engng. Dept. Imperial College, London, England, Report ON16 [1968].
14. Launder, B.E. and Spalding, D.B., "Mathematical Models of Turbulence," Academic Press, New York [1972].

15. Launder, B. E. and Spalding, D. B., "Turbulence Models and their applications to the prediction of internal flows," Heat fluid Flow, 2, 43-54 [1972].
16. Launder, B. E. and Spalding, D. B., Computer Meth Appl. Engng. 3, 269, [1974].
17. Launder, B. E., Reece, G. J. and Rodi W., "Progress in the Development of a Reynolds Stress Turbulence Closure," J. Fluid Mech. 68, 537 [1975].
18. Lumley J. L., "Toward a Turbulence Constitutive Relation," J. Fluid Mech. 41, pp. 413-434 [1970].
19. Lumley, J. L. and Khajeh-Nouri, B., "Computation of Turbulent Transport," Advances in Geophysics A18, 169-192 [1974].
20. Lumley, J. L., "Advances in Applied Mechanics," Vol. 18, Academic Press, New York [1978], p. 123.
21. Lumley, J. L., "Turbulence Modeling," J. Appl. Mech., Trans. ASME 50, pp. 1097-1103 [1983].
22. Newman, G. R., Launder, B. E. and Lumley, J. L., J. Fluid Mech. 111, 217 [1981].

23. Paul, R.N., "A Numerical Study in the Developing Region of Coaxial Axisymmetric Confined Jet," M. Sc. Thesis, Mechanical Engineering Department, BUET [1992].
24. Prandtl, L., ZAMM, 5, 136 [1925].
25. Prandtl, L., Nachrichten Akademie der Wissenschaften, Gottingen, Math. Phys. Klasse, 6, [1945].
26. Reynolds, W. C., "Annual Review of Fluid Mechanics," Vol. 8, ed. M. VanDyke, Wehausen, V. and Lumley, J. L.) Palo Alto, CA [1976], p. 183.
27. Rodi, W., "A new algebraic for calculating the Reynolds stresses," ZAMM, 56, T219-T221 [1976].
28. Rodi, W., "Examples of Turbulence Models for Incompressible Flows," AIAA J. 20. pp. 872-889 [1982].
29. Spalding, D. B., Turbulence Models, a Lecture Course, Imperial College of Science and Technology [1982].
30. Speziale, C. G., J. Fluid Mech. 178, 459 [1987].
31. Taylor, G. I., Proc. Roy. Soc. London, A135, 685 [1932].

32. Tennekes, H. and Lumley, J. L., A First Course in Turbulence, MIT Press, Cambridge [1972].
33. Yoshizawa, A., "Statistical Analysis of the Derivation of the Reynolds Stress from its Eddy Viscosity Representation," Phys. Fluids 27, 1377-1387 [1984].
34. Yoshizawa, A., "A Statistically Derived System of Equations for Turbulent Shear Flows," Phys. Fluids 28, 59-63 [1985].
35. Zeman, O., "Annual Review of Fluid Mechanics," Vol. 13, ed. VanDyke, M. Wehausen V. and Lumley J. L.) Palo Alto, CA [1981], p. 253.



$$r_1 = 0.012 \text{ m}$$

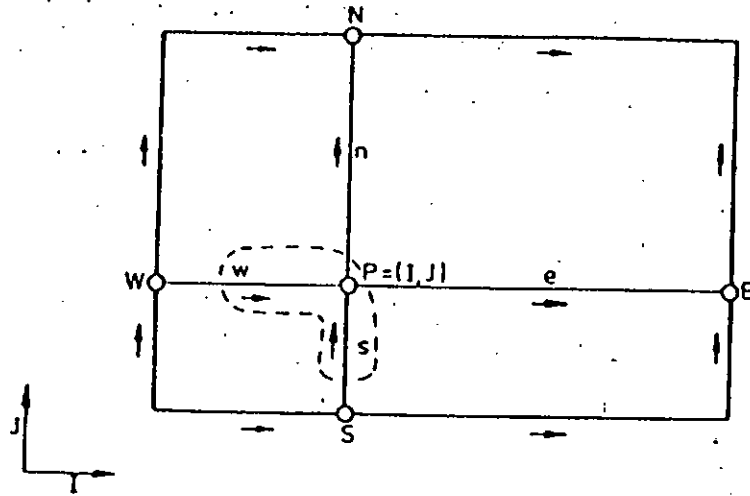
$$r_2 = 0.0295 \text{ m}$$

$$R = 0.061 \text{ m}$$

$$U_1 = 0.52 \text{ m/s}$$

$$U_2 = 1.66 \text{ m/s}$$

FIG.1 Geometry of Confined Coaxial Jet Expansion Setup.



THREE GRIDS : FOR ρ, k ETC. - AT POSITION MARKED (O)
 FOR U VELOCITY - AT POSITION MARKED (—)
 FOR V VELOCITY - AT POSITION MARKED (|)

FIG. 2 Staggered grid.

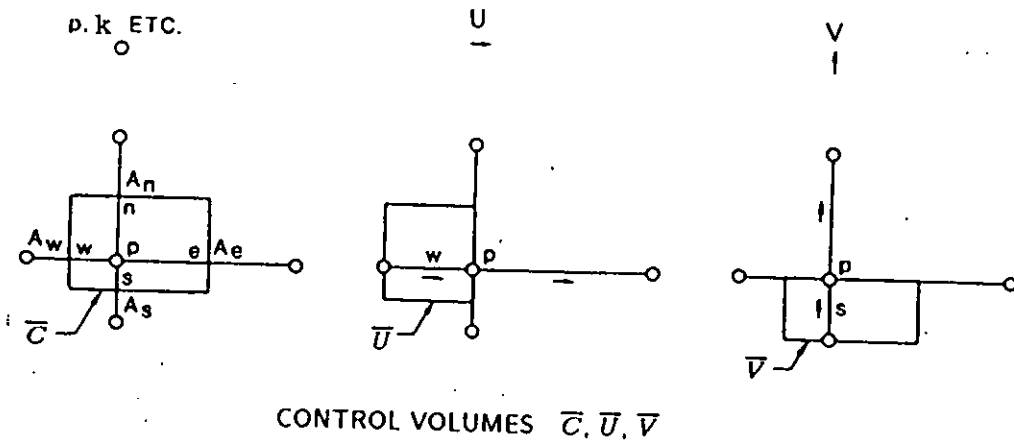


FIG. 3 Three control volumes associated with points of the three grids.

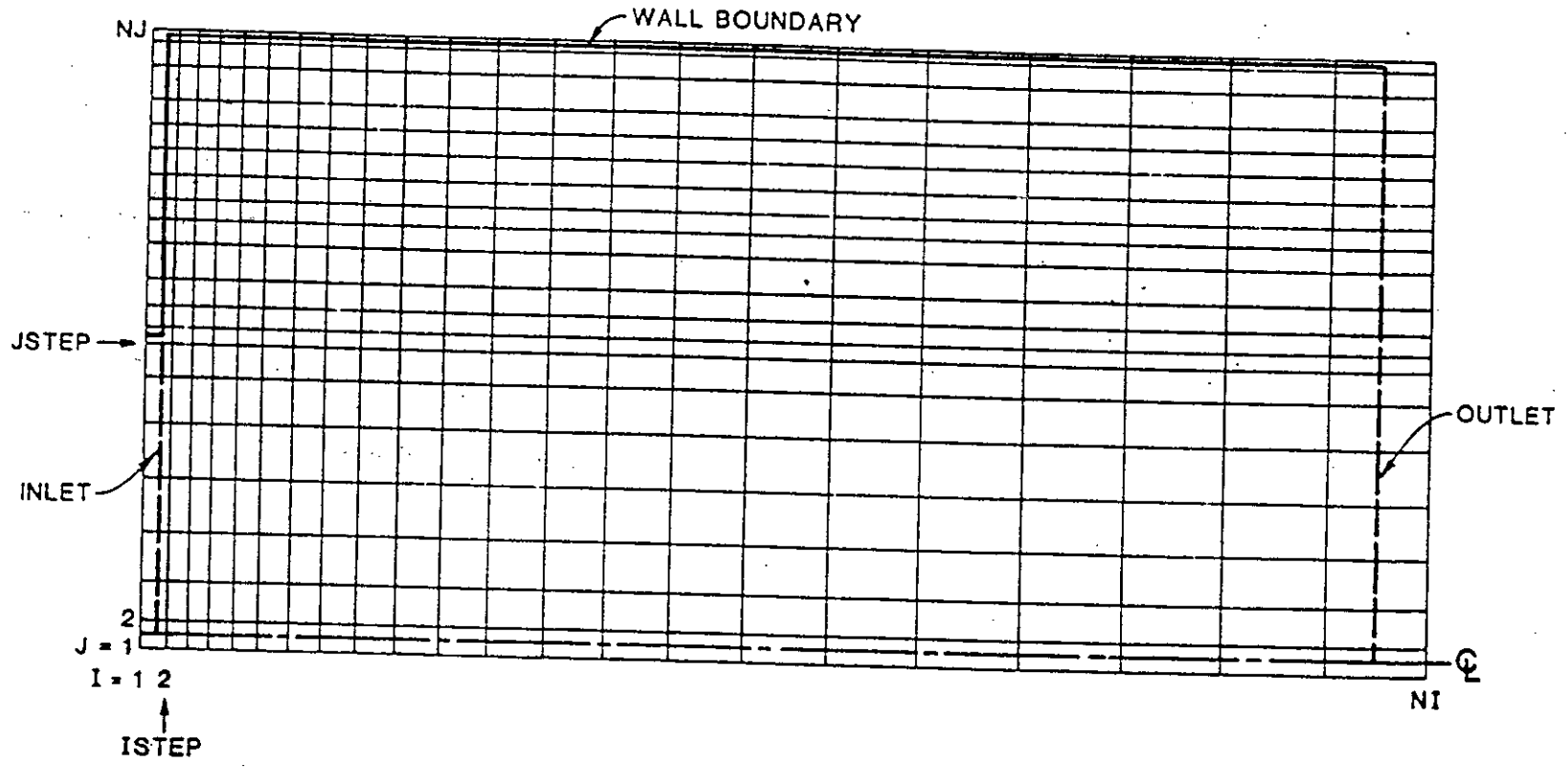


FIG. 4 Nonuniform rectangular grid system.

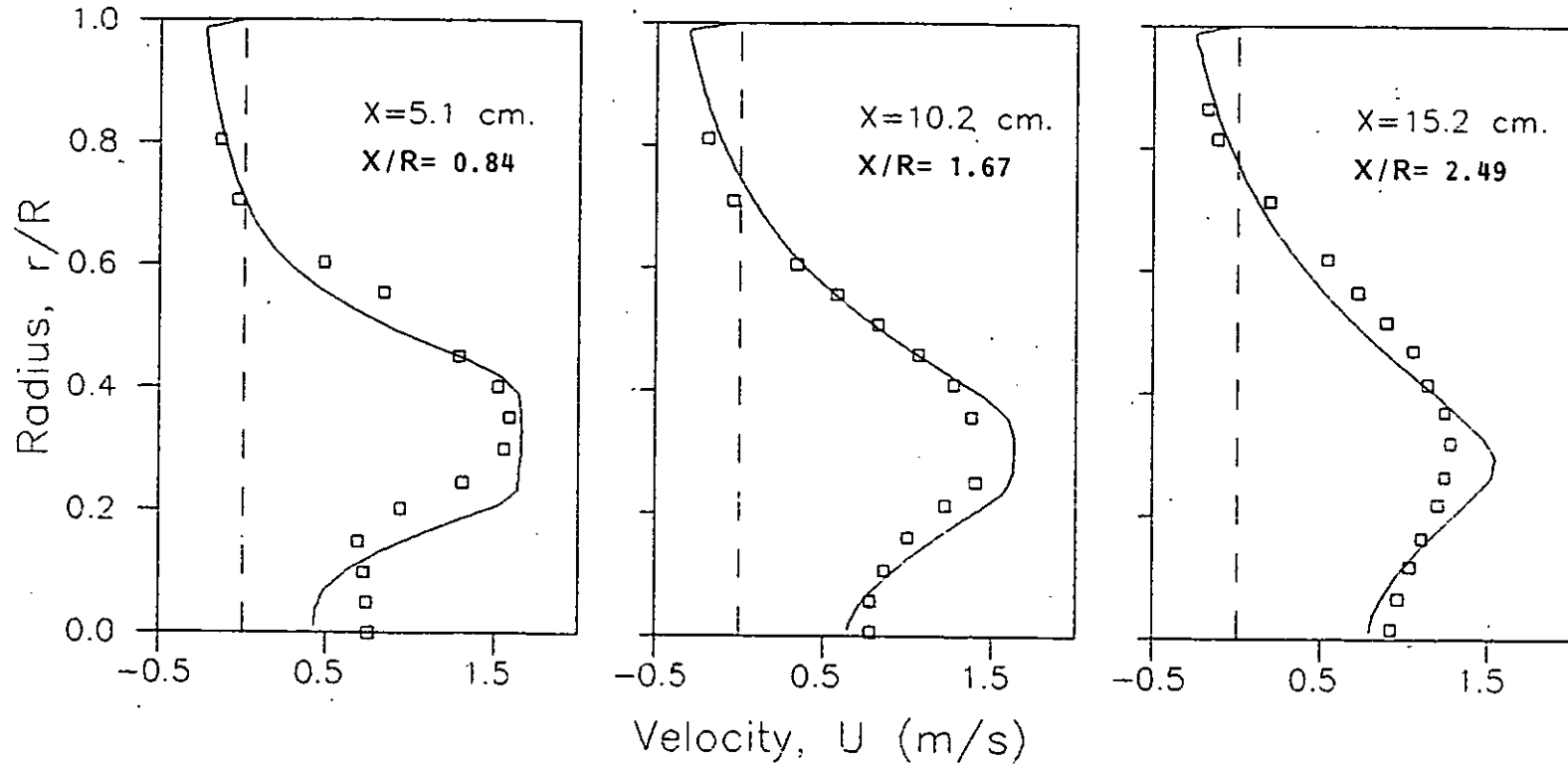


FIG.5. Comparison of mean axial velocity profiles: \square , experimental data of Johnson and Bennett; —, present numerical prediction.

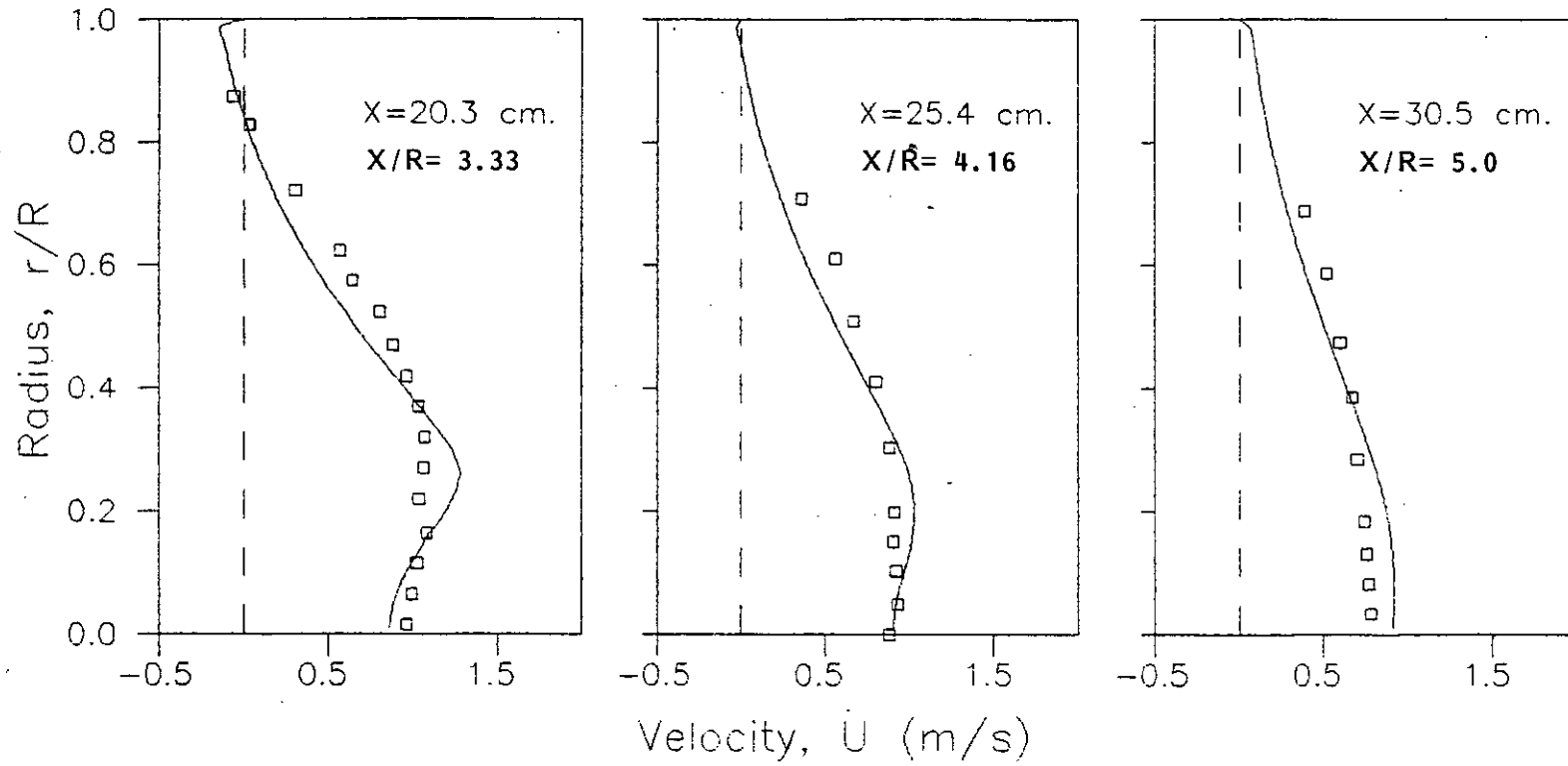


FIG.5.(Contd.) Comparison of mean axial velocity profiles.

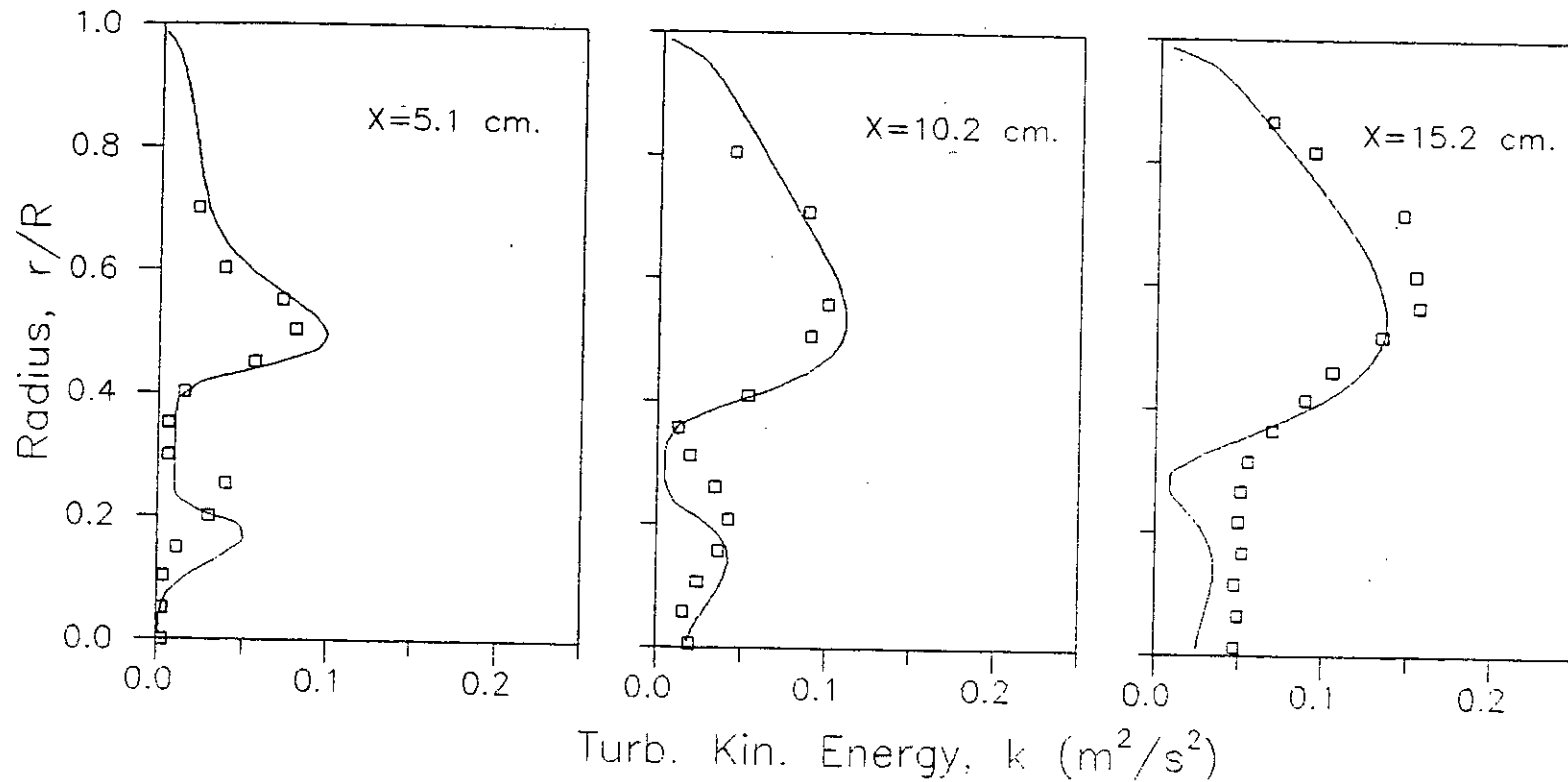


FIG.6. Comparison of turbulence kinetic energy profiles: \square , experimental data of Johnson and Bennett; —, present numerical prediction.

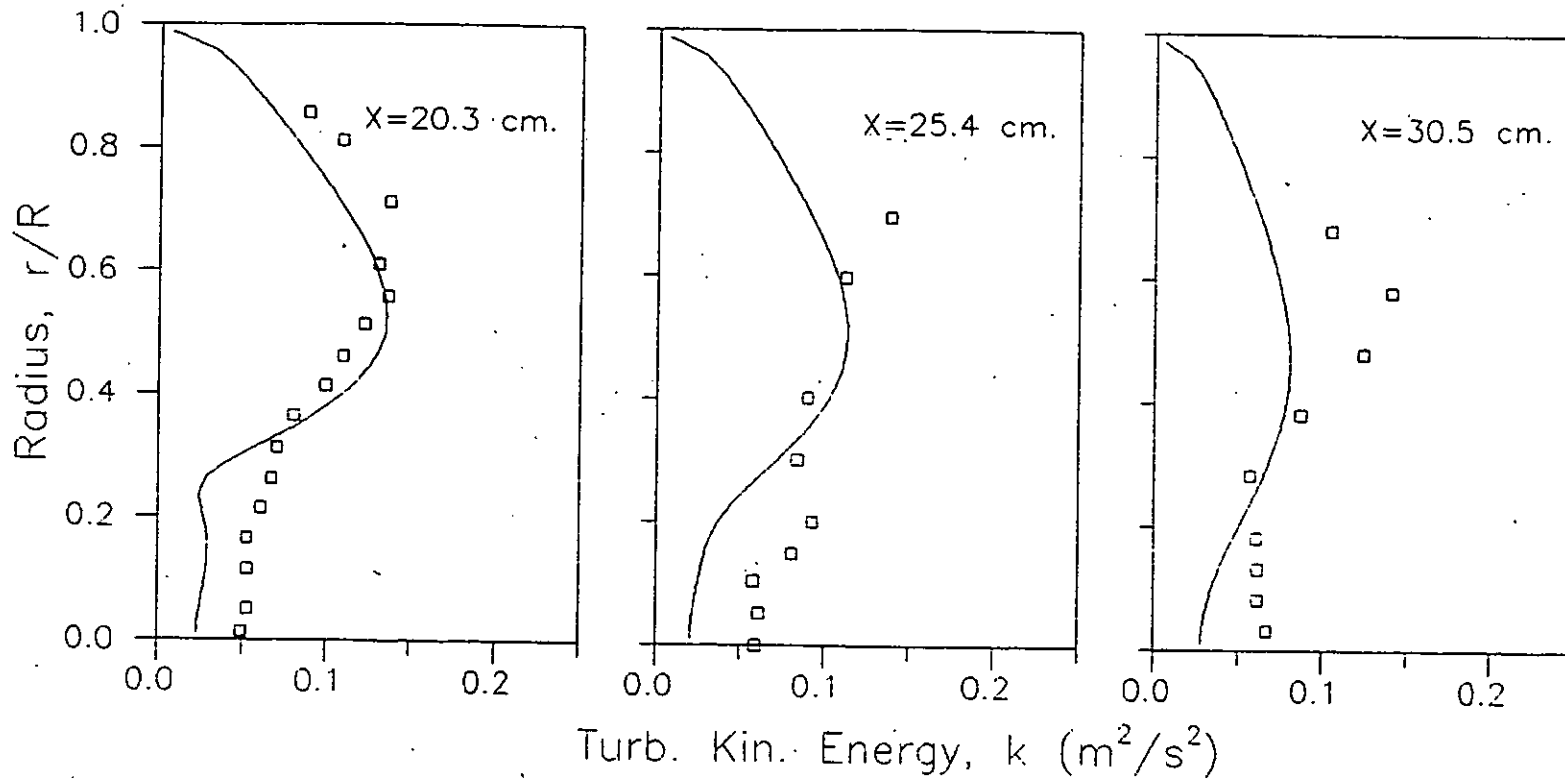


FIG.6. (Contd.) Comparison of turbulent kinetic energy profiles.

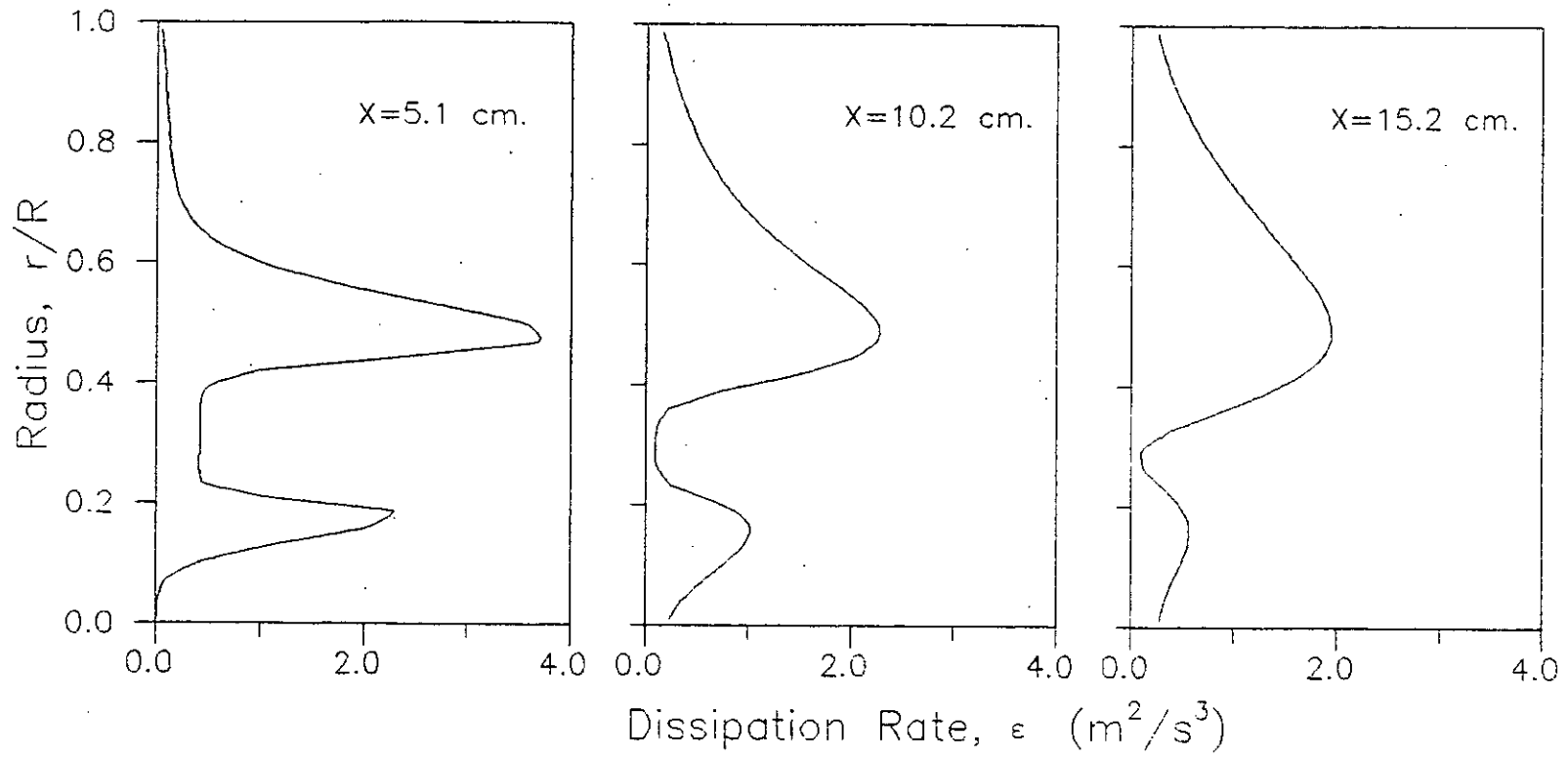


FIG.7. Dissipation rate profiles at different axial locations.

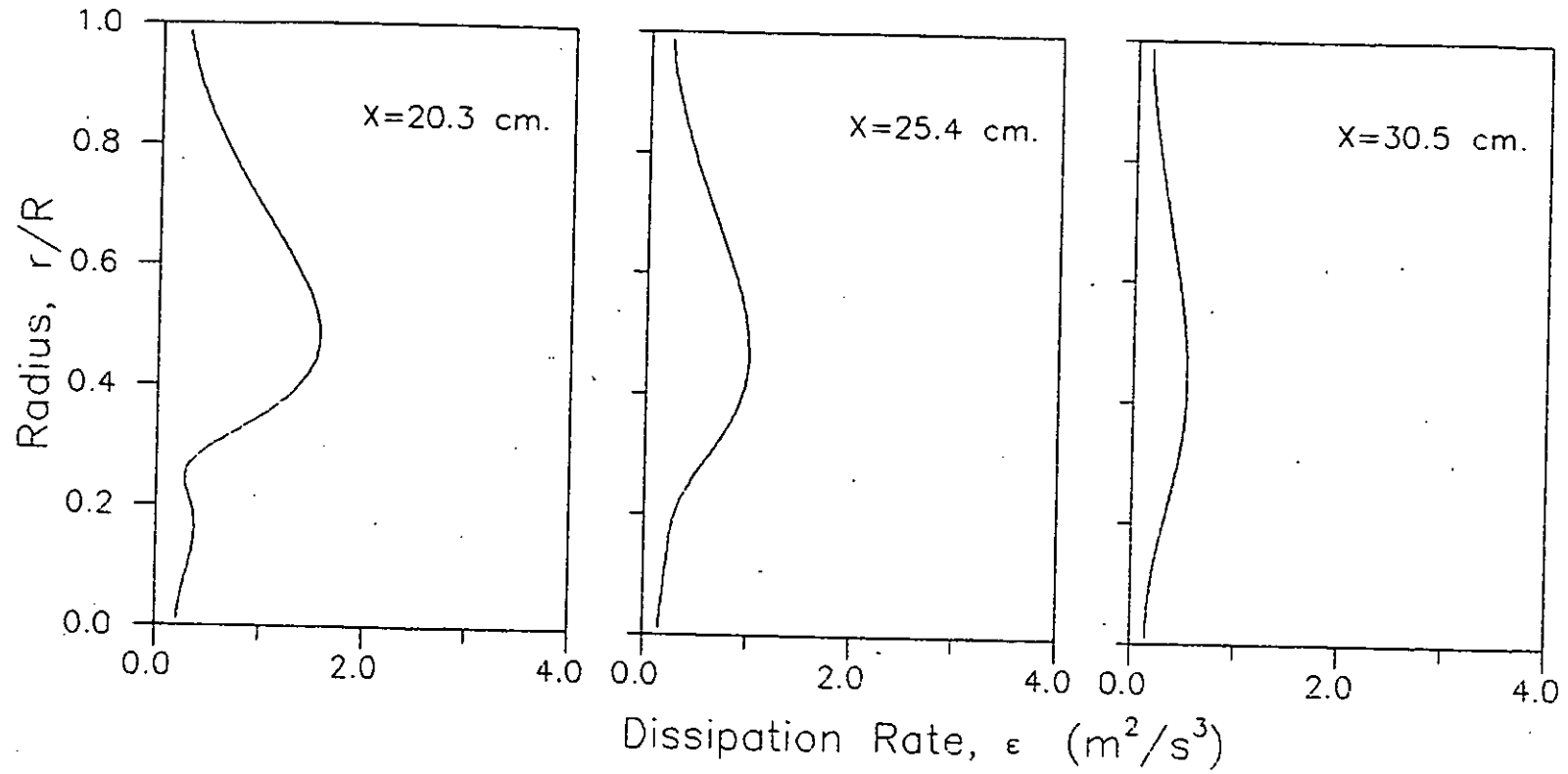


FIG.7. (Contd.) Dissipation rate profiles at different axial locations.

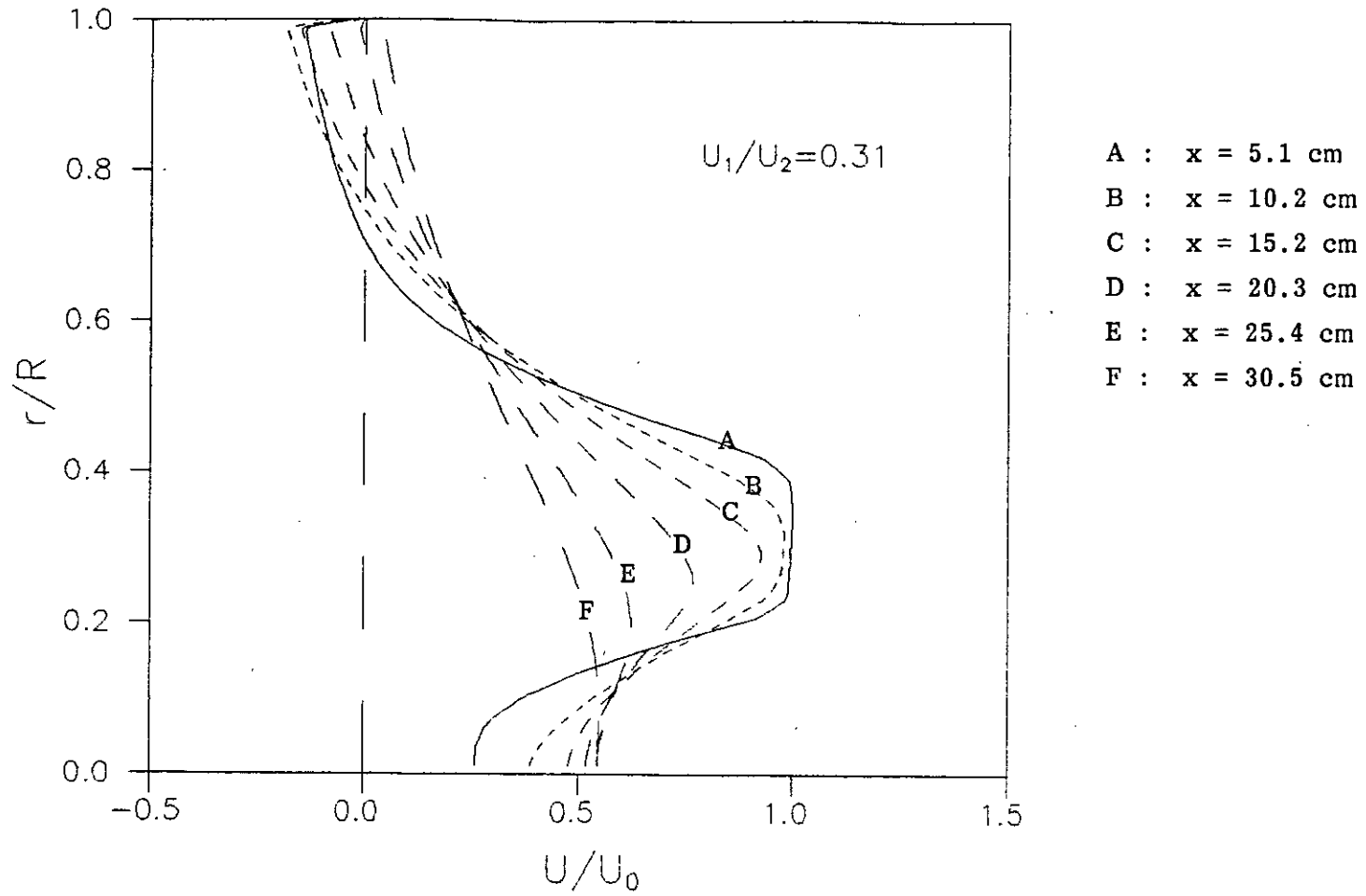


FIG.8. Dimensionless mean axial velocity profiles for different axial locations.

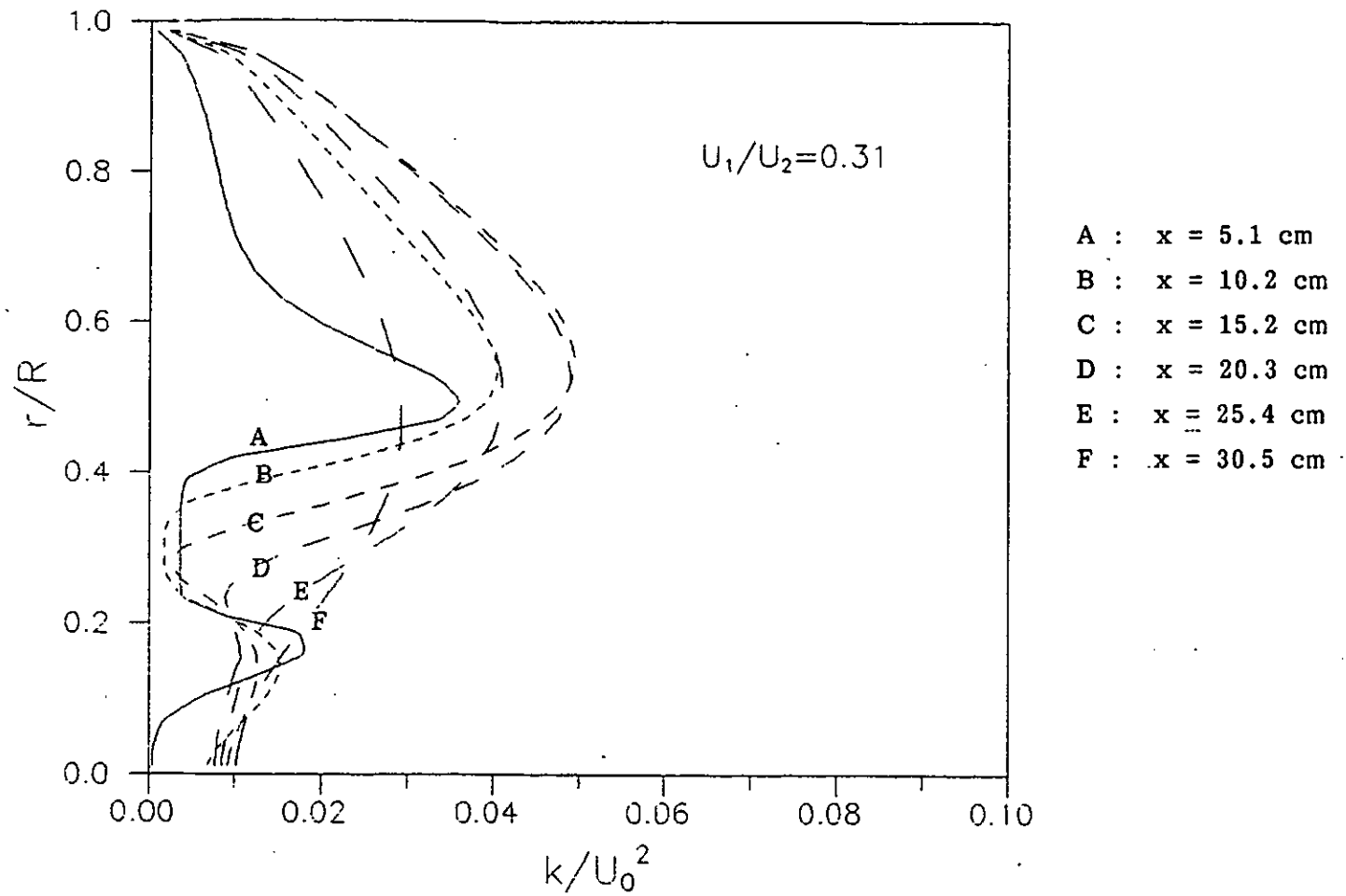


FIG.9. Dimensionless turbulent kinetic energy profiles for different axial locations.

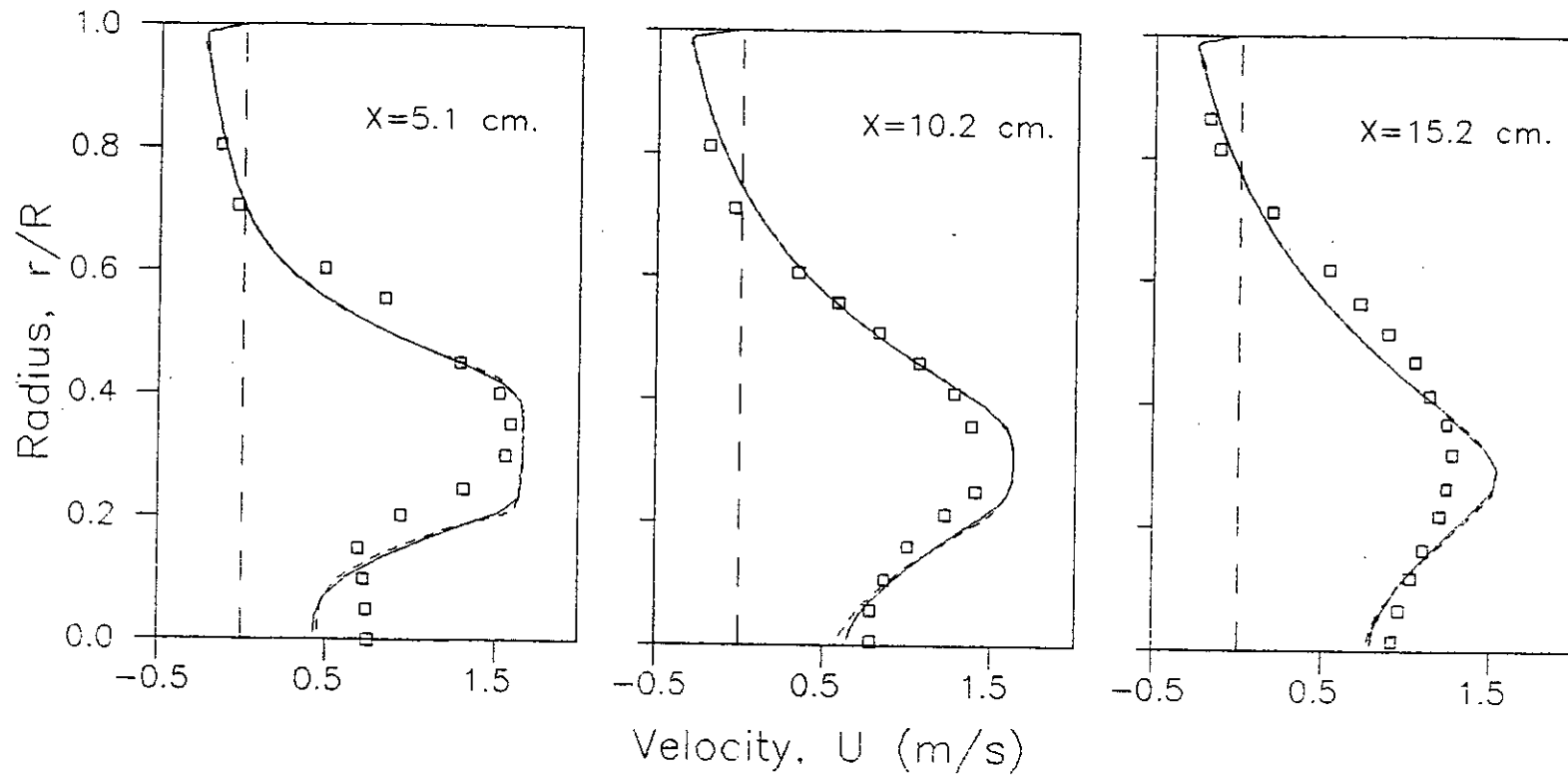


FIG.10. Comparison of mean axial velocity profiles: —, 46×34 grid; - - -, 46×24 grid.

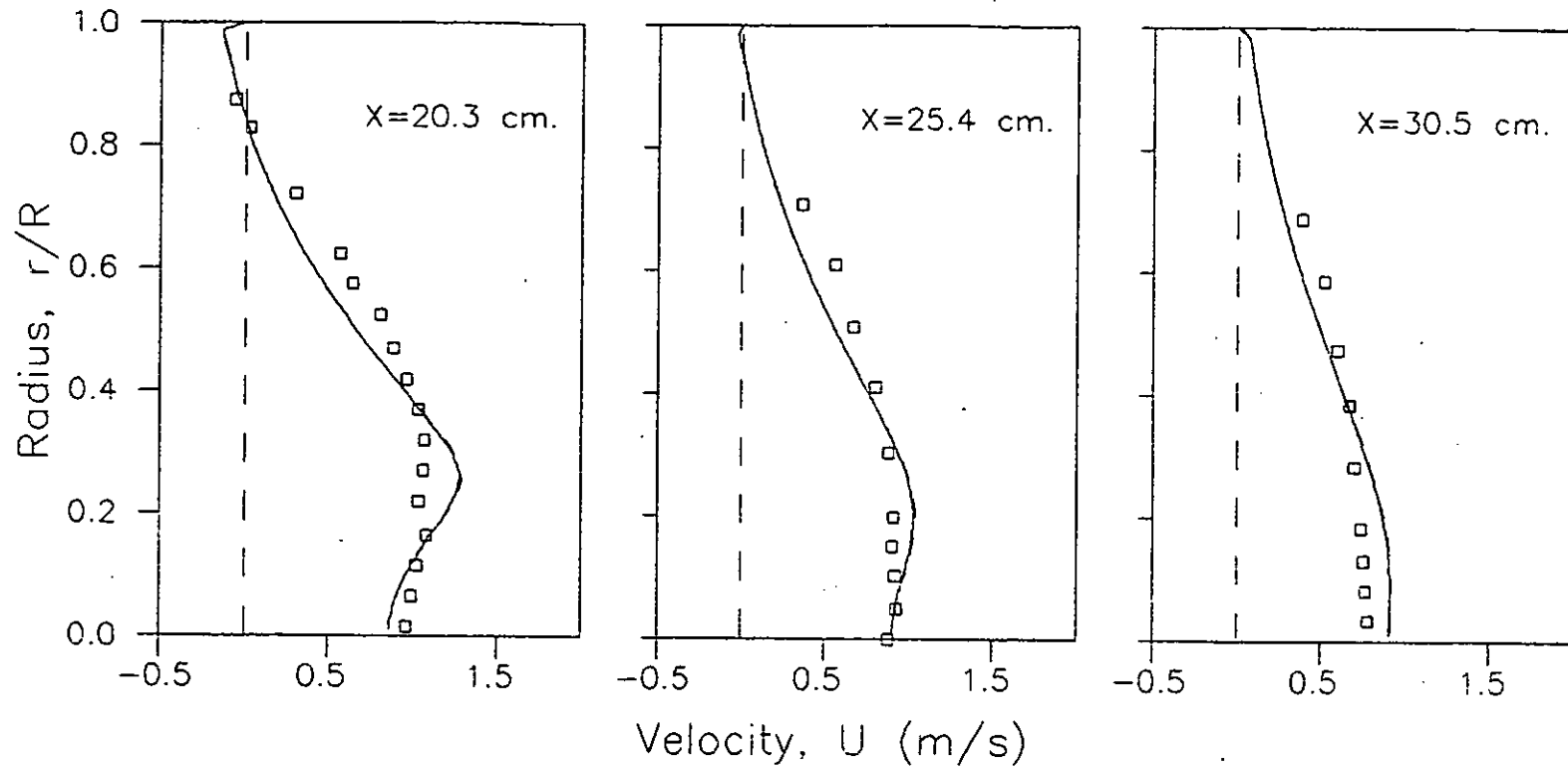


FIG.10.(Contd.) Comparison of mean axial velocity profiles.

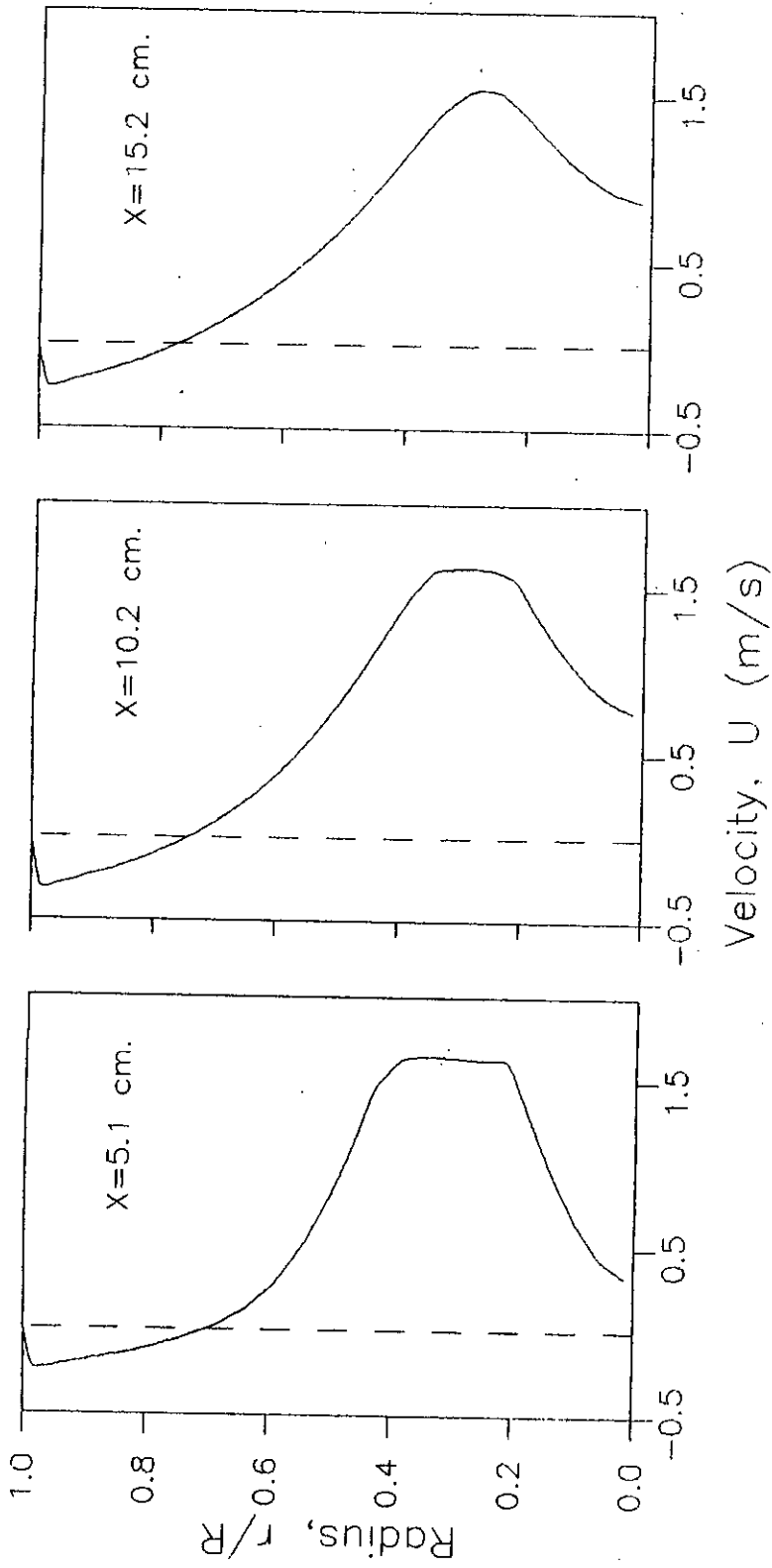


FIG.11. Mean axial velocity profiles for $U_1/U_2 = 0.2$.

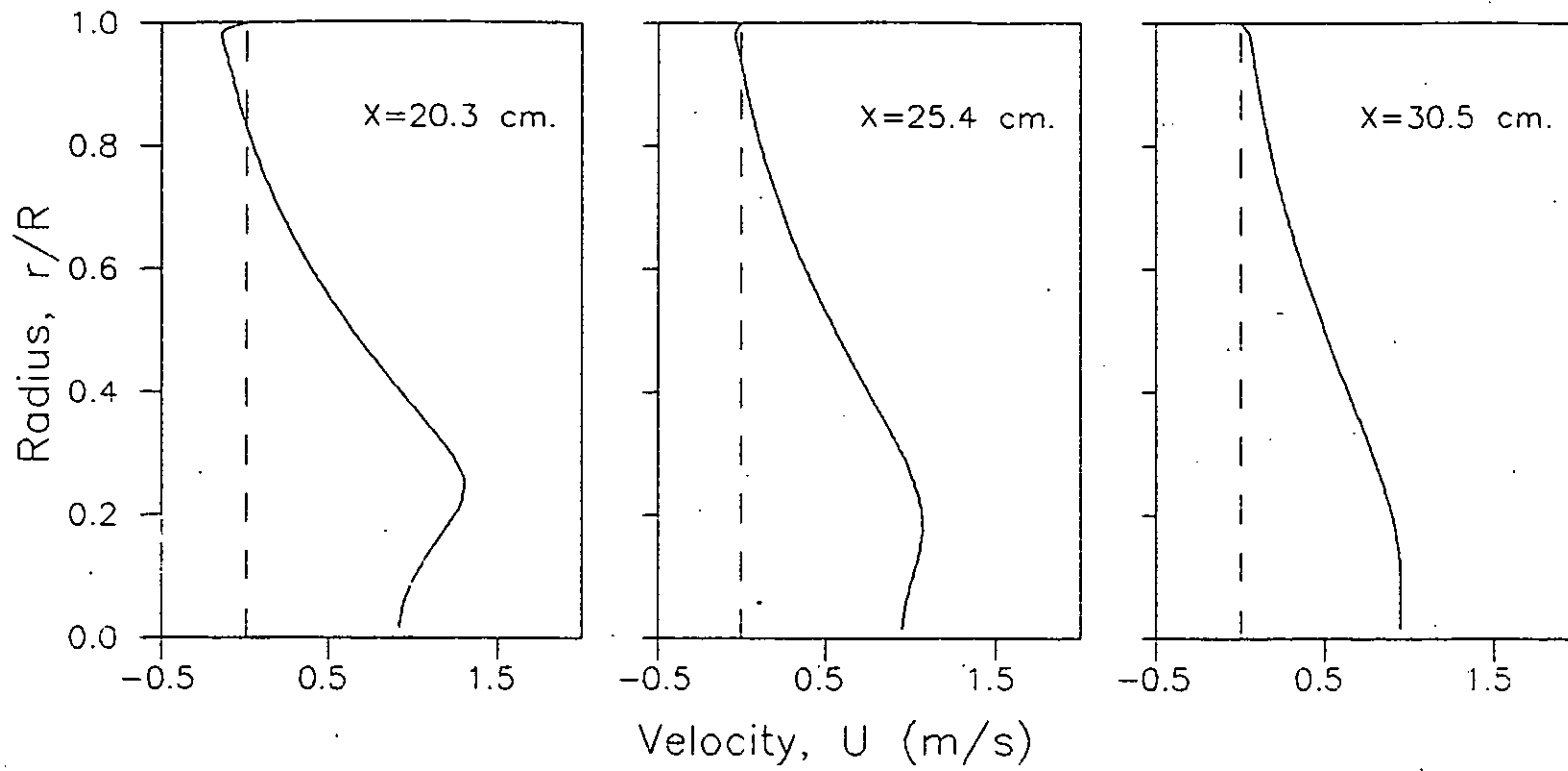


FIG.11.(Contd.) Mean axial velocity profiles for $U_1/U_2 = 0.2$.

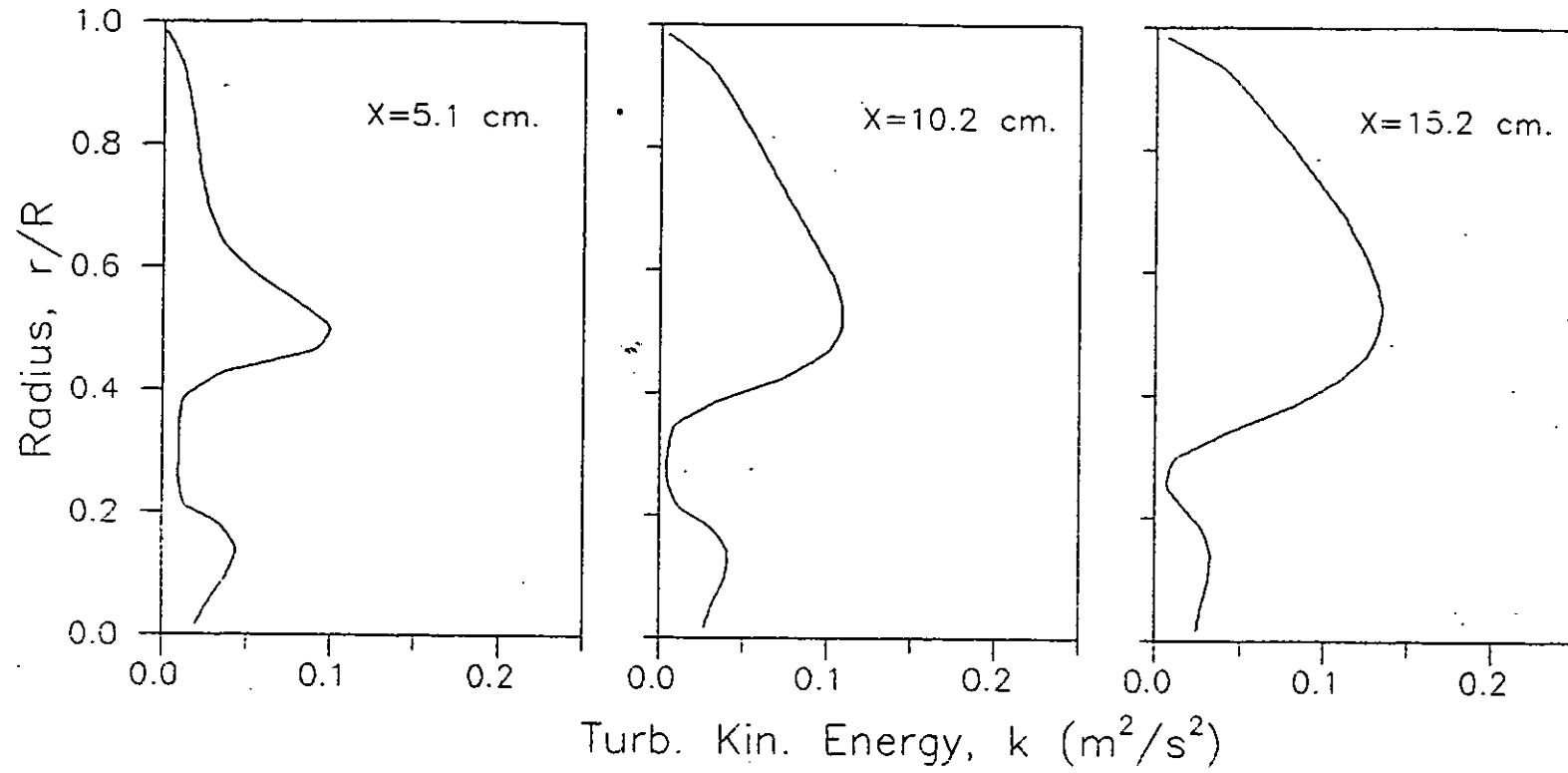


FIG.12. Turbulent kinetic energy profiles for $U_1/U_2 = 0.2$.

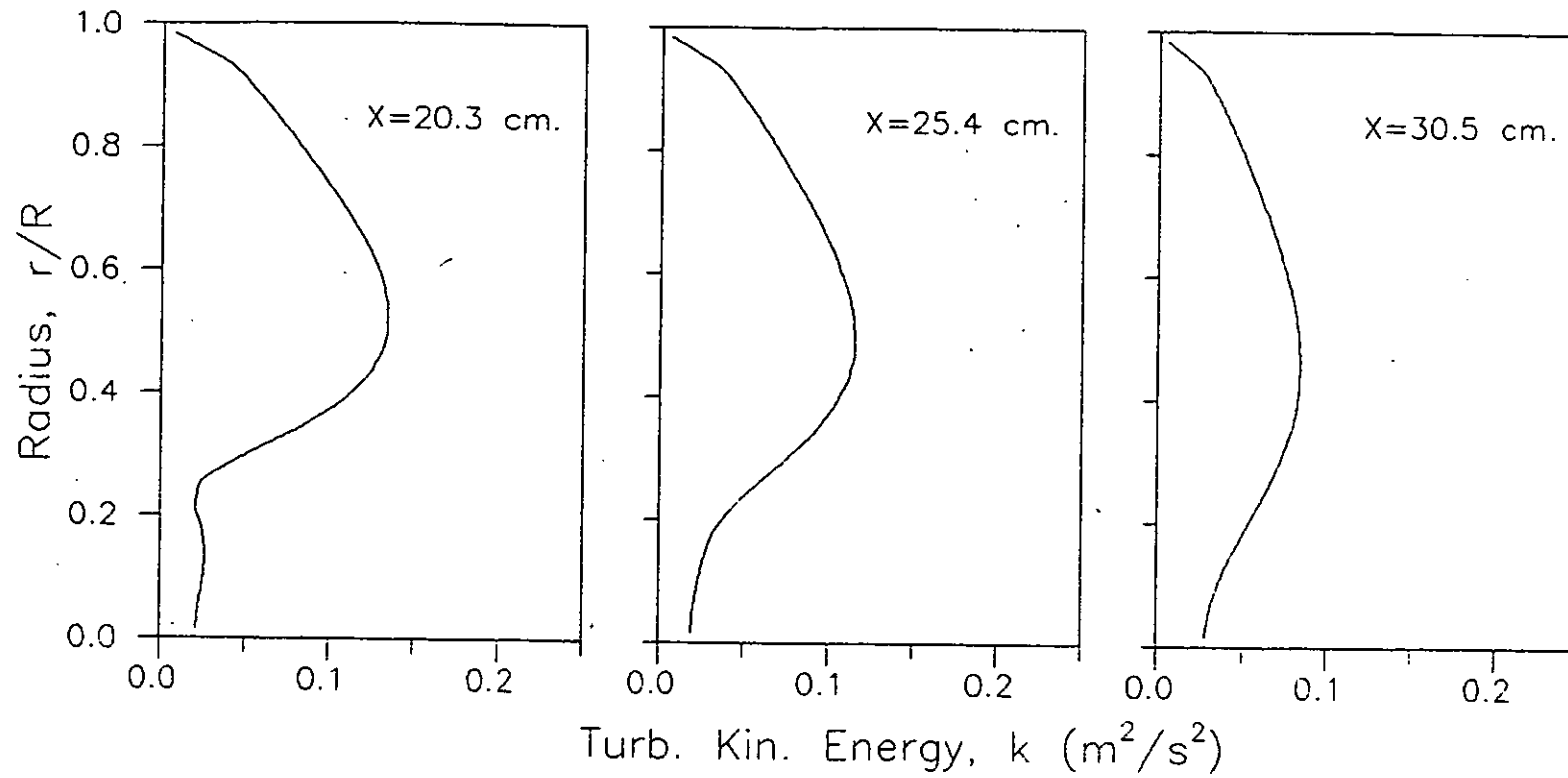


FIG.12.(Contd.) Turbulent kinetic energy profiles for $U_1/U_2 = 0.2$.

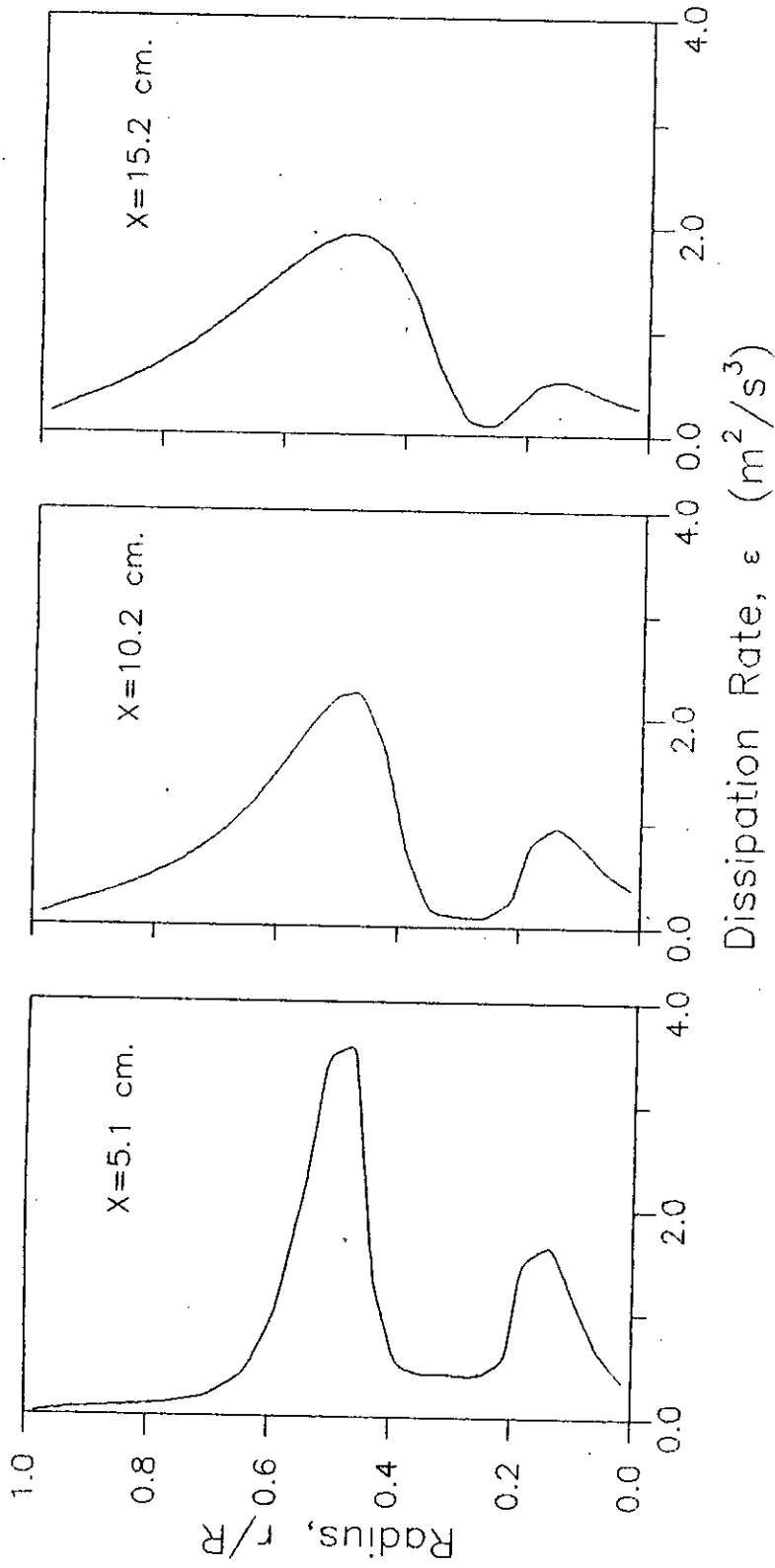


FIG.13. Dissipation rate profiles for $U_1/U_2 = 0.2$.

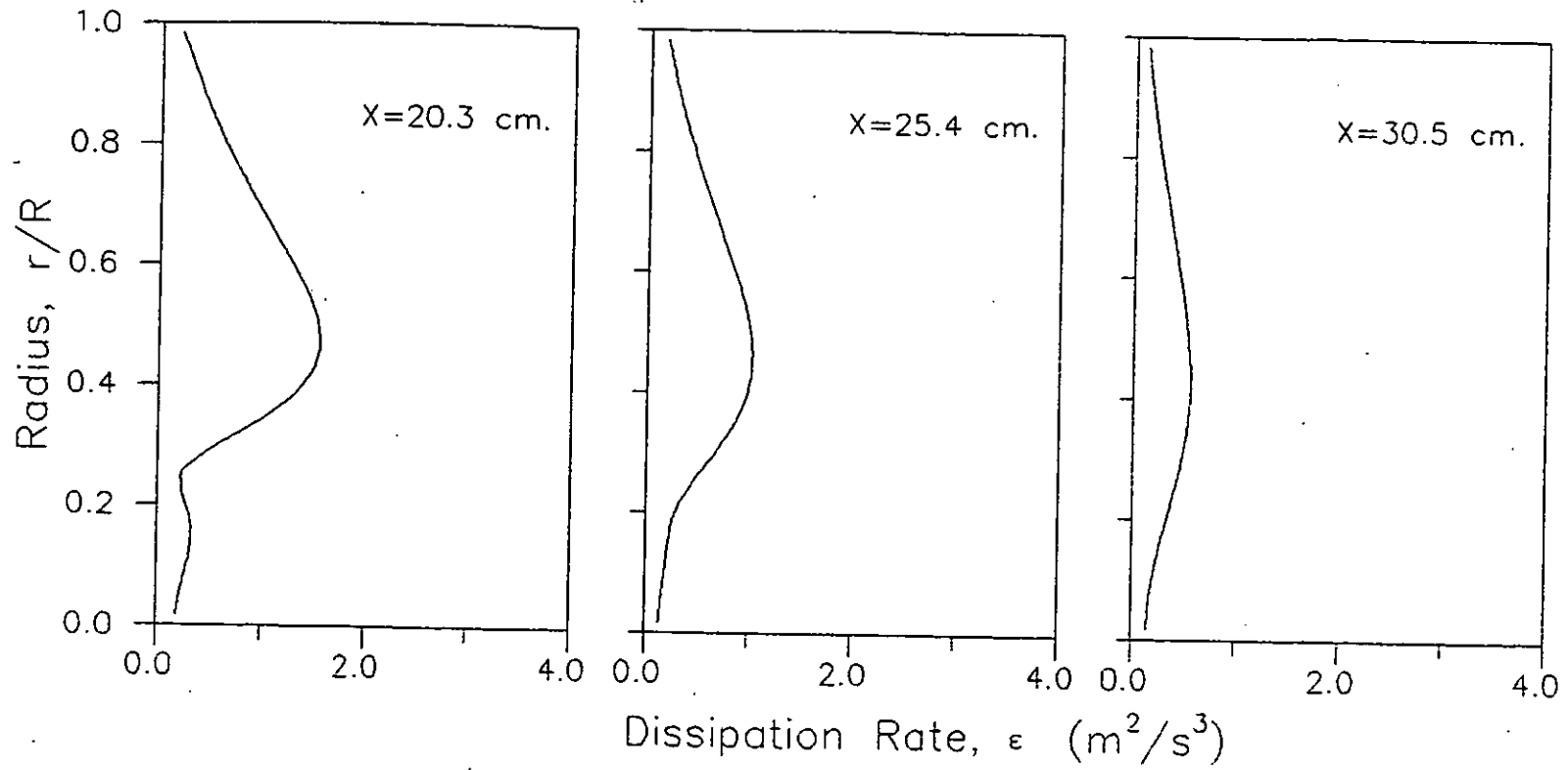


FIG.13.(Contd.) Dissipation rate profiles for $U_1/U_2 = 0.2$.

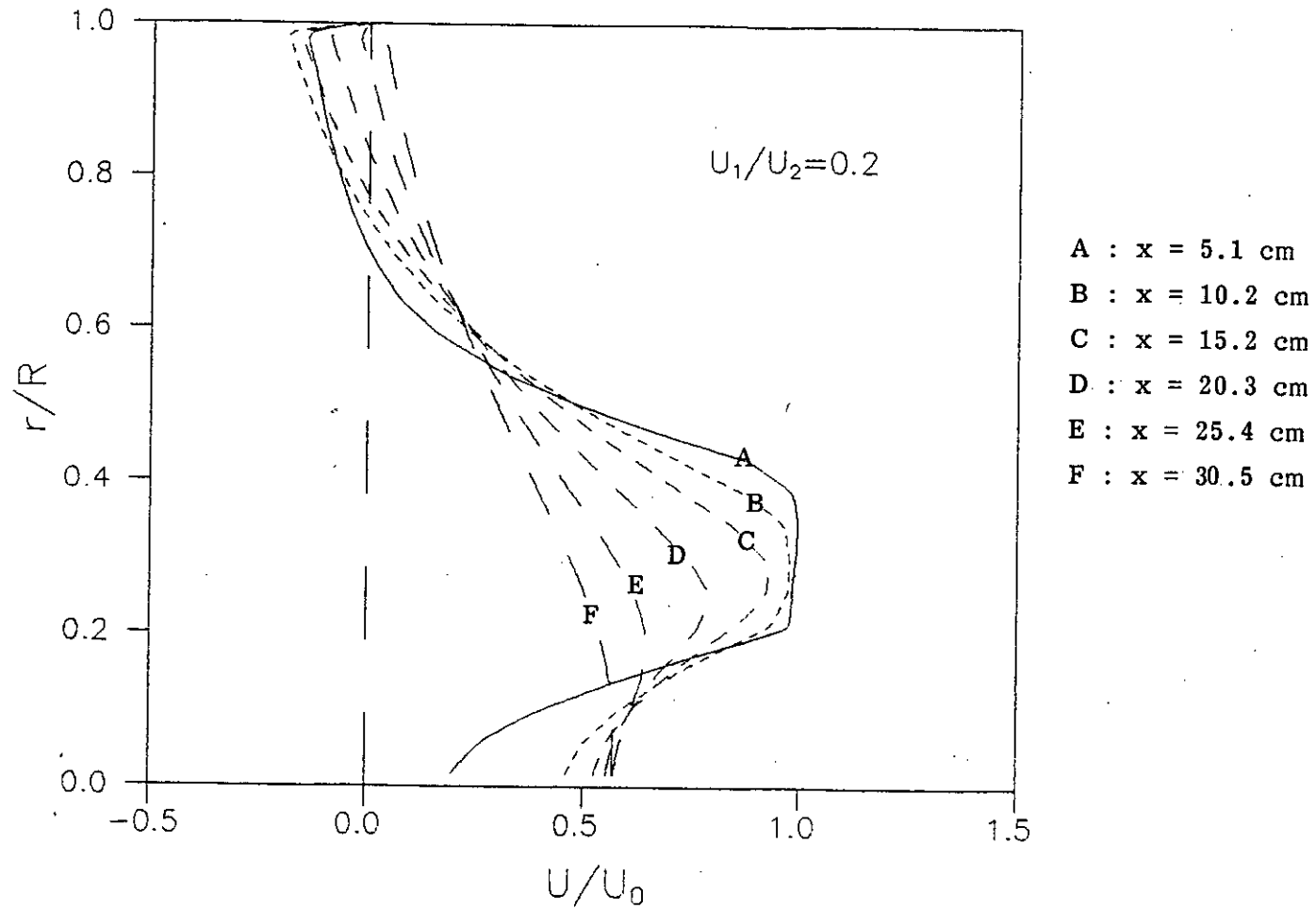


FIG.14. Dimensionless mean axial velocity profiles for different axial locations.

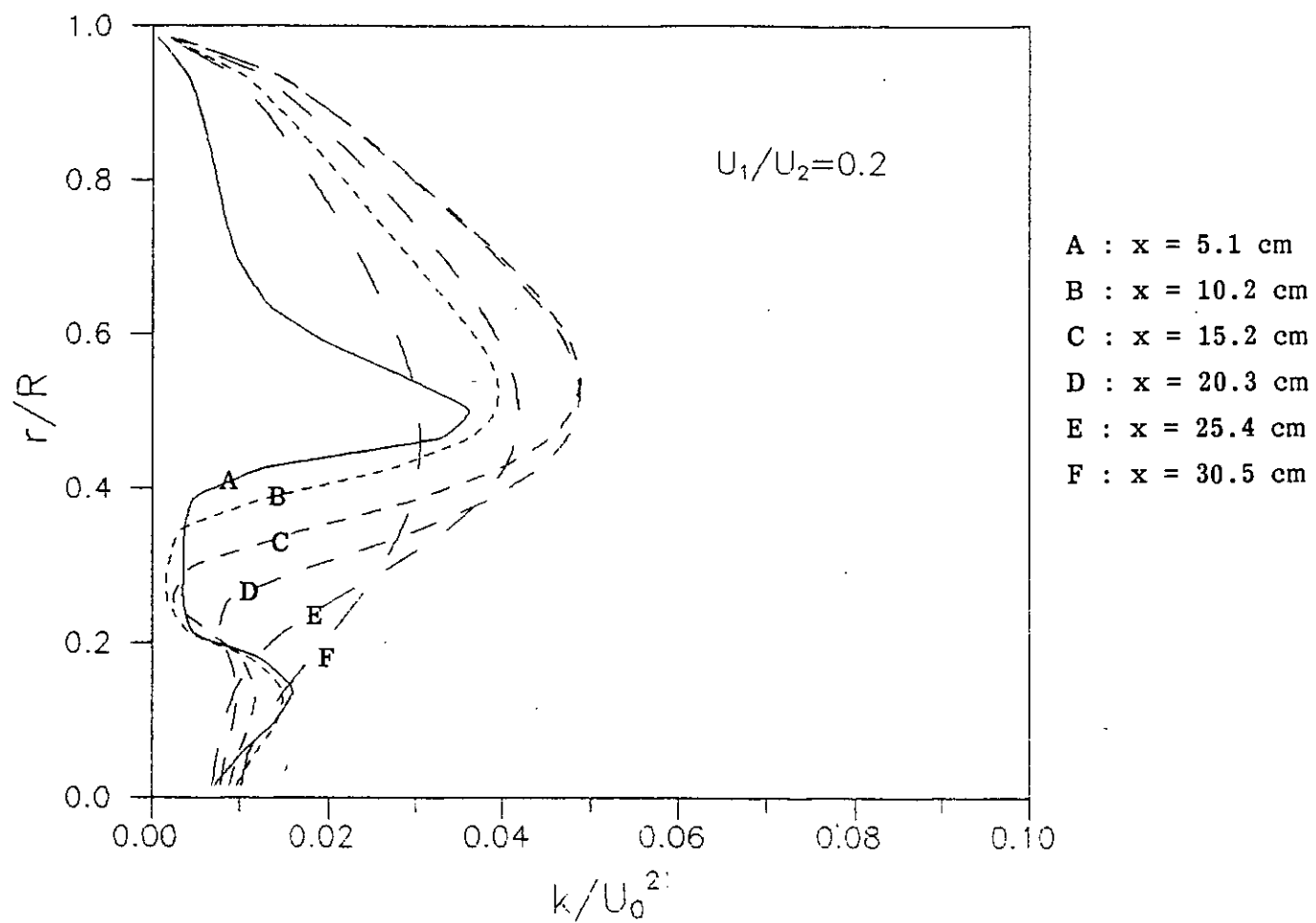


FIG.15. Dimensionless turbulent kinetic energy profiles for different axial locations.

85784

63

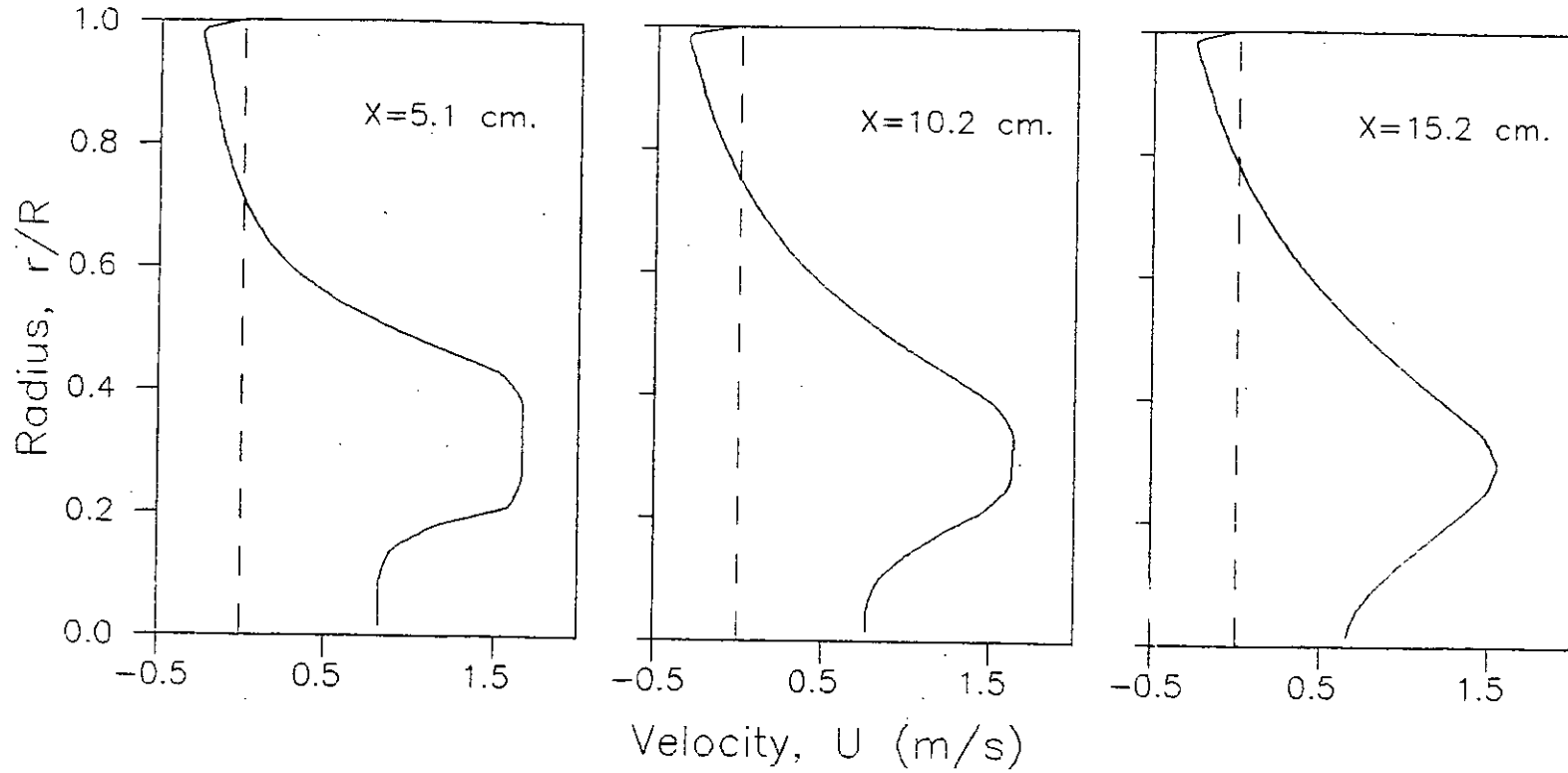


FIG.16. Mean axial velocity profiles for $U_1/U_2 = 0.5$.

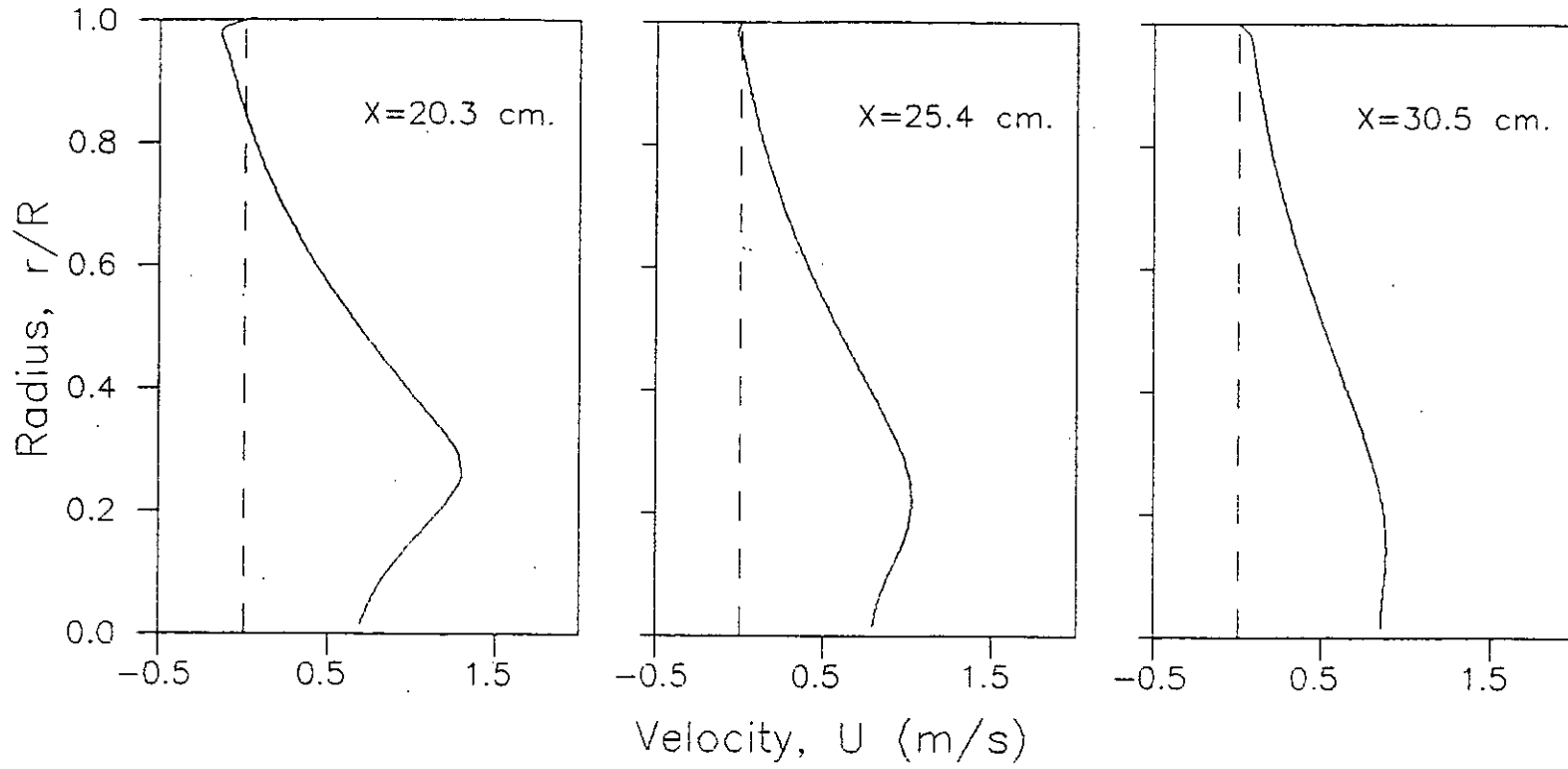


FIG.16.(Contd.) Mean axial velocity profiles for $U_1/U_2 = 0.5$.

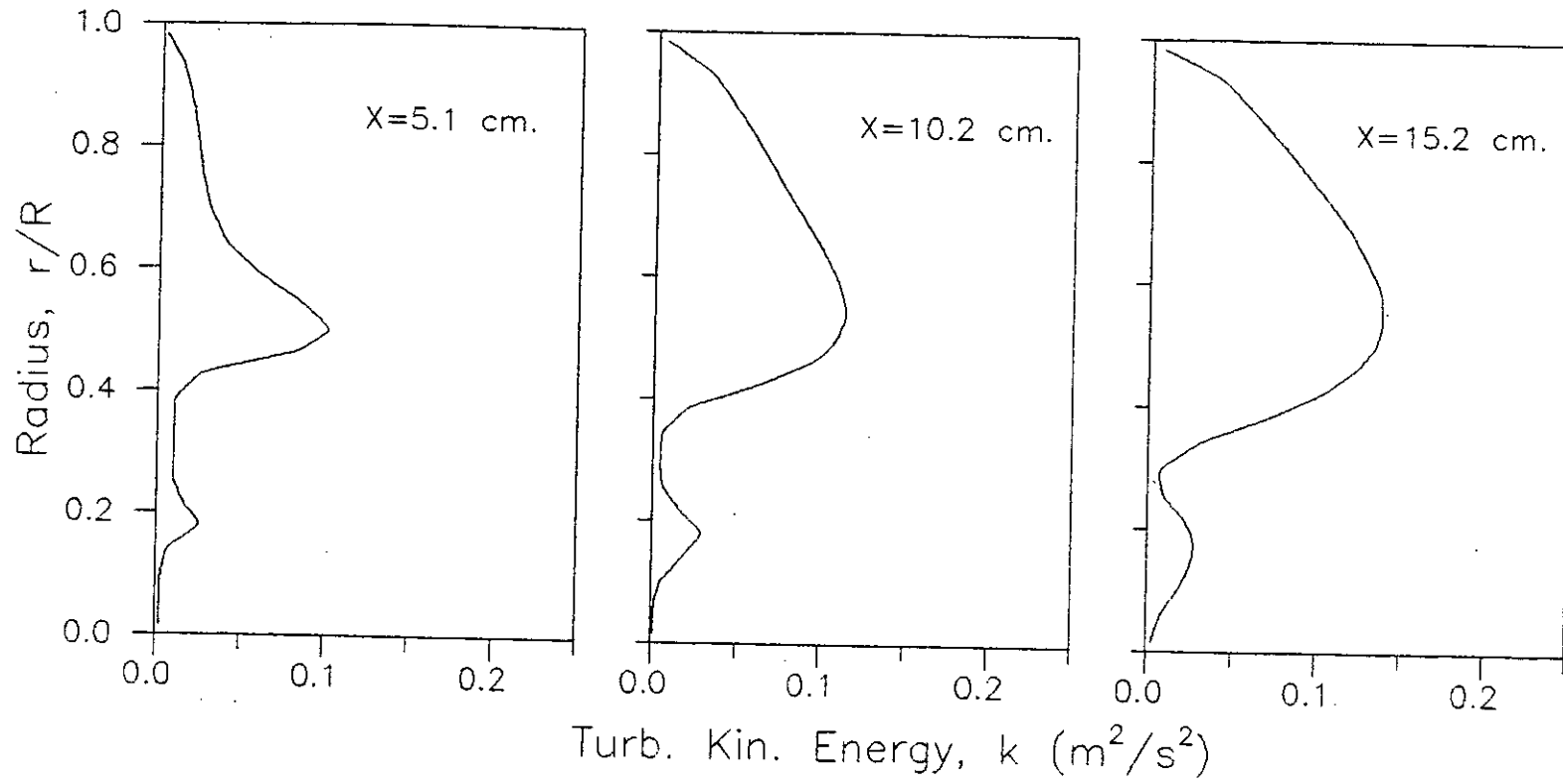


FIG.17. Turbulent kinetic energy profiles for $U_1/U_2 = 0.5$.

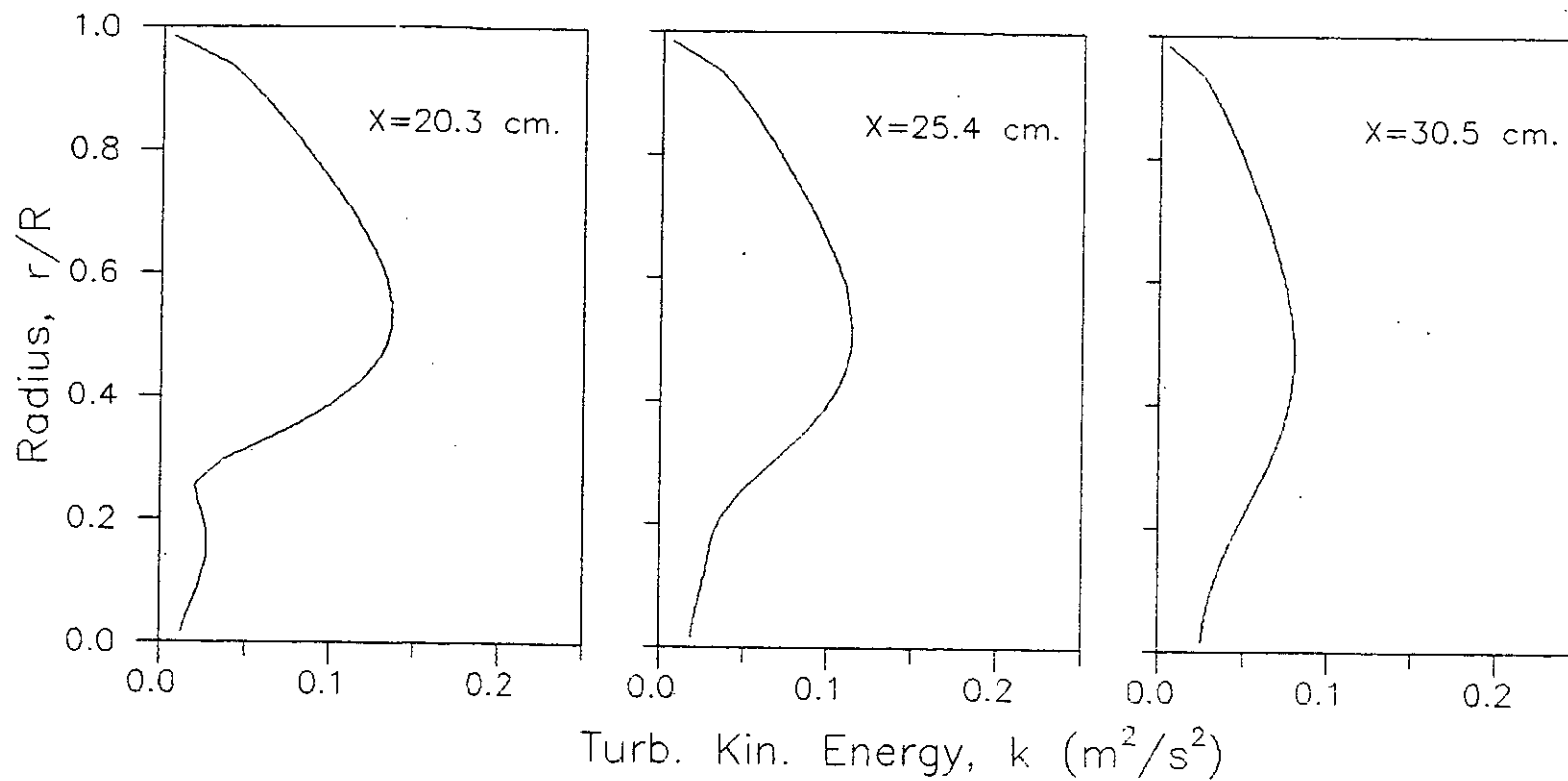


FIG.17.(Contd.) Turbulent kinetic energy profiles for $U_1/U_2 = 0.5$.

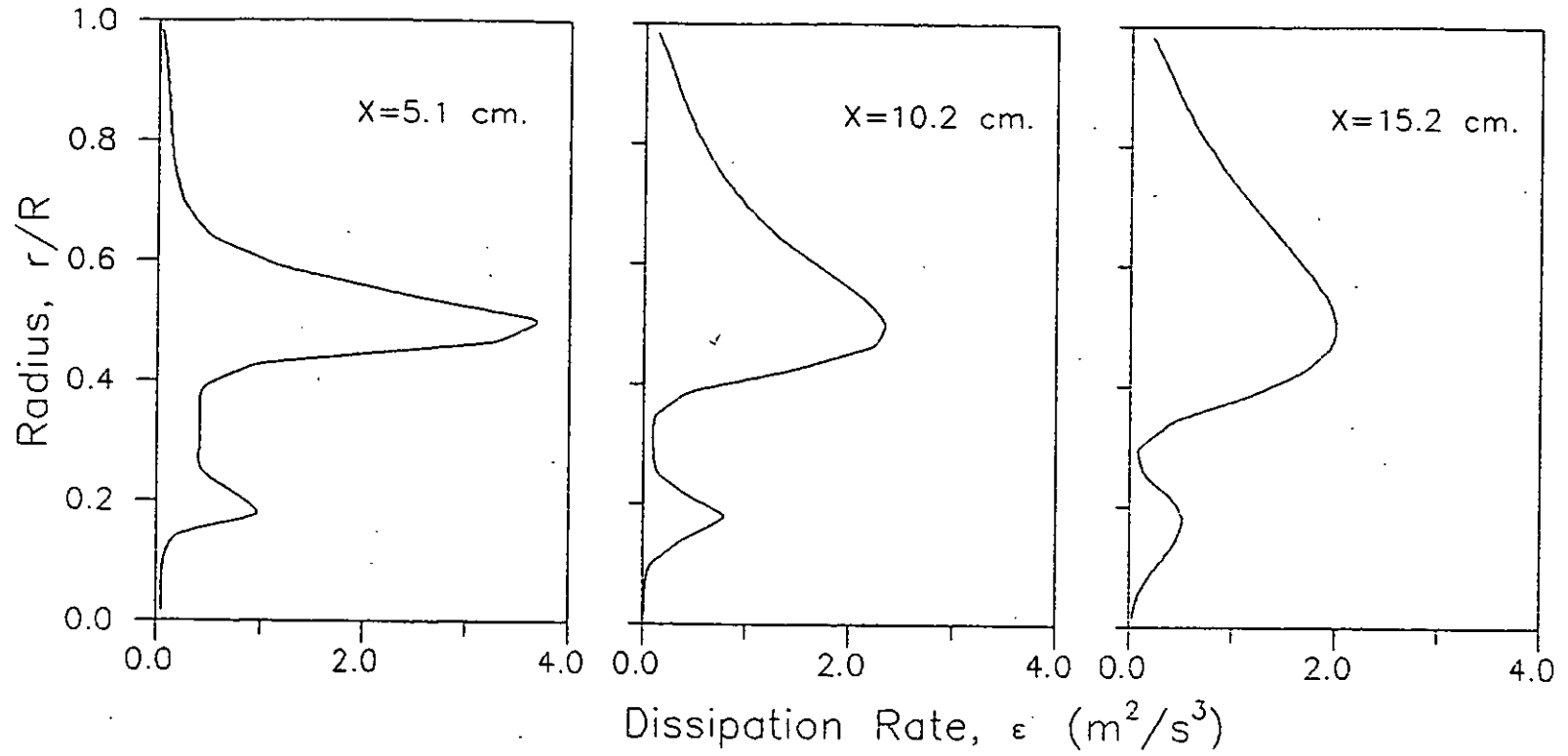


FIG.18. Dissipation rate profiles for $U_1/U_2 = 0.5$.

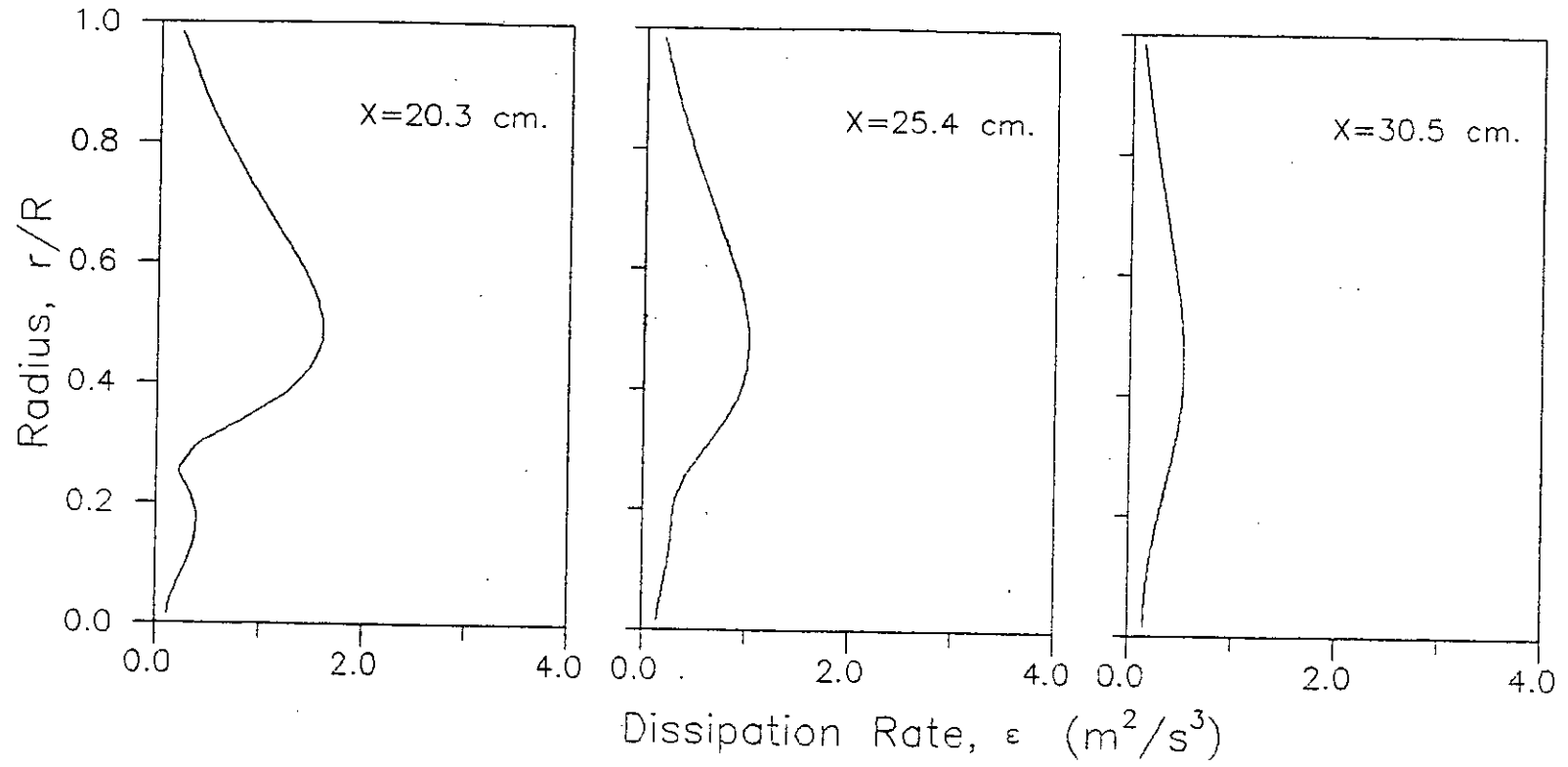


FIG.18.(Contd.) Dissipation rate profiles for $U_1/U_2 = 0.5$.

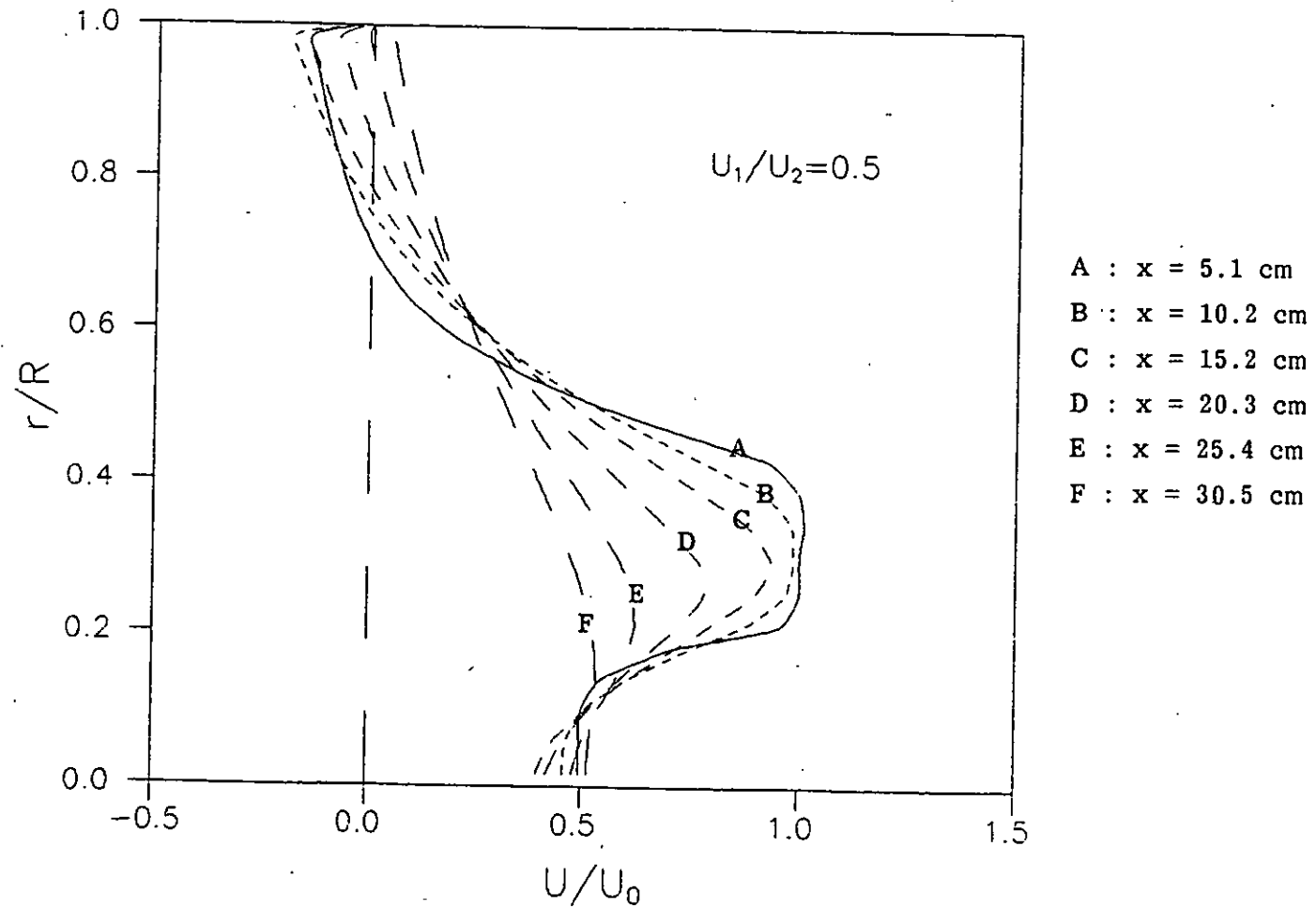


FIG.19. Dimensionless mean axial velocity profiles for different axial locations.

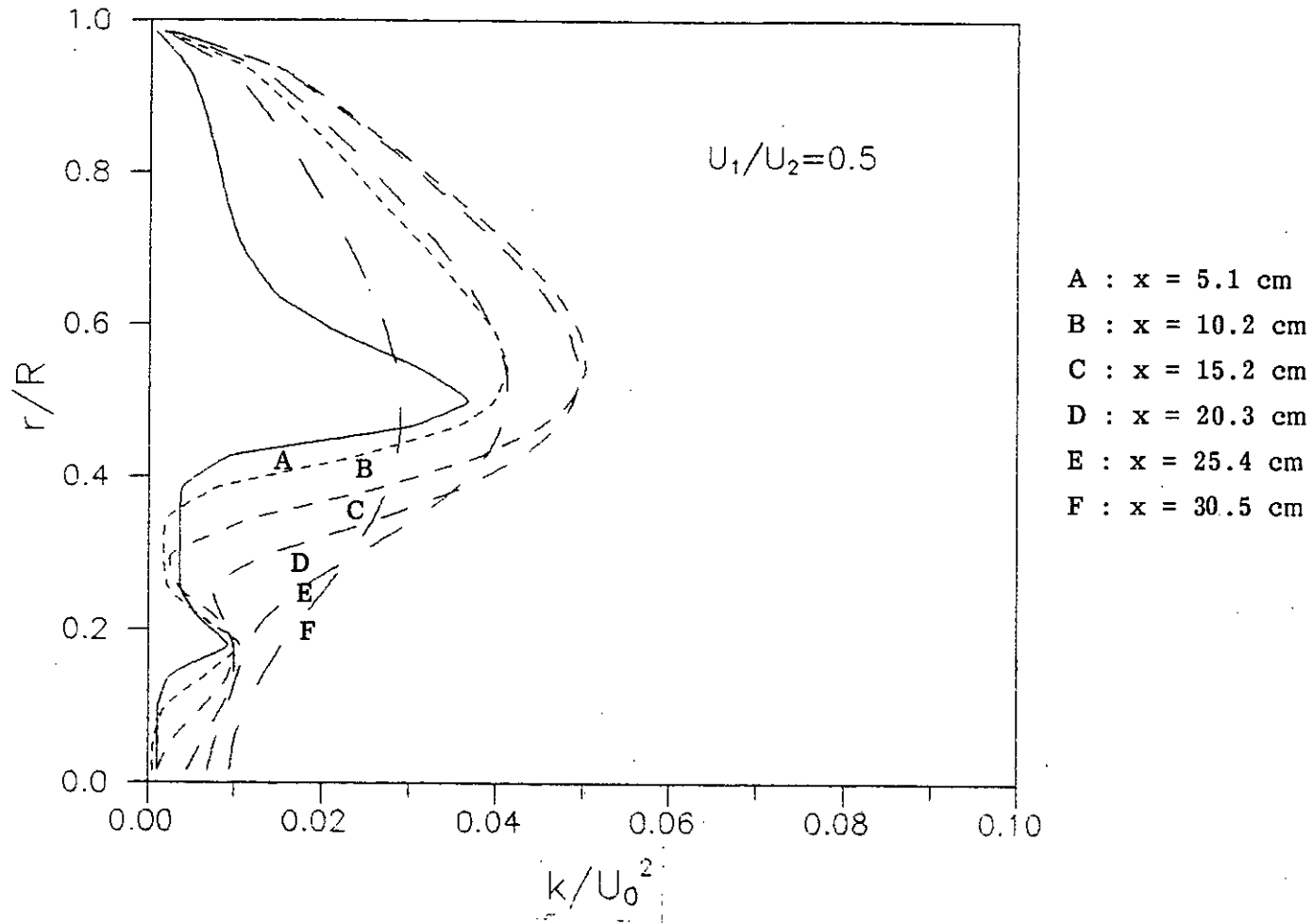


FIG.20. Dimensionless turbulent kinetic energy profiles for different axial locations.

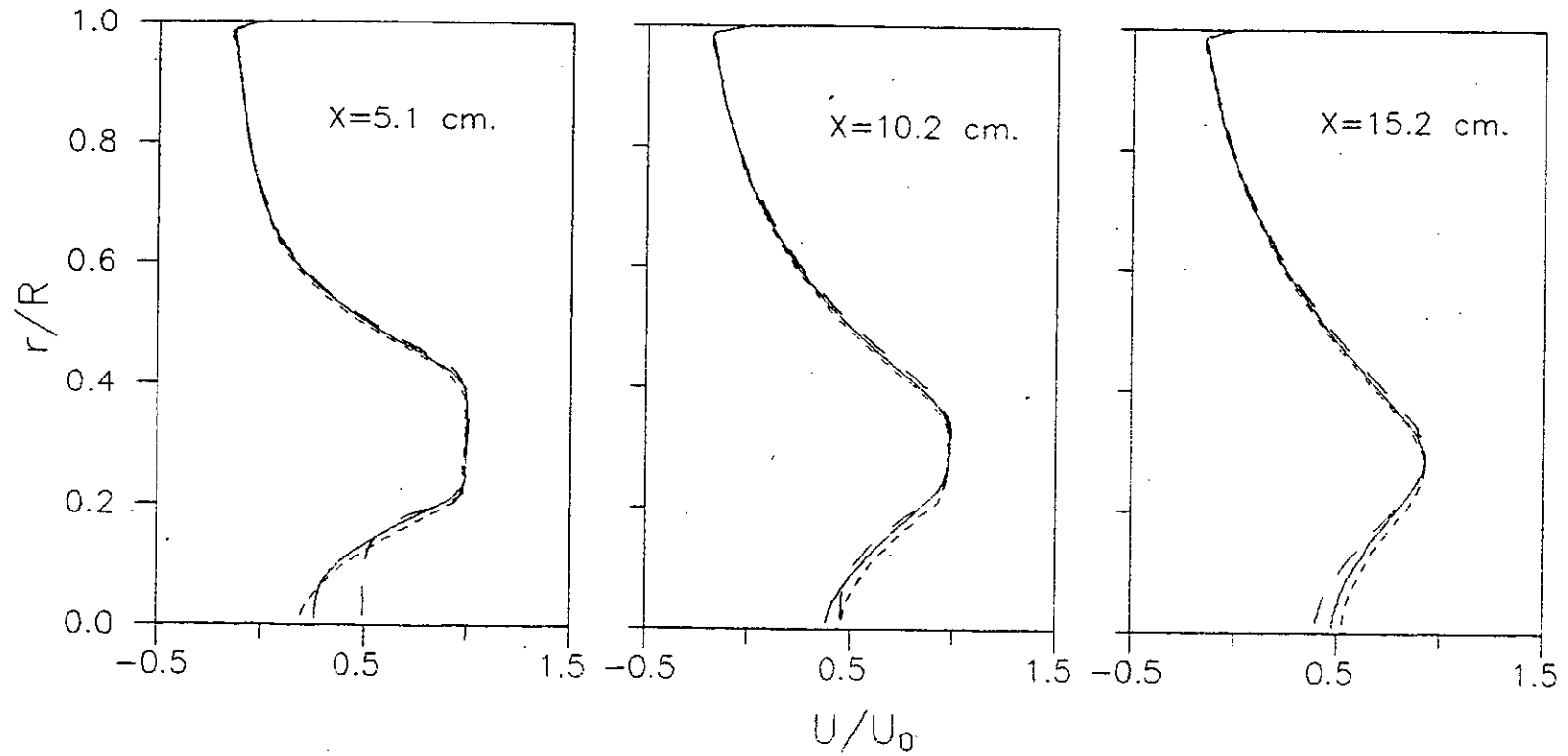


FIG. 21. Comparison of dimensionless mean axial velocity profiles: —, $U_1/U_2 = 0.31$; ---, $U_1/U_2 = 0.2$; - · - ·, $U_1/U_2 = 0.5$.

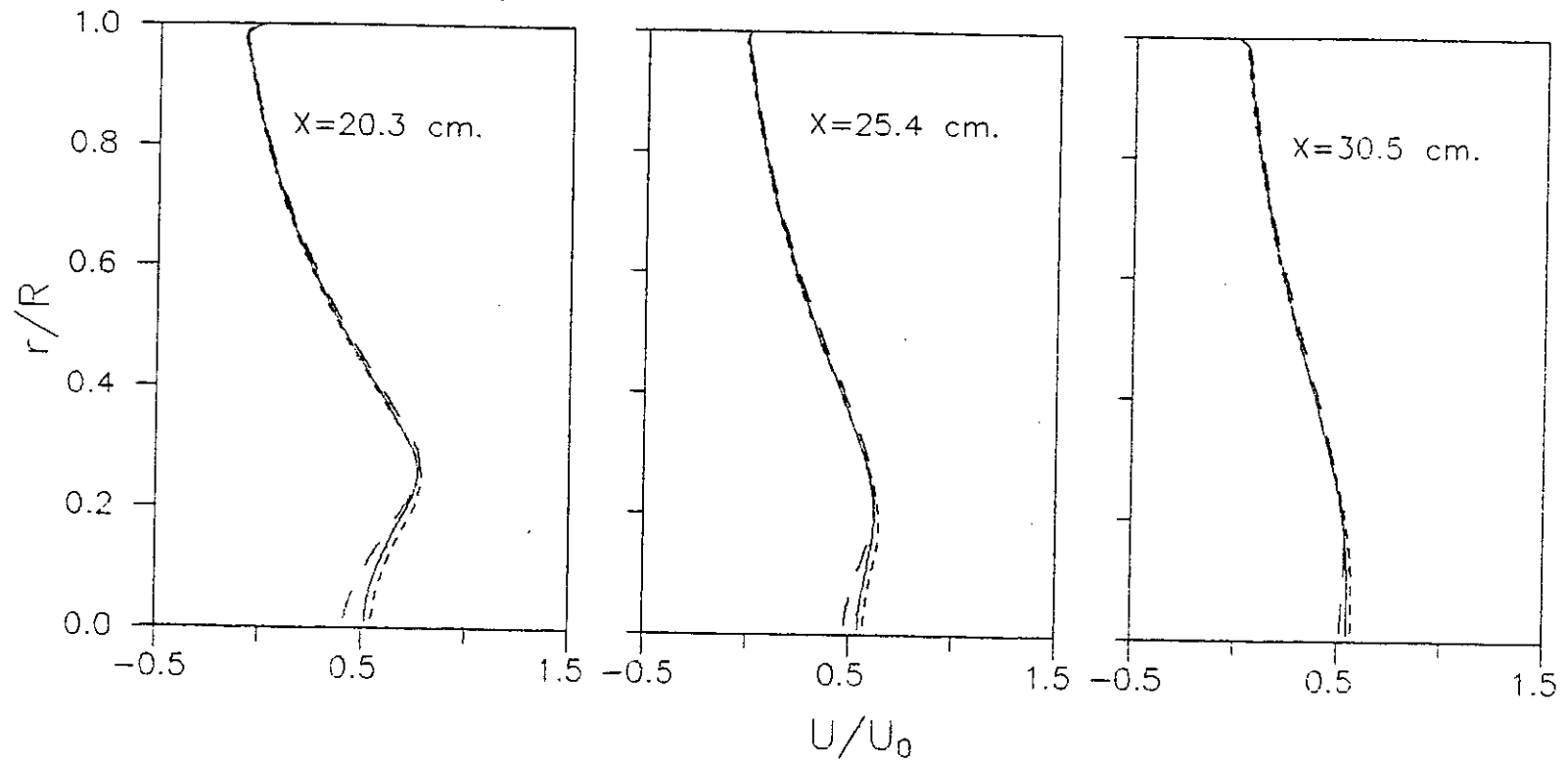


FIG.21. (Contd.) Comparison of dimensionless mean axial velocity profiles.

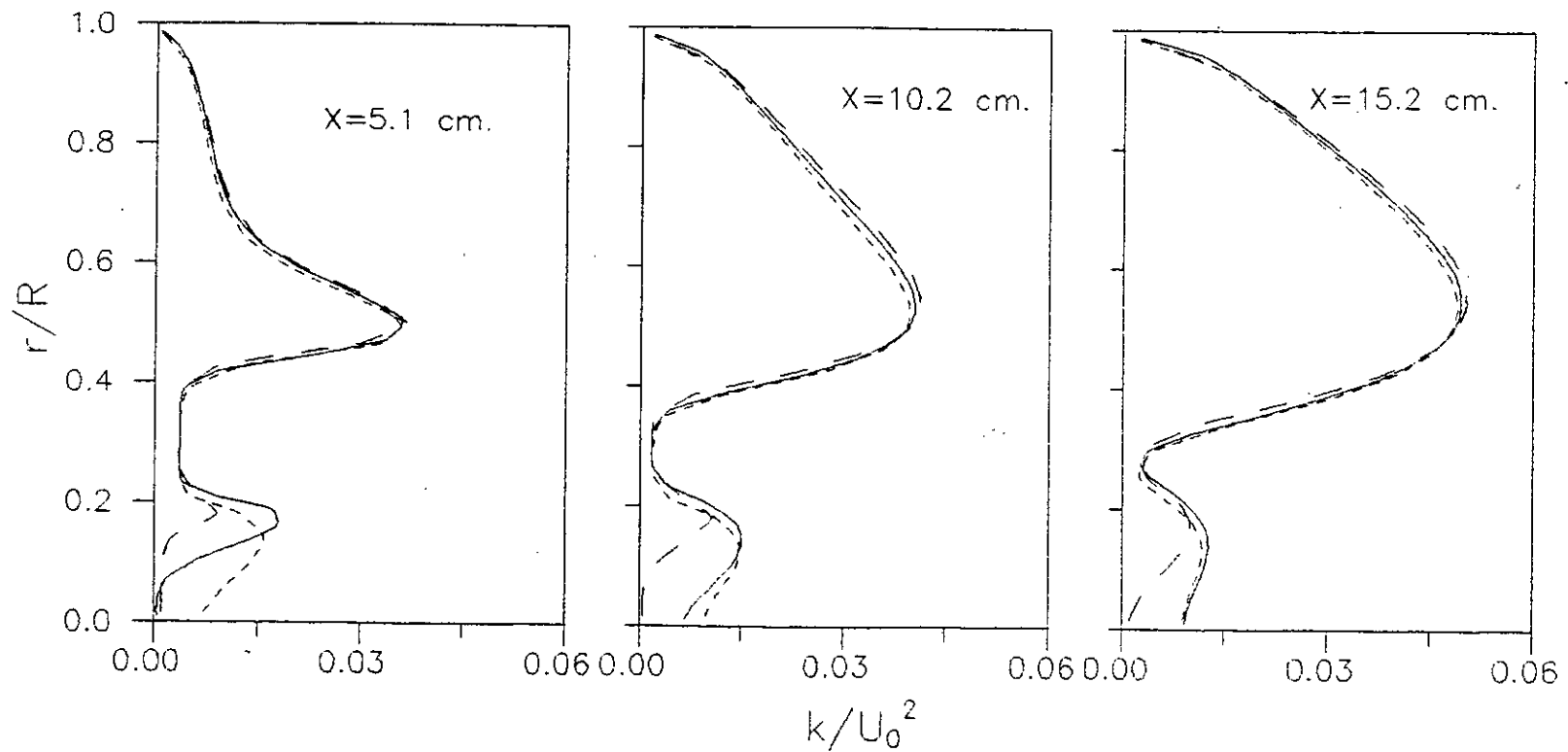


FIG.22. Comparison of dimensionless turbulent kinetic energy profiles:—, $U_1/U_2 = 0.31$; ---, $U_1/U_2 = 0.2$; - - -, $U_1/U_2 = 0.5$.

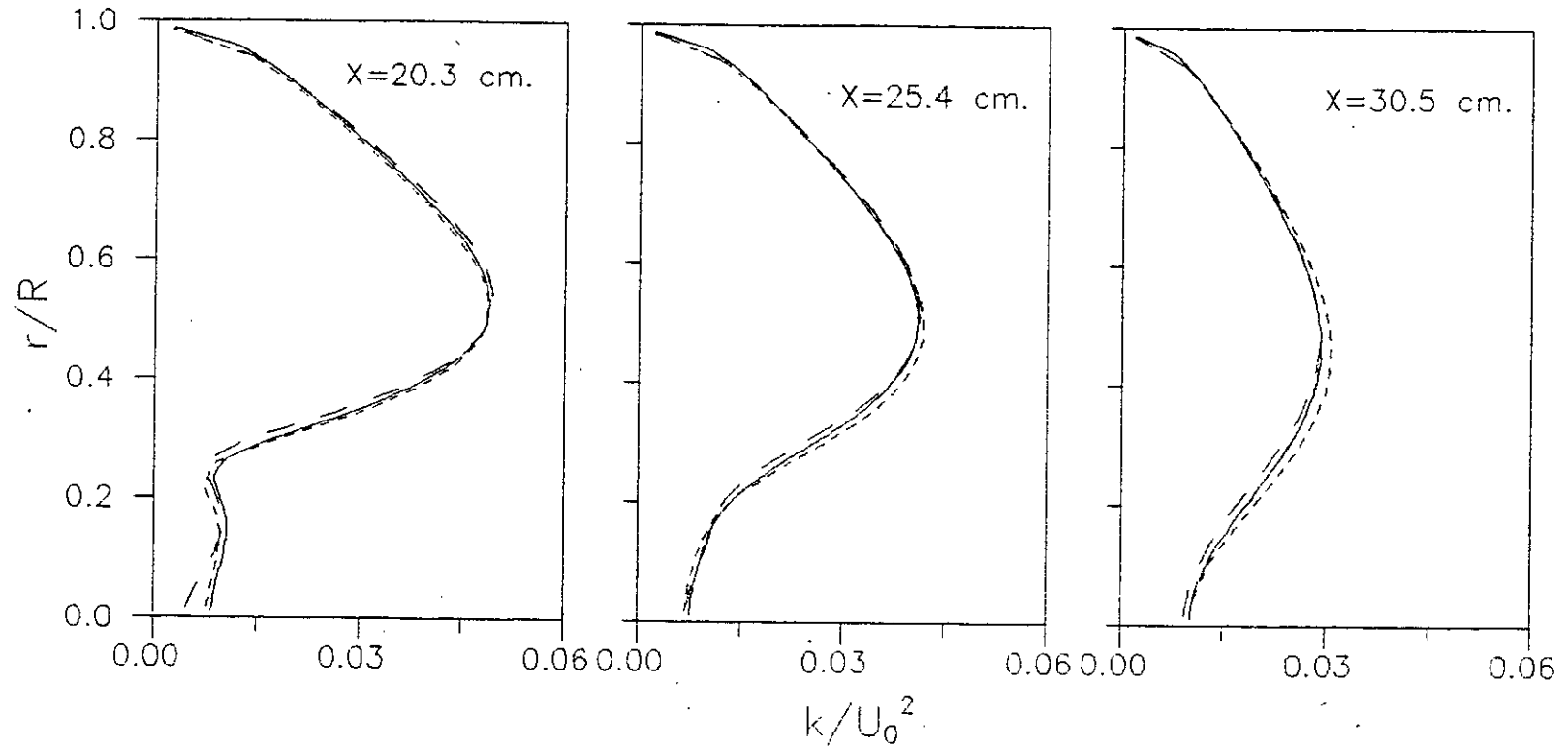


FIG.22.(Contd.) Comparison of dimensionless turbulent kinetic energy profiles.

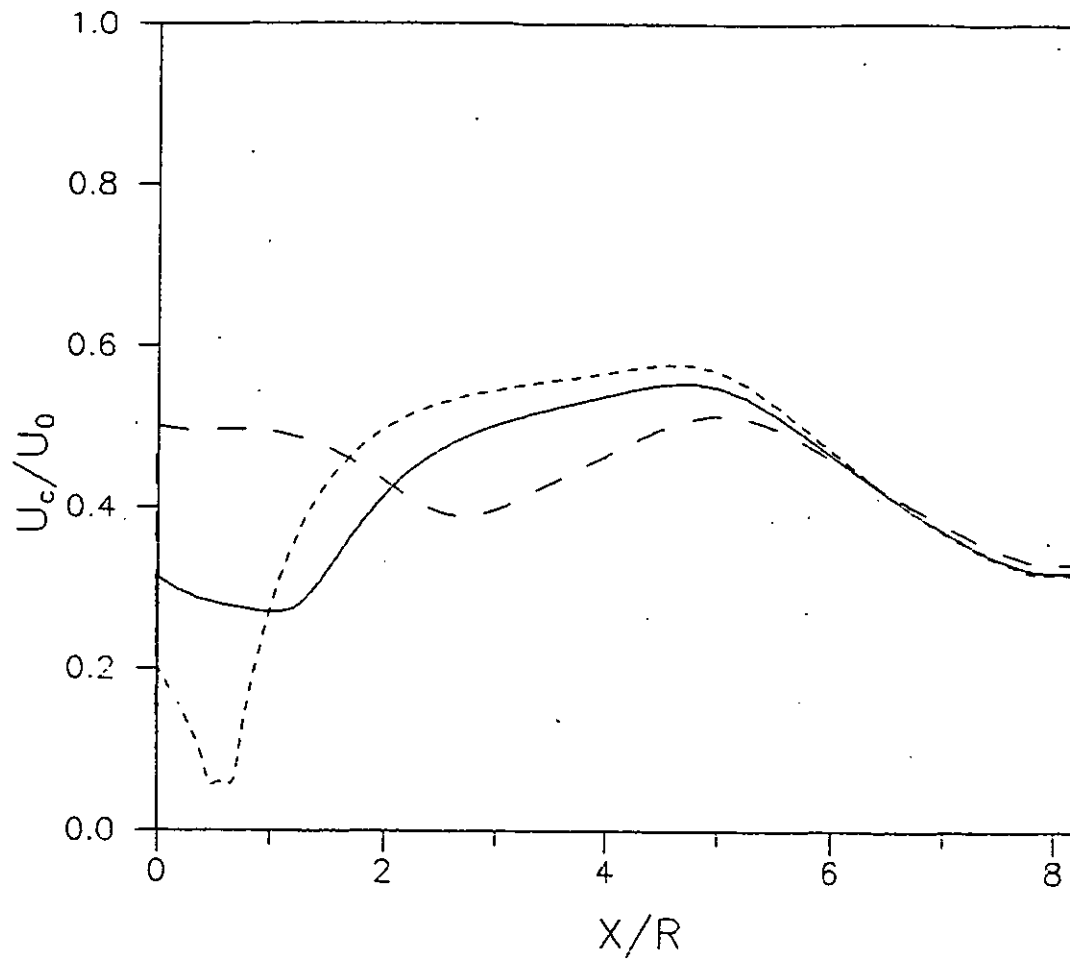


FIG. 23. Comparison of nondimensional centreline velocities:
—, $U_1/U_2 = 0.31$; ---, $U_1/U_2 = 0.2$; — — —, $U_1/U_2 = 0.5$.

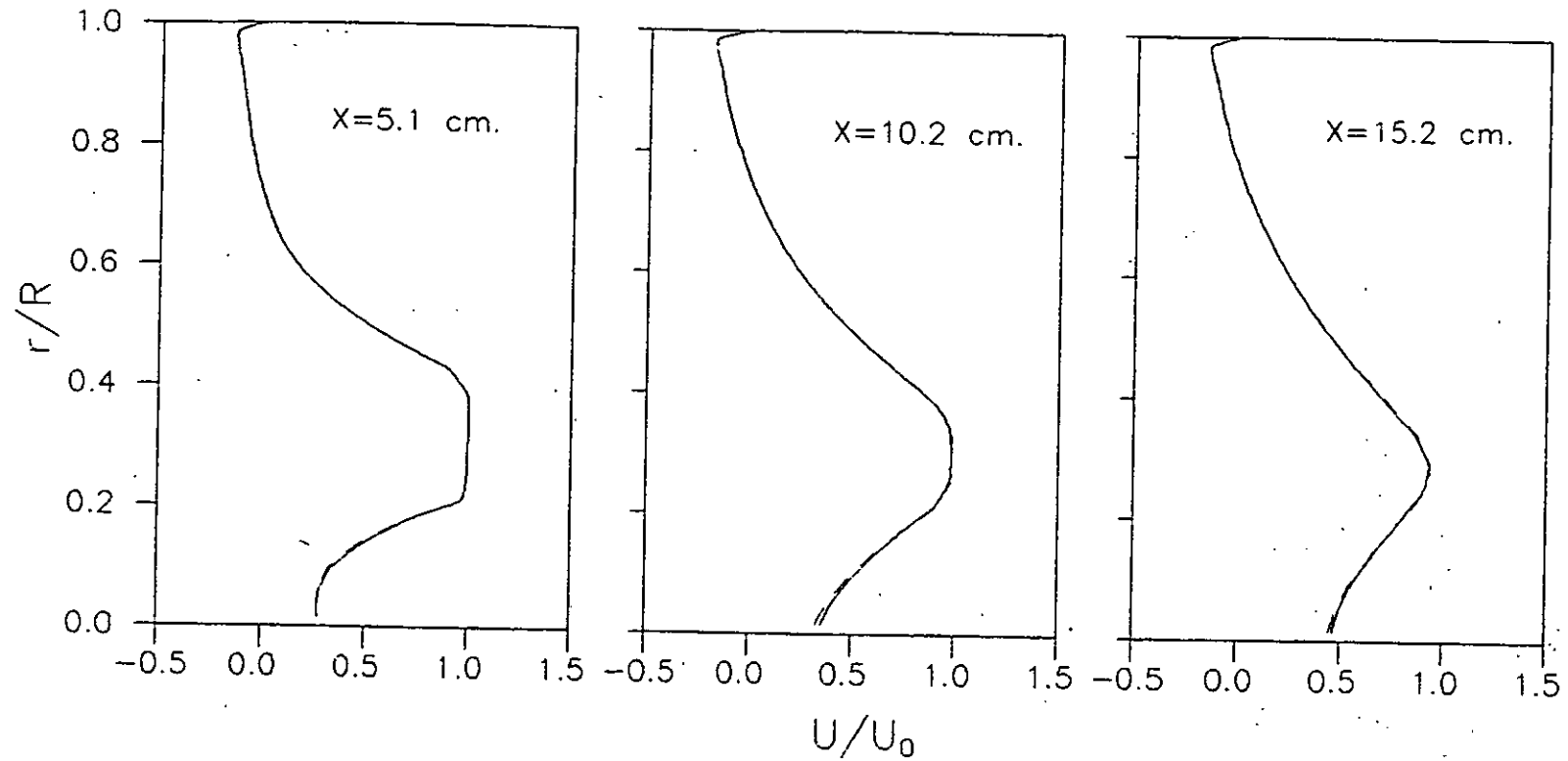


FIG.24. Comparison of dimensionless mean axial velocity profiles:—, $Re=97000$;
---, $Re=194000$.

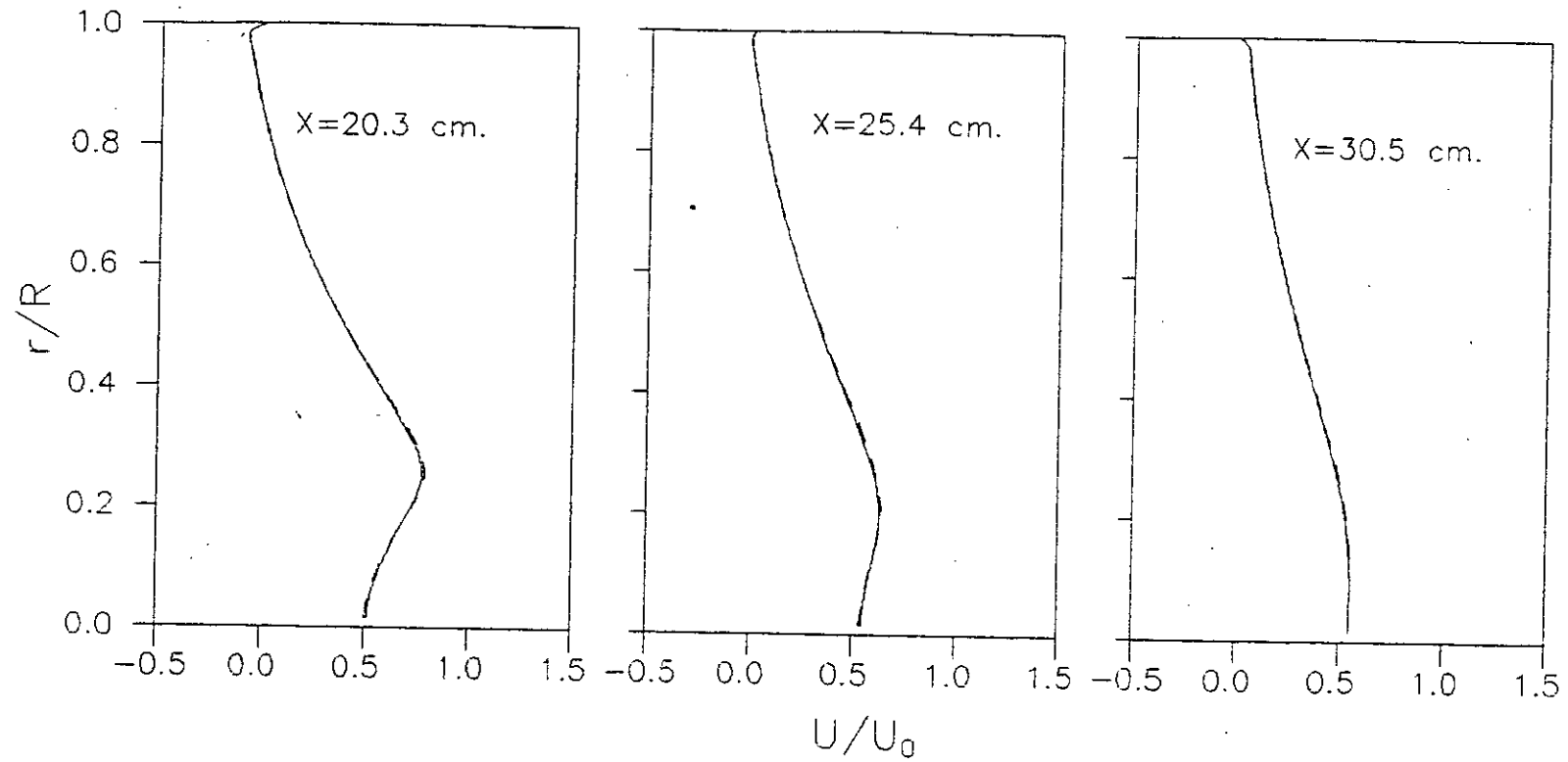


FIG.24.(Contd.) Comparison of dimensionless mean axial velocity profiles.

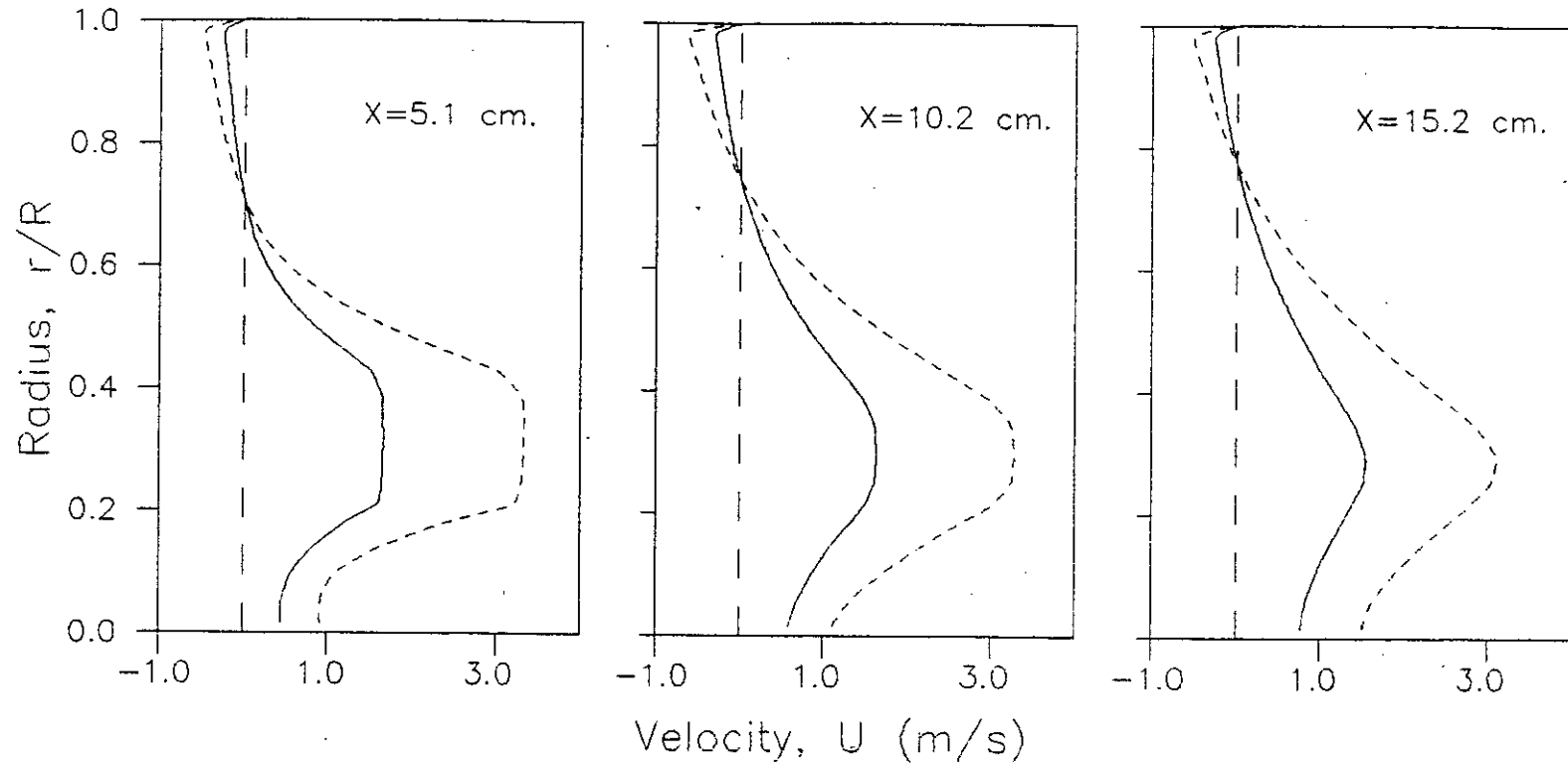


FIG.25. Comparison of mean axial velocity profiles:—, $Re = 97000$; ---, $Re = 194000$.

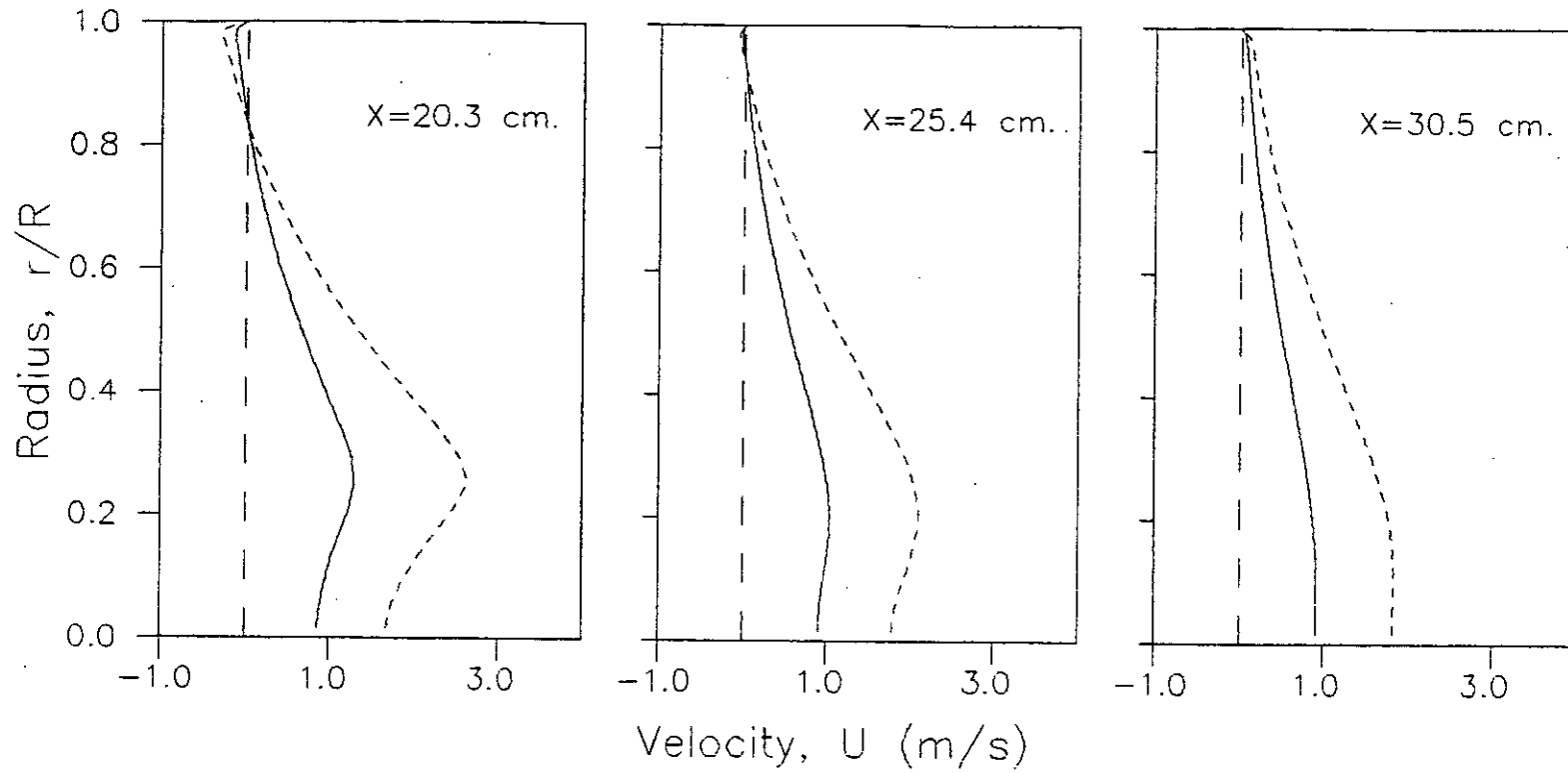


FIG.25. (Contd.) Comparison of mean axial velocity profiles.

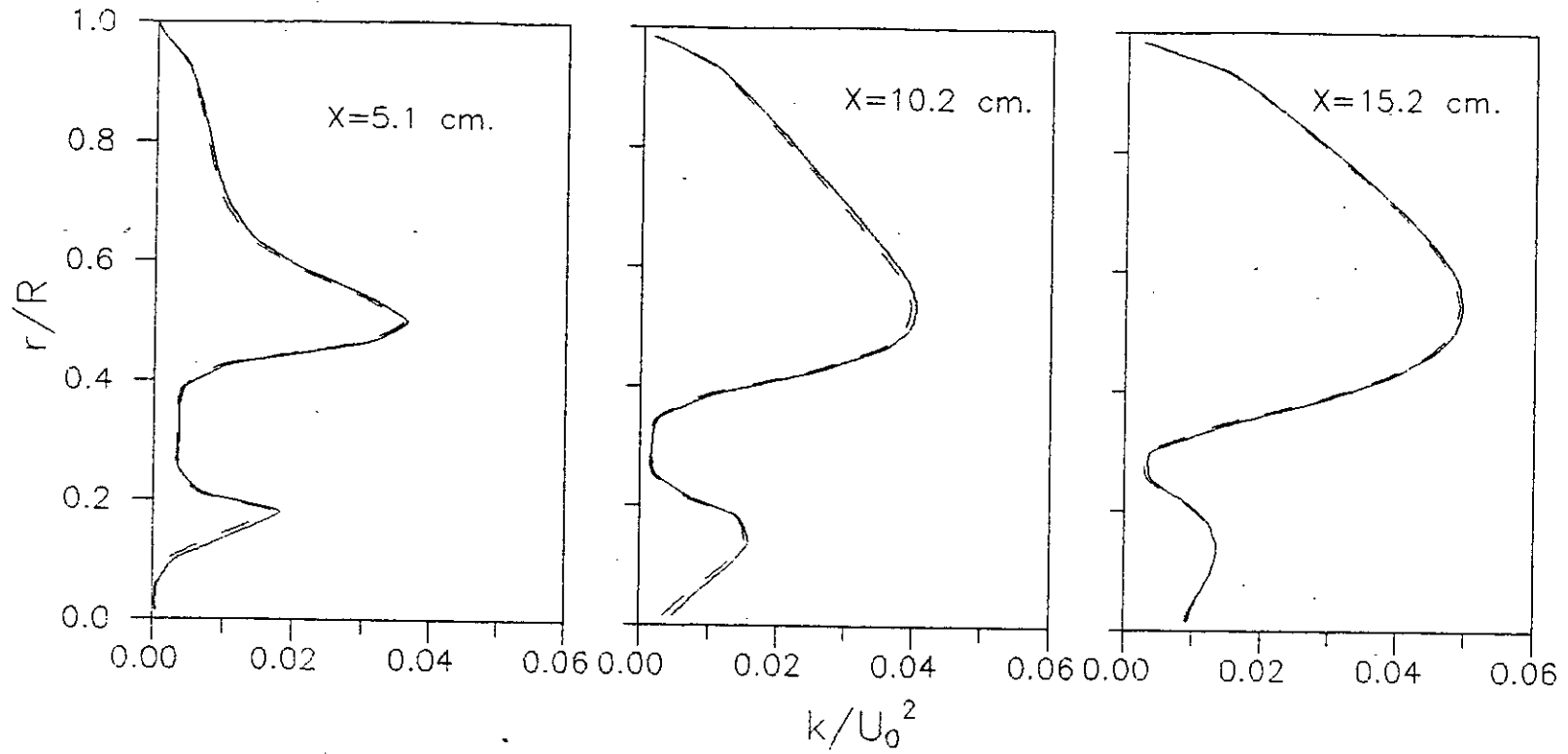


FIG. 26. Comparison of dimensionless turbulence kinetic energy profiles:—, $Re = 97000$; ---, $Re = 194000$.

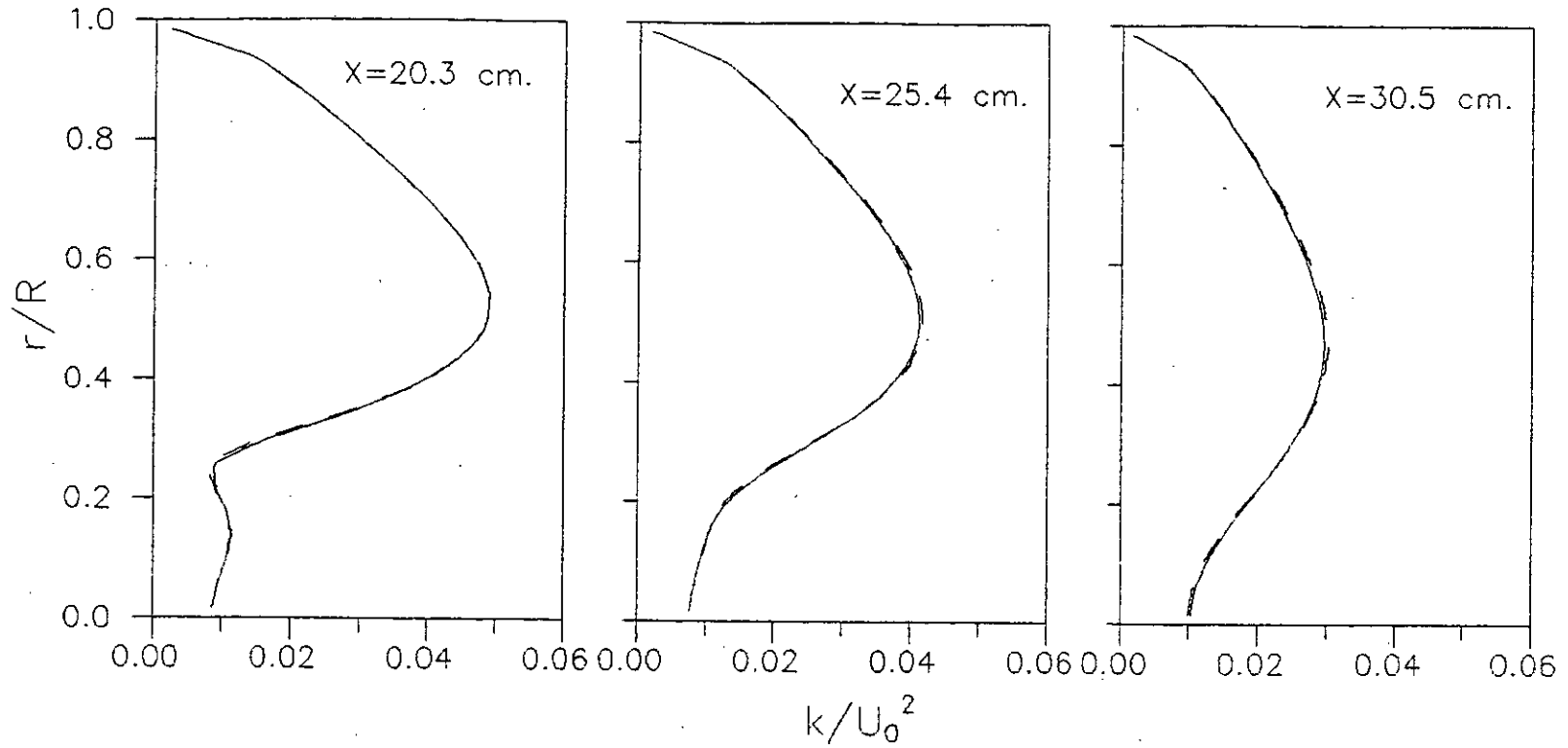


FIG.26. (Contd.) Comparison of dimensionless turbulence kinetic energy profiles.

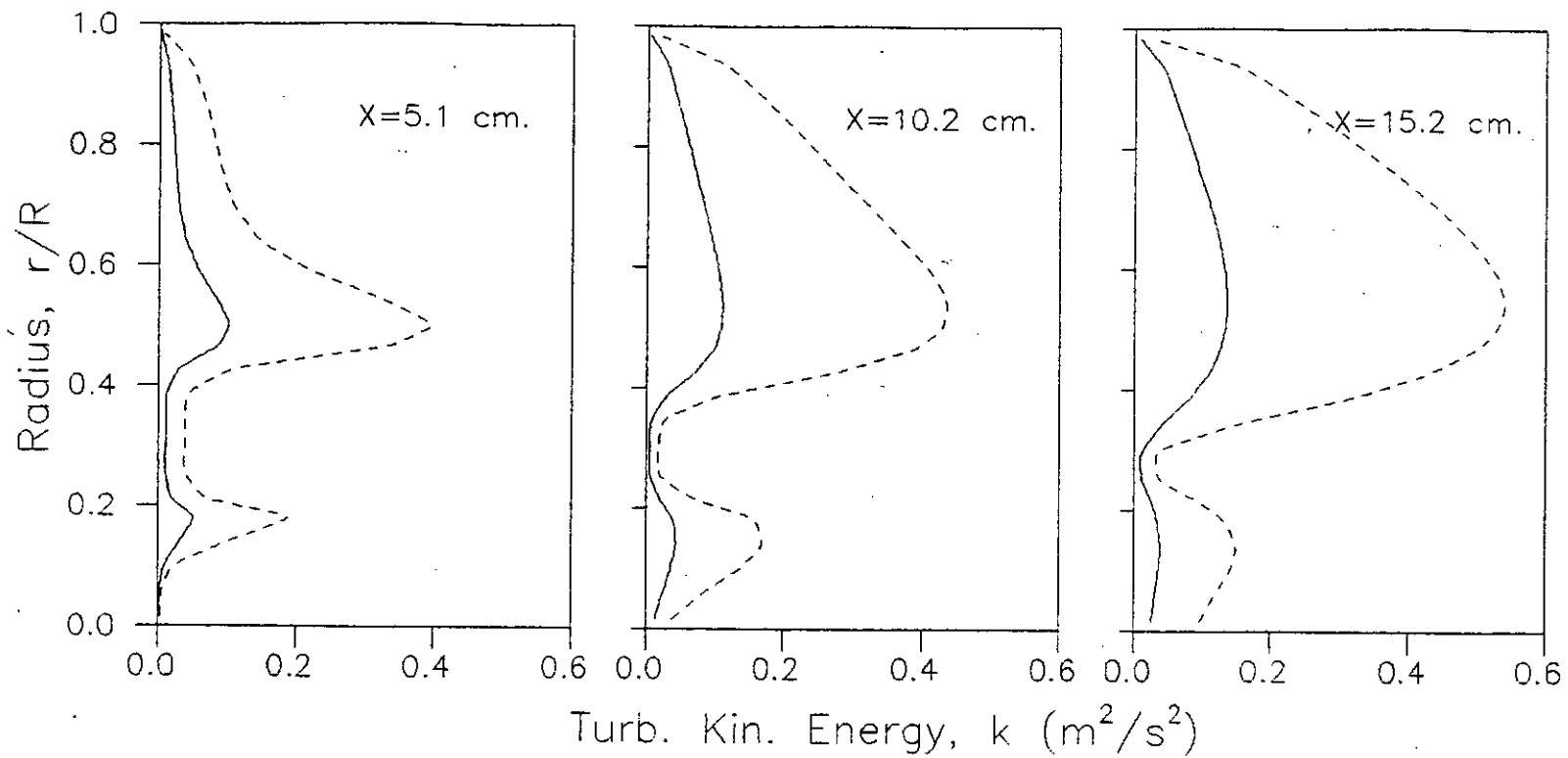


FIG.27. Comparison of turbulent kinetic energy profiles:—, $Re = 97000$; ---, $Re = 194000$.

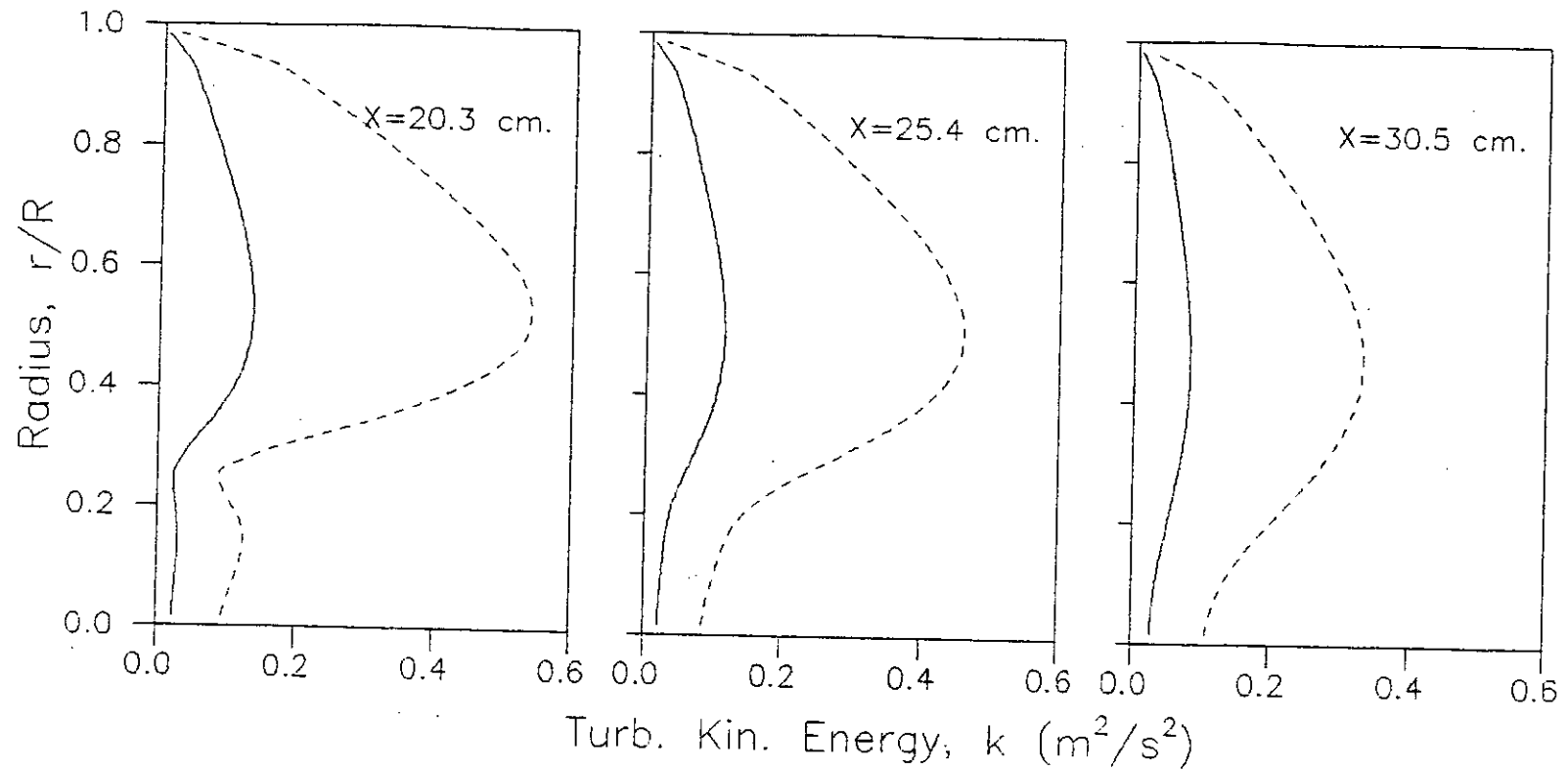


FIG.27.(Contd.) Comparison of turbulent kinetic energy profiles.

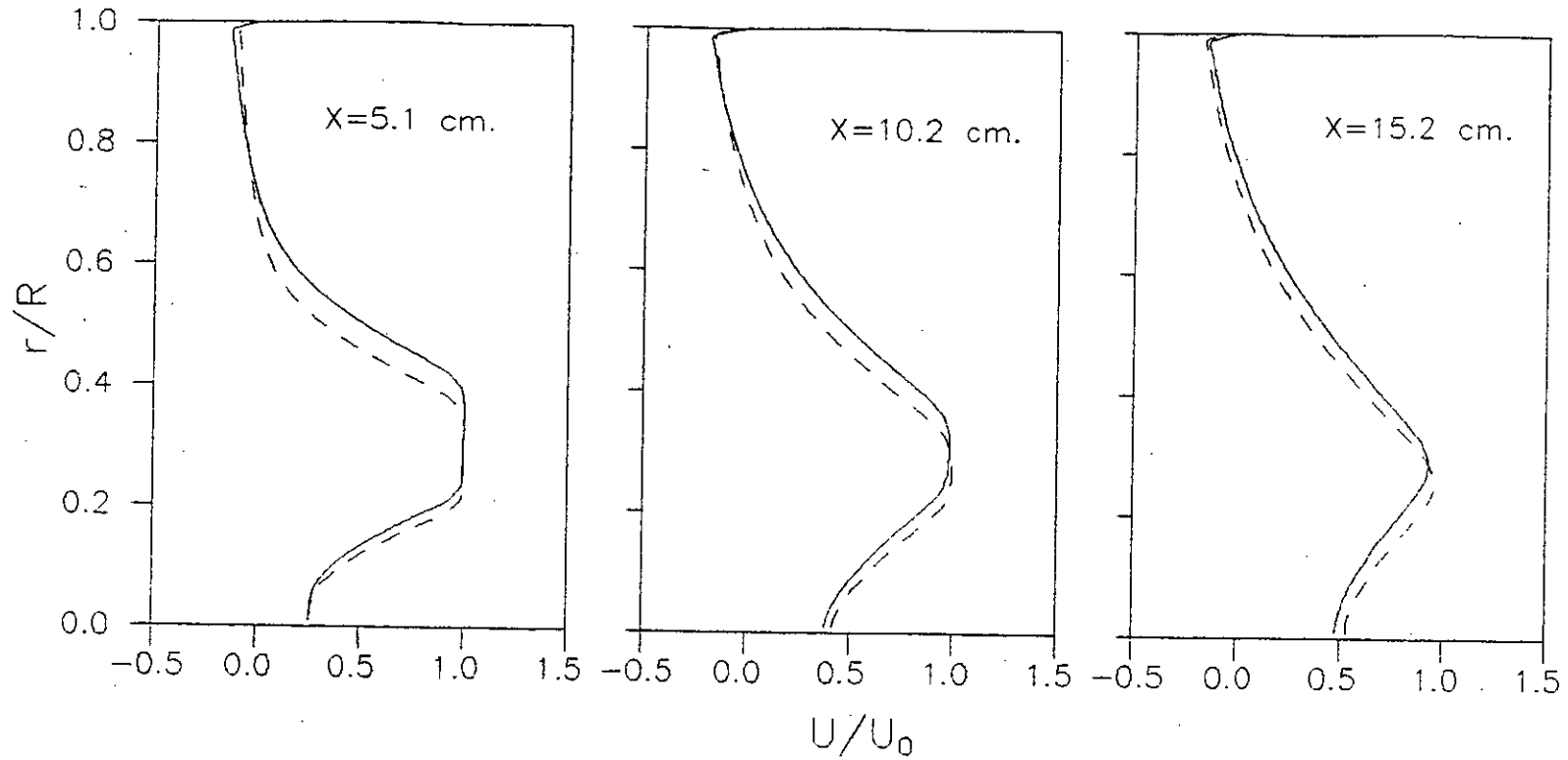


FIG.28. Comparison of dimensionless mean axial velocity profiles: —, $R/r_2 = 2.07$;
---, $R/r_2 = 2.27$.

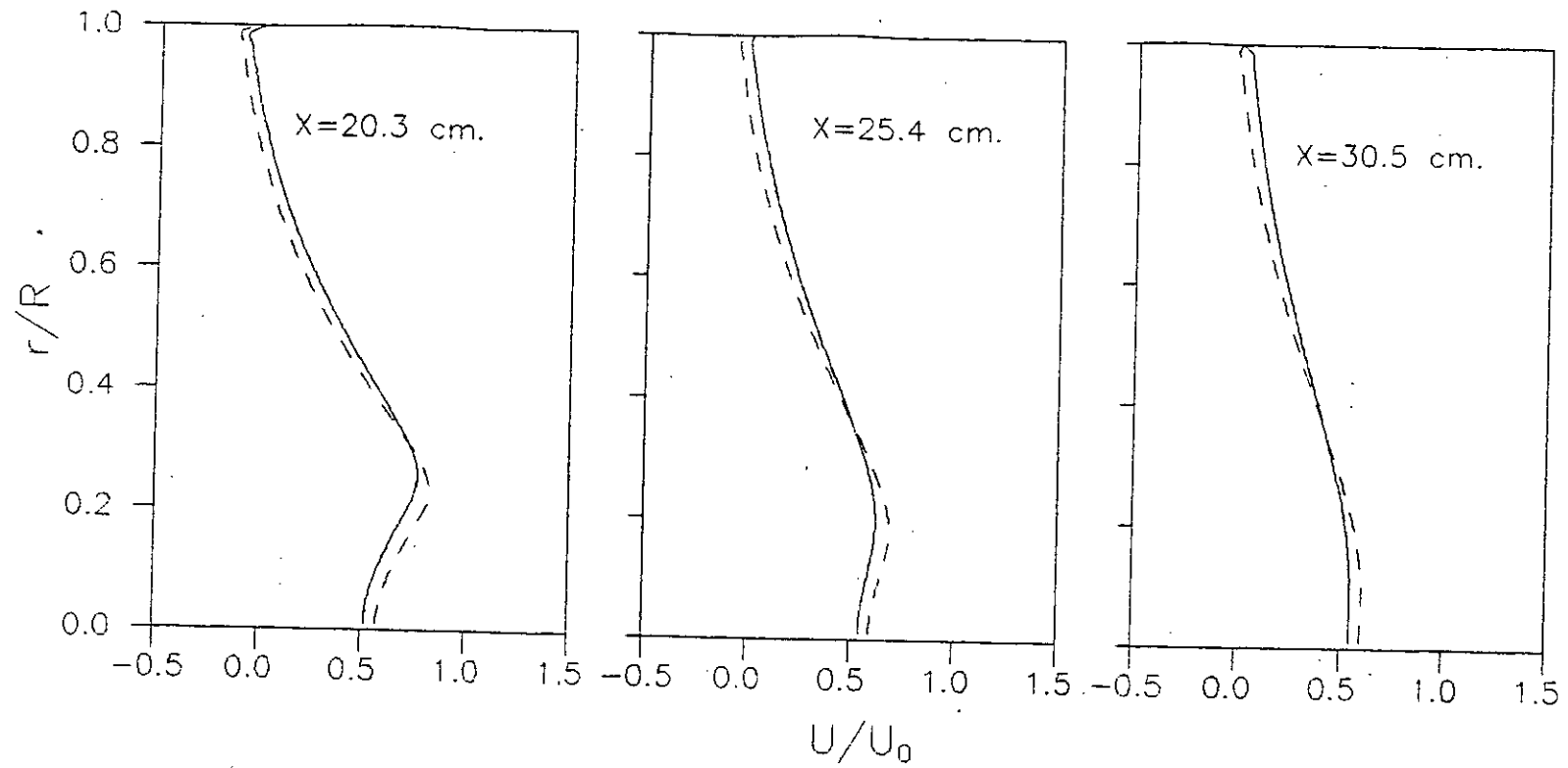


FIG.28.(Contd.) Comparison of dimensionless mean axial velocity profiles.

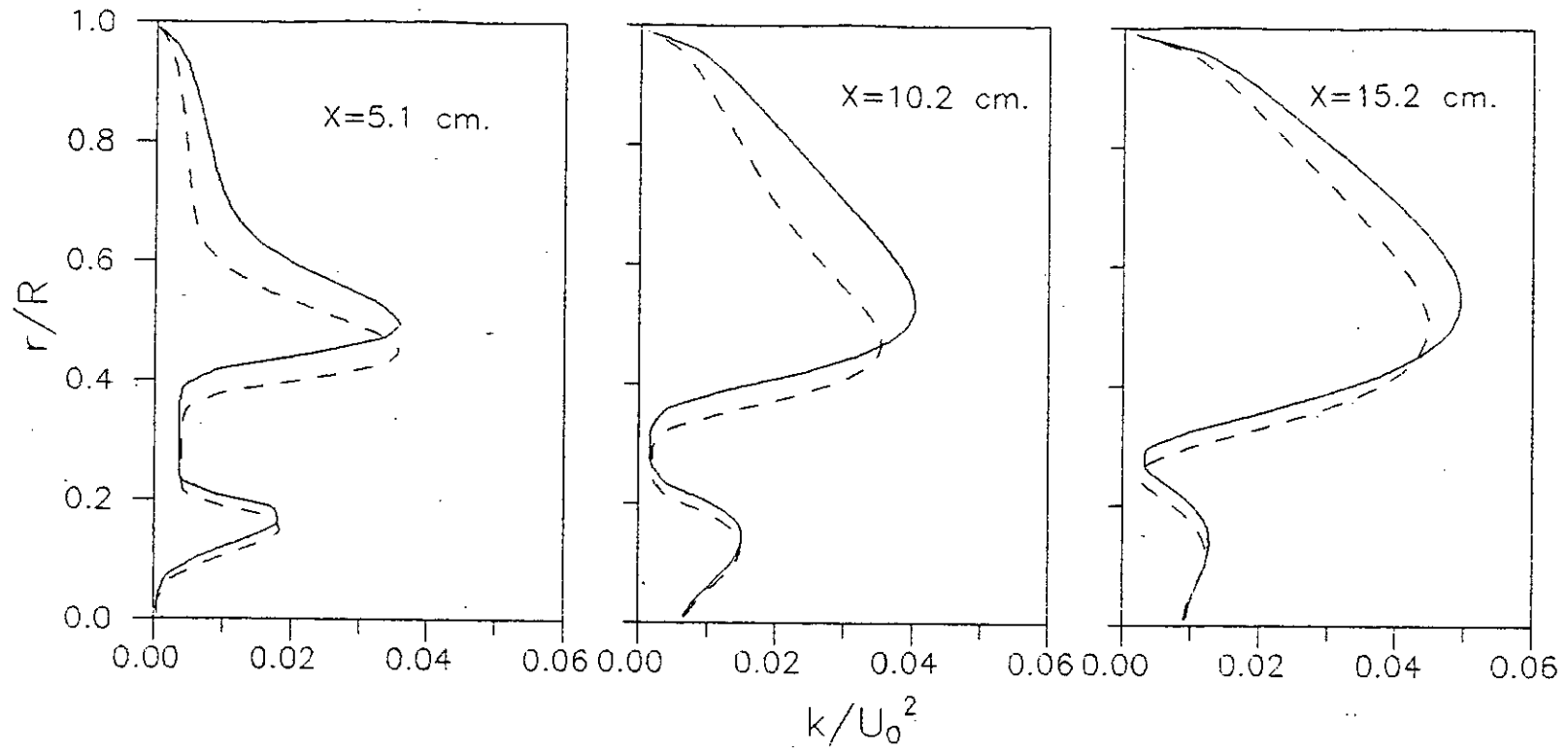


FIG.29. Comparison of dimensionless turbulent kinetic energy profiles: —, $R/r_2 = 2.07$; ---, $R/r_2 = 2.27$.

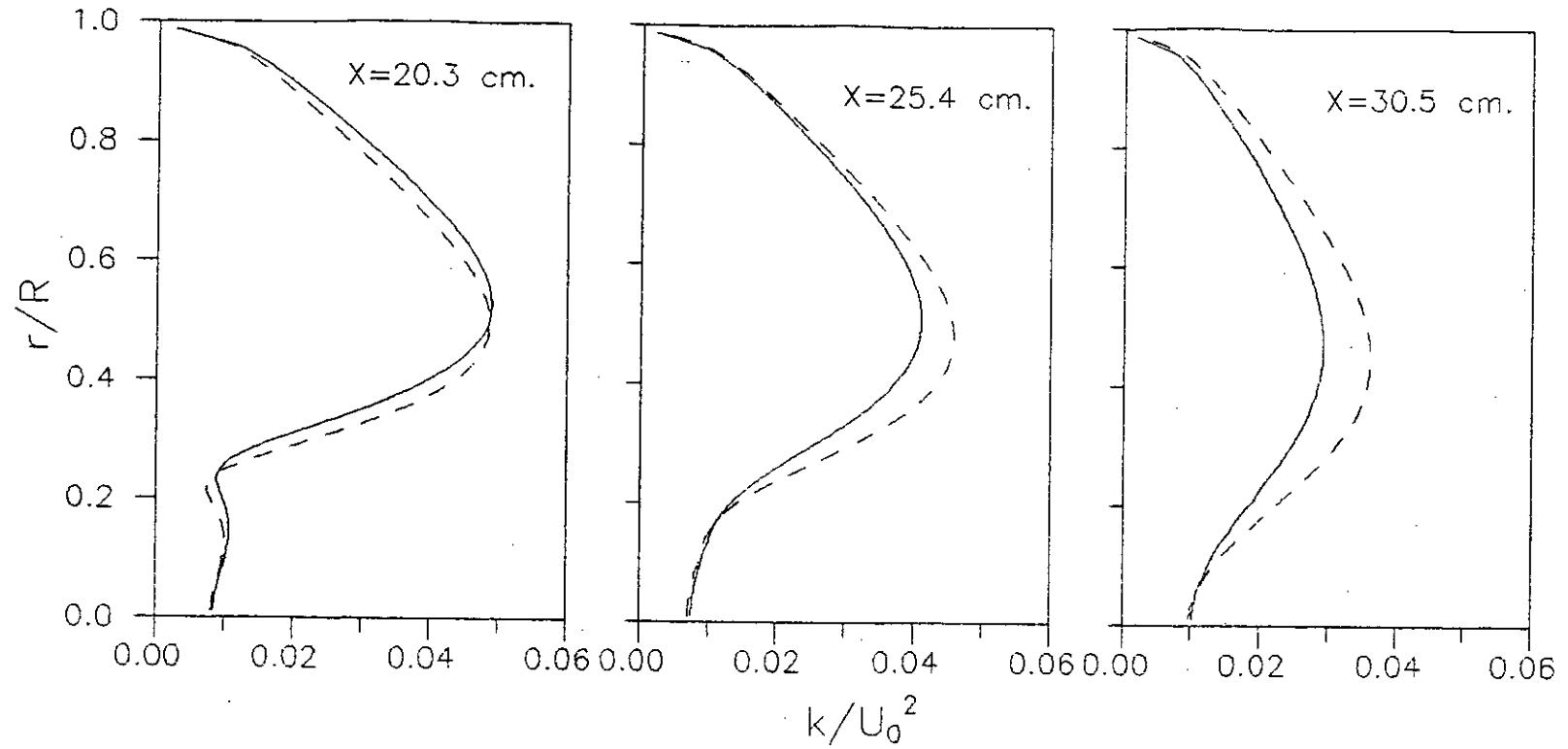


FIG.29.(Contd.) Comparison of dimensionless turbulent kinetic energy profiles.

APPENDIX - A

COMPUTER PROGRAMME FLOW CHART

